ACOUSTIC REPLICATION IN SMART STRUCTURES USING ACTIVE STRUCTURAL/ACOUSTIC CONTROL

A Thesis
Presented to
The Academic Faculty

by

Steven F. Griffin

In Partial Fulfillment
of the Requirements for the Degree
Doctor of Philosophy
in Aerospace Engineering

Georgia Institute of Technology
November 1995

ACOUSTIC REPLICATION IN SMART STRUCTURES USING
ACTIVE STRUCTURAL/ACOUSTIC CONTROL

Approved:

Sathya V. Hanagud, Chairman

Krishan K. Ahuja

Yves H. Berthelot

Wassim M. Haddad

Date Approved Nov 22 '95

ACKNOWLEDGMENTS

I would first like to thank my advisor, Dr. Sathya Hanagud, for time spent, knowledge imparted, and confidence invested in me over the course of this research.

I would also like to thank Dr. Yves Berthelot, Dr. Wassim Haddad and Dr. Manohar Kamat for spending so much time discussing acoustics, control and finite element modeling with me. I also thank Dr. Krishan Ahuja for providing insight into applied acoustics problems and allowing me to use the anechoic facility.

I also have received invaluable help from Hugang Luo, with structural modeling and experimentation, and from Jeff Hsu, with acoustic testing, for which I am extremely grateful.

I am also indebted to the Air Force Palace Knight Program for supporting me financially in the course of my studies and would especially like to thank Alok Das, who served as my mentor.

I also thank my mother Donna, father Edward, and sisters Kristine and Karen, who have all provided love, support and advice and served as wonderful examples. Finally, I would like to thank Carolyn, whose love, knowledge and moral support were truly indispensable in completing this research.

TABLE OF CONTENTS

LIST OF TABLES

LIST OF FIGURES

LIST OF SYMBOLS

w	out-of-plane plate displacement
D	plate stiffness
ρ	mass of the plate per area
c	equivalent viscous damping coefficient of plate
S	plate area
P_b	pressure behind plate
P_p	pressure in front of plate
F_p	point force applied to plate
λ	acoustic wavelength in air
γ	specific heat ratio
P_o	ambient pressure
V	cavity volume
z	displacement of air mass in the vent
R_p	viscous resistance term for plate motion
R_h	viscous resistance term for the air mass motion
R_t	$R_p + c$
M_h	air mass (continuous model)
m_h	air mass (discrete model)
ρ_0	ambient density
t	plate thickness
r_h	radius of the vent

S_h	area of the vent
a_0	ambient speed of sound
η_i	time-dependent modal coefficients
ϕ_i	spatially-dependent shape functions
R	distance from a point source to an observer
q	source strength
k	wavenumber in the acoustic medium
T	kinetic energy
U	potential energy
W_e	electrical energy
$\dot{\mathbf{w}}$	vector of velocities of the piezoceramic and structural materials
$\dot{z}$	velocity of the air mass
ρ_p, ρ_s	volume densities of the piezoelectric and structural materials
S, T	material strain and stress vectors
E	vector of the electric field
D	vector of electrical displacements
β	effective spring constant for the air cavity
ζ	viscous damping ratio
ξ	2ζ
C_h	proportional damping coefficient or air mass
x	state variable vector
H_w	displacement transfer function
H_a	accelerance transfer function
H_p	pressure transfer function
ω	angular frequency
C_{lpf}	low pass filter transfer function

$\omega_{i'}, \xi_{i'}$	measured guitar frequency and damping values (i = h,1 and 2)
ω_i, ξ_i	model input guitar frequency and damping values (i = h,1 and 2)
v	electric potential
σ	charge density
$\mathbf{c}^E$	short circuit elastic stiffness matrix
E	dielectric tensor at constant mechanical strain
e	piezoelectric tensor
d	matrix of piezoelectric constants
$\mathbf{m}_p, \mathbf{m}_s$	piezoelectric and structural mass matrices
$\mathbf{k}_{uu}, \mathbf{k}_s$	piezoelectric and structural stiffness matrices
$\mathbf{k}_{uv}, \mathbf{k}_{vu}$	piezoelectric stiffness matrices
$\mathbf{k}_{vv}$	dielectric stiffness matrix
$\mathbf{F}_p$	applied point forces
Cs	blocked sensor capacitance
v_s	sensor voltage
v_a	actuator voltage
Θ_a, Θ_s	piezoelectric actuator and sensor coupling matrices

SUMMARY

There has been a great deal of research on the use of active vibration control with the goal of changing the vibration characteristics of structures. These vibration characteristics may result in undesirable acoustic fields that radiate from the structure. Traditional active noise control approaches center around canceling the offensive acoustic field using loudspeakers to set up opposing fields. A more recent approach is to use active vibration control techniques to directly modify the vibration characteristics and thus the acoustically radiative properties of the structure. A very effective way of achieving this structural/acoustic control is through the use of smart structures in which sensors and actuators are integrated into the structure itself. The subject of this thesis is to explore the potential for the use of active structural/acoustic control and smart structures in acoustic replication. In acoustic replication, an offensive acoustic response of an acoustically radiative smart structure is modified to match a desired acoustic response using active structural/acoustic control. The desired goal, in this case, is not necessarily suppression but to match the acoustic response of a similar structure that has desired acoustic properties. The model that is developed in detail is an elastic plate with piezoceramic sensors and actuators backed by a rigid, vented cavity. One specific application explored is the acoustic guitar. Detailed information on desired acoustic response of guitars is readily available in the literature, and experimental specimens are relatively easy to

obtain. The way such an instrument vibrates in response to excitation of the strings determines the acoustic field that results. The feasibility of changing these vibrational characteristics using active structural/acoustic control is examined in detail including analytical and experimental results. The feasibility of applying acoustic replication to an aircraft cockpit is also examined including an experimental study on noise transmission reduction and an analytical study on acoustic signature modification.

CHAPTER I

INTRODUCTION

1.1 Motivation

In 1990, the "Mendelssohn" Stradivarius violin sold at Christie's in London for $ 1,686,700. A good violin at a typical music store sells for around $ 2,000. What is it about the Stradivarius that makes it cost almost 1,000 times as much? The structure and geometry of the two instruments are very similar, yet subtle differences in the structural dynamics of the two instruments cause them to vibrate differently in response to an excitation by a violinist's bow. This, in turn, causes differences in the sound produced by the two instruments which ultimately determines quality and, to a large extent, price. If it were possible to force the less expensive violin to vibrate like the Stradivarius, the legendary sound would follow.

The relatively new field of smart structural/acoustic control is centered around changing the structural dynamics of an acoustically radiative structure to change, usually to suppress, the sound resulting from vibration of the structure. This is done by connecting actuators that are integrated into the structure in a control loop with sensors that are either in the acoustic field or also integrated in the structure. Smart structural/acoustic control also has the potential to force one acoustically radiative structure to behave like a target acoustically radiative structure, thus replicating its acoustic properties. The

less expensive violin might be forced to sound like a Stradivarius. The concept of acoustic replication using smart structures has far reaching implications, from the field of acoustic musical instruments to aircraft cockpits.

1.2 Background

To provide a background, a brief review of active acoustics leading to smart structural acoustics is presented. Smart structural acoustics is a relatively recent subset of the broader field of acoustic control wherein an acoustically noisy structure may be controlled at the structure through integrated sensors and actuators. This integration is such that the sensors and actuators are load-carrying parts of the structure as well as control elements. The field of smart structural acoustics has emerged in a natural progression: first, acoustic control by acoustic sources; then, by vibration inputs; and finally, by integrated sensors and actuators or smart structural acoustic control.

Additionally, a review is given of literature on the acoustic guitar. This instrument has inspired a significant amount of analytical and experimental research from the perspective of acoustics and structural dynamics. As such, there are identified dynamic parameters in the literature that could potentially be further "tuned" using active acoustic control to accomplish desired changes in acoustic parameters.

1.2.1 Acoustic Control by Acoustic Source Actuation

In most applications, acoustic control is implemented in order to suppress unwanted noise through attenuation or other mechanisms. Sound attenuation is usually implemented through sound-absorbing materials for sounds of medium and high frequencies. Because the thickness of the sound

absorption material necessary to produce constant attenuation increases with decreasing frequencies, there is a practical limit on its use at relatively low frequencies [1]. In this low frequency region, active acoustic control has found applications.

The principles underlying active acoustic control have been understood at least since 1802 when Young's principle of interference was introduced [2]. The principle suggests cancellation of a sound wave propagating in space by the addition of an inverse wave. This principle forms the basis of active noise control [3]. Huygen's principle, as applied to acoustics, is an extension of Young's principle for multiple dimensions. Huygen's principle states that the sound field inside a surface that is produced by a source outside the surface can be exactly reproduced by an infinite array of secondary sources distributed along the surface [4]. Since an infinite array of secondary sources are not realizable, in practice, a finite number of secondary sources can be "field-fitted" to achieve an optimum result [5].

Despite the longevity of the underlying principles of active noise control, one of the first practical implementations was described by Lueg [6] in a German patent in 1933 and in a U.S. patent in 1934. Phase reversal in Lueg's one-dimensional duct was accomplished by considering the electronic system as a transmission line whose length determined the time delay. Lueg also proposed cancellation in a space very near a loudspeaker and in an open space using a microphone and a loudspeaker. It has been found more recently that cancellation at a point is done at the expense of increased noise at other locations in the field [7, 8]. Also, Lueg's approach to control of noise in an open space was probably not viable since successful

experiment implementations of this are much more recent and inevitably involve more than one microphone and speaker.

Little was published in the field of active control following Lueg's patent until the 1950's. In 1953, Olson published research on an electronic sound absorber and Conover made early attempts to control transformer noise using a single loudspeaker [9,10] . Frequency performance range of Olson's devices were limited at low frequencies by loudspeaker performance and at high frequencies by phase errors and electronics. An attenuation is achieved of almost 25 dB in the range of 60 to 80 Hz accompanied by an almost linearly decreasing attenuation up to around 500 Hz where there is an increase of sound pressure of 5 dB. This early work started to map out the frequency range of usefulness of active versus passive noise control, where active is most effective in the range of near DC to 500 Hz and passive is most effective above 500 Hz. This upper limit on active control should continue to increase as theory develops, computing power continues to increase, and computing equipment cost continues to decrease.

Applications in which modern active noise control research continue are plentiful, including approximately one-dimensional problems such as ducts and noise-reducing headsets and multidimensional applications such as cylinder interiors and transformers. Cylinder interiors are of particular interest because of their natural extension to fuselages [3] and launch vehicles.

The idea of noise reducing headsets started as a more advanced version of Lueg's system for controlling duct noise and was implemented by Olson [9]. For low frequencies, sound waves in ducts propagate as approximately one-dimensional plane waves. As the sound frequency

increases, the sound propagation becomes multidimensional and much harder to control as the plane wave assumption breaks down and transverse resonances cause pressure fluctuations through a cross section [11]. Active noise control has been applied to fan-induced duct noise in commercial air handlers at low frequencies [12]. The limiting frequency for noise reduction of up to 20 dB for most duct structures is around 500 Hz. This limitation is also imposed by sampling and processing speeds [3].

Internal cylinder noise can be a pseudo two-dimensional problem or a three-dimensional problem depending on whether the noise sources and secondary sources lie in the same cross-sectional plane and the frequency of the noise. In 1976, Kempton [13], put forth one of the first illustrations of a multidimensional active acoustic control problem using an array of "anti-sources" to cancel the far-field of a monopole source. Lester and Fuller [14] used four interior monopole control sources to attenuate noise by around 20 dB within a cylindrical cross section caused by 2 exterior monopole noise sources. Later, Fuller, and Jones [15] and Jones and Fuller [16] performed similar studies using a structural control actuator. These will be covered in greater detail in the next section. Elliot *et. al.* [17] determined that as long as secondary sources couple sufficiently with modes that are excited by the primary source, it is possible to achieve noise reduction without locating secondary sources near the primary source. Noise control has also been applied to the characteristic low frequency hum of transformers. Angevine [18] showed attenuation levels of 16 dB using 26 secondary sources surrounding the transformer.

1.2.2 Acoustic Control by Direct Structural Actuation

When the source of noise to be controlled is a structure, the use of acoustic sources for control is available in addition to the option of applying a vibrational source directly to the structure. The addition of a sensor and a control methodology can potentially modify the structure so that noise does not propagate as readily at the frequencies of interest. An advantage for direct structural actuators is illustrated by an inherent disadvantage in acoustic source control. When there are many phase changes across the surface of a noise source, as in a panel structure vibrating in a higher mode, many acoustic sources are needed for control. In the case of the panel, there should be at least one acoustic source for each antinode on the structure [19]. Additionally, it has been found in the control of interior noise of cylinders that direct structural actuation avoids control spillover effects encountered using acoustic sources. Control spillover is the effect of generating additional, unwanted noise when control is implemented due to an inexact match of the control field to the primary field with respect to spatial distribution [20].

Some of the earliest works in the literature involving direct structural actuation to provide vibration inputs were published in the Soviet Union. In 1966, Knyazev and Tartakovskii [21] used vibration pickups and vibration inputs to control plate vibrations by introducing active damping. They also noticed an average reduction of 16 dB in acoustic pressure over the area of the plate when vibrating at 390 Hz. This frequency was located very close to a resonance of the plate. A follow-up paper in 1967, by Knyazev and Tartakovskii [22], was directed primarily at acoustic attenuation of noise radiated by the flexural waves of a plate. Experimental results indicated an

average of 7 dB reduction in acoustic pressure across a frequency range of DC to 1900 Hz. They noted that the tuning of vibration dampers to minimize the noise field does not coincide with the tuning of vibration dampers to minimize vibration and that the maximum radiation attenuation of noise occurs near the location of the damper. In another relatively early publication from the Soviet Union in 1987, Vyalyshev, Dubinin, and Tartakovskii [23] presented a theoretical examination of reductions in sound transmission through a plate with an auxiliary point force used as a control actuator. They observed that reductions in sound transmission through the plate could alternately be viewed as an increase in the impedance of the plate.

Early pioneering work in the United States using direct structural actuators to provide vibration inputs began with Jones and Fuller [15] on active control of a sound field within a cylinder (this followed an earlier reference work by Lester and Fuller [14] using acoustic sources on the same problem). This cylinder study was directed towards the control of cabin noise in the advanced turboprop aircraft. A control relation is derived, in this experimental study, by producing the same sound field at a given microphone location using both an acoustic source that is supposed to simulate noise and a secondary vibration control source. Both sources were then switched on and their phase varied with respect to each other while sound pressure level (SPL) was measured at several interior locations as a function of this variation. Both resonant and off-resonant noise frequencies were investigated. Attenuation of sound pressure of up to 20 dB was obtained. An additional study by Jones and Fuller [16] showed reductions of up to 30 dB at acoustic resonance in the cavity using two vibration control sources and two microphone error sensors. In this case, the control was

formulated by minimizing a quadratic cost function based on error signals from the microphones.

1.2.3 Acoustic Control by Smart Structure Actuation

An enhancement to providing direct structural actuation with a point force is to provide direct structural actuation using actuators that have been developed for smart structures. The use of smart structures started in the field of vibration control. In acoustic control, the objective changes from one of minimizing or altering structural response to one of minimizing or altering acoustic response. These two objectives often require very different control laws, but both may be achievable using the same actuator. A smart structure actuator can either be imbedded in or bonded to the host structure. It provides a source of direct structural actuation without the added space and structural grounding requirements necessary with a shaker providing a point force. In addition, point force actuation is more prone to spillover [24] and shakers exhibit a certain back reactance that may require consideration in the model of the structure [25]. Smart structure actuators only slightly increase the mass and stiffness at the point of application. The primary smart structure actuator used, in vibration applications, is the surface-bonded piezoceramic. Transverse deflections on application of a voltage in the poling direction of the through-the-thickness poled piezoceramic translate into in-plane surface tractions applied to the structure.

The first investigation of what could be called a smart structure actuator was directed at vibration control by Forward [26]. He used bonded piezoceramics as sensors and actuators to control the vibration of a mirror subjected to acoustic excitation. Other early work, which concentrated on vibration control of beam structures, includes that of Bailey and Hubbard [27],

who investigated the use of poly vinyldene fluoride (PVDF), a piezoelectric polymer, as a distributed parameter actuator on a cantilever beam. Obal [28] and Hanagud, Obal, and Calise [29,30] formulated an optimal control law for vibration suppression of a beam using surface-bonded piezoceramic sensors and actuators. They also found that for the assumptions of uniform beam stiffness and perfectly rigid bonds, piezoceramics could be modeled as concentrated line moments applied to the beam at the boundaries of the actuators. Baz and Poh [31] investigated optimal location and control gains for minimizing beam vibration amplitude using piezoceramic actuators. The interaction between piezoceramic actuators and beam structures was first thoroughly analyzed by Crawley and De Luis [32] and later by Crawley and Anderson [33]. An important conclusion was that the bonding layer should be very thin and that the piezoceramic actuator should be stiff compared to the host structure for maximum force at a given voltage. They also came to a similar conclusion as references 28-30 that, under these conditions, the action on the beam by the piezoceramic can be approximated by line moments proportional to the applied voltage at the boundaries of the piezoceramic. Early work on the incorporation of one-dimensional active piezoceramic elements into more complicated truss structures for vibration suppression was done by Fanson and Chen [34]. More recently, Bronowicki and Betros [35] developed a hybrid method for modeling piezoceramic sensing and actuation of complicated truss-beam combination structures which uses a finite element code to generate structural mode shapes and a thermal analogy to model both sensing and actuation.

Investigations into the more general problem of actuation of plates using surface-bonded piezoceramic actuators are more relevant to acoustic

problems, but also have their background in vibration suppression problems. Approaches to smart structure plate actuation can be divided into two categories: (1) continuous exact or approximate solutions and (2) discrete formulations involving a finite element model (FEM) .

Among continuous solutions, Dimitriadis, Fuller, and Rogers [36] put forward a theoretical paper postulating the interaction between a piezoceramic plate bonded to a plate substructure. A perfect bond and a uniform bending applied by the actuator at all points within the actuator boundaries were assumed, resulting in a spherical deformation of the plate due to the actuator. It was predicted, analogous to the beam case, that the piezoceramic could be replaced by line moments along the borders of the piezoceramic actuator. Also, it was shown that for symmetric distribution of an actuator about a nodal line of a given vibrational mode, excitation of that mode was theoretically impossible. Optimum actuator position for excitation of a vibrational mode was said to be near nodal lines. A more general statement of this principle by Fuller, Rogers, and Robertshaw [37] is that the center of the actuator should be in a region of high structural surface strain of a mode for excitation of that mode. Crawley and Lazarus [38] developed a model of induced strain actuation that was applicable to isotropic and anisotropic plates. The model was experimentally verified for the case of piezoceramic material covering the majority of both surfaces of cantilevered plate test articles in static deflection due to voltage applied to the actuators. Kim and Jones [39] included the effect of a finite thickness bonding layer in actuation of a plate by surface-bonded piezoceramic actuators. They also presented some results on optimal thicknesses of the actuator for a constant applied field. In a study of segmentation of piezoceramic sensors and

actuators bonded onto plates, Tzou and Fu [40, 41] found that proper segmentation of piezoceramics result in the ability to sense and actuate modes for which piezoceramics are evenly distributed about a nodal line of the mode.

The inherent limitation in all of the continuous models is that the plate substructure problem must be amenable to a continuous exact or approximate solution in order to solve the combined piezoceramic/plate problem. For evaluation of potentially more complex problems, approaches have been developed which fall into the category of discrete solutions involving FEM. The first piezoelectric finite element for structural dynamics that could be found was derived by Allik and Hughes [42]. Also, McDearmon [43] published a method to add piezoelectric properties to structural finite elements through a matrix manipulation of elastic and heat transfer element matrices. In a much more recent study, Ha, Keilers, and Chang [44] developed a composite finite element with piezoceramics included as outer layers of the element. The specific element was eight-noded, with three displacement degrees of freedom and one voltage degree of freedom per node. A modal expansion was used to show the feasibility of introducing active damping although no explicit control algorithm was formulated. Comparisons were also made between predictions of static and dynamic deflections using an assembled model that included the composite element and experimental data on cantilevered plates.

Piezoceramics are also used as actuators in the majority of smart structure acoustic control research found [24, 25, 36, 37, 45-58]. Piezoceramics offer the necessary frequency response and force authority for active acoustic control. In addition, the distributed nature of the

piezoceramic wafer can be used to spatially filter selected modes that are acoustic radiators by proper placement of the actuator material [49, 36, 25]. Rogers, Fuller, and Liang [60] have also proposed using embedded nitinol fibers, a shape memory alloy, to control sound transmission through a panel. Activation of the nitinol fibers results in a static change in mechanical properties and mode shapes of the panel that can reduce sound transmission.

There have been a number of theoretical papers considering smart structural acoustic control applied to both beam and plate structures. Clark and Gibbs [48] investigated the use of a simply supported plate with one piezoceramic actuator to demonstrate a higher harmonic control approach. Control of sound radiation due to subsonic vibrational waves impinging on structural discontinuities was researched by Guigou and Fuller [52]. In this study, active control forces due to bonded piezoceramics and shakers, were both shown to be effective at minimizing the radiated acoustic field. Clark and Fuller [50] present a theoretical paper examining model reference-based control on the acoustic field resulting from a simply supported beam with piezoceramic actuators and structural sensors. The structural response is driven by a controller to some predetermined reference response which results in favorable acoustic response. It was shown analytically that the same degree of control that can be achieved by any number of error sensors in the acoustic field and n actuators can also be achieved by using n structural sensors and n actuators. This provides a means to get a high degree of acoustic control through a detailed initial survey using many microphones in the acoustic field, and to maintain that control with a reduced number of structural sensors.

There have also been studies that include experimental validation implementing smart structural acoustic control of plates. In a purely experimental study, Fuller, Hansen, and Snyder [25] achieve a global attenuation on the order of 45 dB using a piezoceramic actuator and a form of open-loop control which varies the phase between the disturbance and the control signals. This was done at two distinct resonant frequencies of a simply supported plate. In another experiment, Clark and Fuller [24] compare the number of piezoceramic actuators used to control on-resonant and off-resonant excitation of a simply-supported plate. They found that for on-resonant excitation, more piezoceramic actuators failed to elicit better performance, while for off-resonant cases more piezoceramic actuators increased performance. Also, Clark and Fuller [49] give an optimal placement methodology for piezoceramic actuators and PVDF structural sensors on a baffled, simply-supported plate. A Rayleigh integral approach is used to predict pressure fluctuation as a result of plate movement. Analytical results formulated using a linear quadratic optimal control theory are compared to experimental results. It was found that a single optimally-placed piezoceramic actuator and PVDF sensor can rival performance achieved with three arbitrarily-placed actuators and three microphone sensors. Van Niekerk, Tongue, and Packard [53] used a pair of surface-bonded piezoceramic actuators mounted on a circular plate that was mounted in a duct to suppress a transient pressure pulse due to a loudspeaker that was also mounted in the duct. They found reductions of up to 15 dB in a microphone that was placed downstream of the plate when the controller was active.

Smart structural acoustic control applied to flexible plates that are backed by sealed rigid cavities has also been the subject of a small body of recent research [54-58]. This model is important because it adds insight to problems of sound propagation into aircraft cabins, where the primary noise source is due to new, more efficient, but noisier turboprop engines [54] and into spacecraft launch vehicles where excitation of the payload fairing can create a harsh enough internal acoustic field to interfere with sensitive payloads [56]. Lyon [61] was the first reference found to investigate passive suppression of sound propagation into a sealed, cavity-backed plate, but the first references investigating smart structural acoustic control on the related problem of sound propagation into a two-dimensional cavity with a flexible beam boundary were by Banks and Fang [54, 55] almost 30 years later, in 1991. In this later theoretical work, piezoceramic actuators were bonded to both sides of a clamped, flexible beam boundary, and a time domain state space formulation was derived for coupled structure/fluid system and used to investigate active control of noise in the cavity and beam amplitude due to a periodic beam excitation. Kohsigoe, Gillis, and Falangas [56] investigated sound transmission through an elastic, simply-supported plate into a three-dimensional cavity with rigid sides, a lightly damped back wall, and a rigid inner box located at the center of the cavity. The theoretical development includes a formulation for the equation of motion of the plate and equations for resulting pressure inside and outside of the cavity. Active noise control is investigated for controlling noise transmission into the cavity using the piezoceramics as actuators. In an entirely experimental study, Ellis and Koshigoe [57] constructed a cavity with rigid sides and back and clamped a flexible plate to the front with a piezoceramic actuator and accelerometer

sensor in order to study control of harmonic noise transmission due to an external loudspeaker. In a theoretical study, Koshigoe and Ellis [58] considered decreasing harmonic noise transmission through a simply-supported plate with surface-bonded piezoceramic actuators into a rigid cavity with a time-varying mean air density. Hill et al. [59] conducted an experimental investigation of decreasing harmonic sound transmission due to a loudspeaker through a clamped plate with a pair of surface bonded piezoceramic actuators into a sealed, rectangular cavity with acoustically reflective sides and back. Low-order models, which captured the modes to be controlled, were fit to measured data for state space control design.

1.2.4 Sensors

Two approaches are available for sensing in acoustic control of structures. The traditional approach is to sense the acoustically radiated field directly using microphones in the acoustic field. The second approach is to use any one of the smart structural sensors that have been developed for vibrational control. These include optical fibers, nitinol or constantin strain sensors, and PVDF or piezoceramics.

Piezoceramic sensors can be used as independent sensors or their functionality as sensor and actuator can be shared to form the sensoriactuator [46]. In this embodiment, piezoceramic wafers serve as a collocated sensor and actuator. One advantage to smart structure sensors is the ability to spatially weight acoustically radiative modes by placing sensors in regions of high in-plane strain corresponding to the radiative mode [49]. Another advantage is the compactness of locating the sensor on the structure. A disadvantage is the necessity of formulating a relationship between a measurable structural parameter and the radiated acoustic

pressure. This is only possible analytically for very few circumstances, as with the use of the Rayleigh integral to relate surface velocity to acoustic pressure when the structure is infinitely baffled. In the general case of a complex structure, this relationship between structural parameters and acoustic pressure is beyond the state of the art [62].

The determination of which modes are important as acoustic radiators and thus which modes to control, has been greatly simplified by the introduction of the wave-number transform, also called the k-transform [63, 64]. The k-transform is obtained by calculating the Fourier transform of a structure's spatial response. The resulting portion of the wavenumber spectrum below the wavenumber in the acoustic medium corresponds to the far-field radiation. The portion of the wavenumber spectrum above the wavenumber in the acoustic medium corresponds to the near-field radiation. This transform can be used to predict whether a vibrating structure will produce sound which propagates into the far field and to examine how changes introduced by active control will affect that propagation.

1.2.5 Control Approaches

The majority of the active control approaches reviewed so far have been formulated in response to steady state sinusoidal disturbance inputs at one or multiple frequencies. The simplest control approach under these conditions is open-loop control. This can only be implemented when a very accurate representation of the disturbance signal can also be used to drive the actuators at a desired phase with respect to the radiating structure. The disadvantage of this approach is that it is not always possible to have a very accurate disturbance signal. A more sophisticated extension of this is the feedforward LMS adaptive approach. In this approach a quadratic cost

function constructed of the acoustic error signals is minimized using superposed signals introduced by the actuator. An advantage of this approach is that it does not require a good estimate of the system and that it is relatively easy to implement in hardware [37]. Smith, Fuller, and Burdisso [45] found that for a broadband excitation, single-input-single-output (SISO) feedforward control did not give satisfactory performance in the attenuation of radiated sound from a plate. They found a multi-input-multi-output (MIMO) feedforward controller is necessary for significant acoustic attenuation.

When the disturbance is broadband, a different approach is necessary for single-input-single-output systems. In order for the control to react quickly enough to the variable nature of the input, a feedback control approach must be formulated [46]. Meirovitch and Thangjitham [62] published one of the first theoretical studies using direct structural actuation and feedback control, but their approach was to minimize the vibration of a simply-supported elastic plate and to use the Rayleigh integral to check the effect of the control in the acoustic field. Also, they only attempted to control a harmonic disturbance. Bauman, Saunders, and Robertshaw [65] used a Linear-Quadratic-Regulator (LQR) optimal method to suppress acoustic radiation from a beam that was excited by impulsive forces. They theorized that sound radiation from the beam would be suppressed by 73% with the controller configured to suppress vibration using LQR. Bauman, Ho, and Robertshaw [66] also published a theoretical study investigating active acoustic control of broadband disturbances. Here, a feedback controller was designed for a clamped-clamped beam using a Linear-Quadratic-Gaussian (LQG) theory to minimize total radiated acoustic power.

References [62, 65, and 66] all assumed direct structural actuation via an out-of-plane control force. There were also a few references found that investigated feedback control approaches using smart structural actuation. As was mentioned before, Banks and Fang [54, 55] described an acoustic cavity with one flexible beam boundary and smart structural actuation. Acoustic control was achieved using an LQR time domain approach, but the excitation was assumed to be periodic. Saunders, Cole, and Robertshaw [46] examined stability criteria for collocated structural acoustic feedback control using sensoriactuators. They found that for partial state feedback of plant velocities and farfield radiation states, stability was not guaranteed, as is the case for direct velocity feedback in vibration control. Van Niekerk, Tongue, and Packard [53] used an H_2 optimal control procedure to design a dynamic feedforward/feedback controller to suppress transmission of a transient pulse through the previously described circular plate in a duct with piezoceramic actuators. Feedforward signals were provided by two microphones in the duct and a feedback signal was taken as the velocity of the center of the plate as measured by a laser vibrometer.

Among the acoustic control of sound transmission through flexible plates into three-dimensional cavities using smart structure actuation, Koshigoe, Gillis, and Falangas [56] proposed a feedback method which makes the applied voltage to the piezoceramic proportional to sound pressure inside the cavity, but with the phase adjusted so as to create damping in the acoustic modes. They theorized that the method should be effective for both plate and cavity controlled modes. In the experimental study by Hill *et al.* [59], several feedback control approaches including LQG/ Loop Transfer Recovery (LTR), $H\infty$, pole placement and LQG were implemented

based on the reduced order state space model, but the only input disturbance considered was harmonic.

1.2.6 Acoustic Guitar Research

A reasonable body of technical research exists for two popular acoustic instruments: the violin and the guitar. Both have been studied with respect to their structural/acoustic properties to some degree. The violin is considerably more complex than the guitar. The primary reasons for this are the asymmetrical vibration characteristics of the assembled violin and the involvement of the entire violin body in the production of sound. Despite the symmetrical shape, the bass bar and the soundpost located approximately on either side of the bridge below the top plate cause the vibration of the violin to be very complex and asymmetric. In fact, the primary purpose of the soundpost is to introduce asymmetry [67]. It also effectively couples the top and back of the violin [68]. Reference [69] provides an extensive review of the history of violin research. In contrast, the sound radiated from the assembled guitar is primarily due to the vibration of the top plate which has lower frequency mode shapes that are relatively simple in comparison. As a result, the guitar is particularly amenable to modeling in its lower frequency function [68, 70-74].

Of technical research that has been devoted to the modeling of acoustic-structural behavior of the acoustic guitar, most reported papers are concerned with the lower band of natural frequencies [68, 70-73]. This domain starts with the air mode at around 100 Hz and extends to the lowest plate mode of the lower bout of the acoustic guitar, which usually occurs around 200 Hz. Successful models of this low frequency behavior have drawn on an analogy to a vented loudspeaker enclosure with a solid piston

representing the lower bout and an air piston representing the air mass that moves in and out of the rose. The pistons are constrained by an equivalent spring and damper whose parameters are derived from experimental measurements.

Firth [70] described an analogous acoustical circuit used to model vented loudspeakers to describe the first two modes of the guitar. Frequency and damping parameters for this model were taken from admittance measurements made on a representative acoustic guitar. The analogous acoustical circuit was then used to predict pressure emanating from the guitar in the frequency range of the air mode and the first plate mode. These predictions were compared to measurements of sound output and its phase with relation to an excitation force at the center of the bridge. Extending this approach, Caldersmith [68] used the analogy of a vented loudspeaker but derived the two coupled differential equations that describe the air mass that moves through the rose of the guitar as an air piston and the lower bout of the guitar as an equivalent plate piston. Stiffness and damping parameters for the pistons were taken from resonance and logarithmic decrement measurements, but an approach was outlined to estimate an equivalent stiffness for the plate piston directly for an assumed clamped orthotropic plate. SPL was calculated as a sum of the contribution of the air piston and the equivalent plate piston. Christensen and Vistisen [71] used a similar approach but derived frequency and damping parameters entirely from top plate mobility measurements. A three-piston model has also been proposed by Christensen [73] as an extension of the two-piston model that also treats the guitar back as an equivalent piston. Similar three-piston models were also described by Rossing, Popp, and Polstein [72] and Fletcher and Rossing

[75]. Christensen [74] also proposed modeling all top plate resonances up to 600 to 800 Hz as harmonically oscillating simple sources. This study included experimental measurements of resonant frequencies, initial guesses at damping and area to mass ratios and subsequent tuning of parameters to match experimental SPL measurements at one point in the acoustic field. It neglects multipole radiation of antisymmetric modes that could be significant in locations other than the measurement point two meters directly above the top plate. No published work could be found that links the spatial distribution of movement at the lower bout directly to the resulting sound pressure. This necessarily precludes consideration of sound pressure generated by antisymmetric plate modes at multiple locations in the acoustic field.

There are several factors in the low frequency regime of the acoustic guitar that have been identified as important in determining the quality of music the guitar is able to produce and, ultimately, the quality of the guitar itself. Specifically, these factors all are identifiable from structural transfer function measurements and SPL measurements made on the guitar. A study on appraisal of quality in guitars and violins was done by Gridnev and Porvenkov [76] based on probabilistic spectrum analysis, but no specific advice on individual resonance properties was given. Christensen and Vistisen [71] observed, based on a study of nine guitars, that the best guitars have the highest quality factors in their first resonance. They also observed that the lowest frequency should be relatively low.

By far the most thorough and conclusive research done on relating guitar quality to measurable quantities was by Meyer [77]. In this work, 15 classical guitars of varying quality were used in a series of subjective and

objective tests. The subjective tests consisted of a series of listening tests to different arrangements of music played on each guitar. The objective tests were performed by measuring frequency response characteristics in the SPL due to excitation of the guitars by an electrodynamic vibration system. Measurements were made using microphones in an anechoic chamber with the strings damped. Statistics were then employed to obtain a correlation between measured frequency response characteristics and subjective evaluations of the guitars. It was found that the three most highly correlated measurements with guitar quality were related to the antisymmetric mode of the guitar that occurs at around 400 Hz. This mode is also known as the (0,1) plate mode [75]. Also, the factor with the highest negative correlation with quality was the quality factor in the air mode, meaning the air mode has high damping in guitars of high quality. Based on the results of the correlation tests, Meyer gives specific criteria for quality in acoustic guitars. Among these is the advice that the air mode and the first plate mode should have as much damping as possible, while the antisymmetric mode should have as little damping as possible. Also, the peak levels of the antisymmetric and first plate modes should be high.

Normally, advice on improving quality in guitars is directed at the skilled guitar luthier who achieves such changes passively by careful adjustments of thicknesses and bracing in the guitar. Christensen [78] points out that strong excitation of the (0,1) antisymmetric plate mode is very difficult to achieve since the bridge is usually very close to its nodal line. The closer the bridge is located to the nodal line of a given mode, the less the excitation, of that mode, when the instrument is played.

1.3 Summary and Specific Studies

There has been a great deal of research in the past in the field of active noise control. Primarily, these efforts have investigated the use of loudspeakers to create anti-noise to cancel out ambient noise, the objective being a lower overall noise level. More recently, work has been done on directly controlling acoustically radiative structures using either attached or integrated actuators with the goal of reducing the radiated sound of the structure. The structures under study have been the building blocks of aerospace applications, beams and plates. Most recently there has been some research in controlling structural systems such as acoustically radiative plates backed by a sealed cavity. This has been directed at applications where decreasing noise transmitted into the sealed enclosure was the primary objective. In the vast majority of these efforts involving direct structural actuation of radiative structures, adaptive feedforward control techniques have been used. The advantage of the embodiment of this control technique that is most often implemented is that little information need be known about the system that is being controlled. The disadvantage is, typically, that the speed of the control algorithm is not sufficient to react to broadband disturbances. Much less research using feedback control approaches exists. The advantage of the feedback approach is the ability to react to broadband disturbances. Very little research was found that explored feedback control techniques with direct structural actuation of radiative structures, and only one experimental study could be found that looked at feedback control of broadband disturbances using smart structural actuation, and this considered a plate substructure in a circular duct only. No experimental studies using feedback control of broadband disturbances

using smart structural actuation in more complicated problems such as cavity-backed plates could be found.

In the modeling of cavity-backed plates, only limited research addresses the case when the cavity is vented. A vented, cavity-backed plate model describes the important commercial application of acoustic musical instruments. Accordingly, most of the research in this area is directed toward the acoustic guitar. All of the previous research that could be found involves assumptions that neglect near field acoustic radiation due to antisymmetric plate modes. This is too limiting in investigating musical quality in these instruments. No research could be found on structural/acoustic control of vented, cavity-backed plates. Moreover, although active structural/acoustic control has the potential to favorably tune many of the most important factors that determine quality in acoustic guitars, no published research was found that investigated its application to guitars or any other acoustic musical instrument.

The control objective in all the research found involving acoustically radiative structures was noise suppression. No research could be found in which structural/acoustic control was used to purposely enhance, as well as suppress, aspects of structurally generated acoustics.

Among available transducer devices for structural/acoustic control, surface-bonded piezoceramics have recently found application, buoyed by their success in vibration control applications, as both sensors and actuators. The published models that describe the interaction between structures and piezoceramics can be grouped into two broad categories: continuous models and discrete models. The continuous models have the advantage of a relatively low order state space model that is suitable for control formulation

but are severely limited in the complexity of the problem they can solve. The discrete models usually take the form of a piezoceramic or a composite piezoceramic/structural finite element. The powerful finite element method (FEM) approach has the advantage of being able to model very complex structural systems, but the disadvantage of a very high order model not suitable for control formulation or specialized finite elements that are not necessarily available in commercial codes. In addition, most of the models available, discrete and continuous, are directed toward beam and plate problems. There is much less research available directed at more complicated structures such as the vented, cavity-backed plate problem, and no research could be found that addressed modeling of the vented cavity-backed plate problem with actuators of any kind. Also, no research could be found that used the discrete method to solve plate substructure or more complicated structural problems in conjunction with a specific control formulation.

To address some of the unresolved areas in the research mentioned above, three specific studies were defined along with experimental validation. First, a spatially-continuous model of a vented, cavity-backed plate was developed to investigate structurally generated acoustics from the plate and cavity vent. This model includes the effects of both symmetric and antisymmetric modes. Second, a spatially-discrete model of the vented, cavity-backed plate, also including the effects of both symmetric and antisymmetric modes, was developed that includes a hybrid approach to modeling piezoceramic sensors and actuators. This approach allows the use of commercial FEM codes to analyze the structural part of the problem and uses those results along with modal superposition [79] to formulate a

reduced order state space model of the cavity-backed plate. The order is reduced with respect to that of the FEM solution. Finally, using the state space model, two feedback control approaches were developed with the control objective of matching the acoustic characteristics of a given structure to those of a target structure with desired acoustic properties, or acoustic replication. This involved the purposeful enhancement as well as suppression of various aspects of the structurally generated acoustics due to a transient excitation. The models and the control approach were also specialized for the commercial application of the acoustic guitar and for an aircraft cockpit. Experimental confirmation of the developed theory was shown in both applications.

1.4 Outline of Thesis

With an introduction to the underlying concepts of acoustic replication in smart structures using structural/acoustic control complete, the remainder of the thesis is composed of general problem development and specific applications. Chapter 2 contains the continuous and discrete model development of the vented, cavity-backed plate including the treatment of piezoceramic sensors and actuators in the discrete model. Chapter 3 contains two control approaches including a classic, frequency response-based method and a pole placement method using state feedback. Chapter 4 contains experimental and analytical results of acoustic replication applied to the acoustic guitar to favorably change structural/acoustic properties that influence quality. Chapter 5 contains the application of acoustic replication to an aircraft cockpit. An experimental study is conducted with the goal of reducing noise transmission, and an analytical study is conducted with the

goal of changing the acoustic signature. Finally, in Chapter 6, conclusions are drawn from all of the studies and recommendations are made relating to future studies in the area of acoustic replication in smart structures using structural/acoustic control. Also included are several appendices containing mathematical development and experimental details.

CHAPTER II

DEVELOPMENT OF ANALYTICAL MODELS

The analytical development of an elastic plate backed by a vented, rigid cavity is considered in this chapter. Lower frequency function of the system is modeled in a continuous and discrete formulation in Sections 2.1.1 and 2.2.1 respectively. The continuous formulation is appropriate to predict the passive behavior of the syventations of the problem where an exact, or approximate, continuous solution can be found. The discrete formulation has the potential to capture more geometric and material details of the passive problem since a finite element model is used in solving the structural part of the problem. It is also shown to be conducive to the incorporation of sensors and actuators. Additionally, a state space model is formulated in Section 2.2.2 to allow investigation of structural/acoustic control. Continuous and discrete forms of the Rayleigh integral are used to predict acoustic pressure as a result of plate movement in Sections 2.1.2 and 2.2.3.

2.1 Continuous Model of Low Frequency Plate/Cavity Function

2.1.1 Structural/Acoustic Equations

The acoustic cavity is rigid except for a flexible isotropic portion of the top plate. It is similar to a model for enclosed loudspeaker dynamics except that the loudspeaker piston is replaced by a flexible plate. The cavity is also assumed to have a vent that contains an entrained air mass that is driven by

the movement of the air in the cavity. Figure 2.1 illustrates the parts of the model. The differential equation for the plate making up the flexible part of the top plate is

$$D\nabla^4 w + c\dot{w} + \rho\ddot{w} = P_b - P_p + F_p\delta(r - r_0, \theta - \theta_0), \qquad (2.1)$$

where w is the out-of-plane plate displacement, D is the plate stiffness, ρ is the active mass of the plate per area, c is the equivalent viscous damping coefficient, P_b is the pressure behind the plate, P_p is the pressure in front of the plate, and F_p is a point force applied to the flexible plate at (r_0,θ_0) [81]. Assuming adiabatic conditions, small w, and cavity dimensions of less than $\frac{\lambda}{2}$ at the frequencies of interest where λ is the acoustic wavelength in air, P_b and the change in cavity volume ΔV can be written as

$$P_b = \frac{-\gamma P_0 \Delta V}{V}, \qquad (2.2)$$

$$\Delta V = \int_S w dS + S_h z, \qquad (2.3)$$

where γ is the specific heat ratio, P_0 is the ambient pressure, S is the domain of the circular plate representing the flexible plate, S_h is the area of the vent, V is the cavity volume, and z is displacement of the entrained air mass in the vent [48]. Neglecting mass loading, at low frequencies the pressure on an incremental area of front plate P_p can be written as

$$P_p = R_p\dot{w}, \qquad (2.4)$$

where R_p is a viscous resistance term for the plate motion due to the air adjacent to the top surface of the plate.

The equation for the air mass, from Borwick [80], is also used to model a vent in a loudspeaker enclosure and can be used when cavity dimensions are less than $\frac{\lambda}{2}$. It is derived by considering a force balance on the air mass. In particular,

$$M_h\ddot{z} + R_h\dot{z} = P_b S_h, \tag{2.5}$$

where z is the displacement of the air mass. In this case, the damping term R_h arises entirely from viscous resistance to the movement of the air mass from the air surrounding it. The actual mass of air, M_h, and damping term, R_h, are given by

$$M_h = \rho_0 S_h (t + \frac{16 r_h}{3\pi}), \quad R_h = \frac{\rho_0 S_h^{\,2} \omega^2}{2\pi a_0} \quad , \tag{2.6}$$

where ρ_0 is the ambient density, t is the plate thickness, r_h is the radius of the vent, and a_0 is the ambient speed of sound.

Combining Equations 2.1-2.4 gives Equation 2.7 and Equations 2.2, 2.3,2.5 and 2.6 give Equation 2.8

$$D\nabla^4 w + \rho\ddot{w} = \frac{-\gamma P_0}{V}(\int_S w ds + S_h z) - R_t\dot{w} + F_p\delta(r - r_0, \theta - \theta_0), \tag{2.7}$$

$$M_h\ddot{z} = \frac{-\gamma P_0}{V}(\int_S w ds + S_h z)S_h - R_h\dot{z}, \tag{2.8}$$

where $R_t = R_p + c$. To solve Equations 2.7 and 2.8, modal superposition is used. It is assumed the displacement of the plate can be represented as $w = \sum_{i=1}^{n} \eta_i \phi_i$, where $\eta_i = \eta_i(t)$ are the time-dependent modal coefficients and $\phi_i = \phi_i(x,y)$ are the spatially-dependent shape functions taken from the vibrations of a clamped isotropic circular plate. This method of solution is taken from Meirovitch [81] for the solution to an equation modeling a damped, continuous system. The solution is approximate when n is truncated to a finite number of modes.

Substituting the expression for w into Equation 2.7, multiplying by ϕ_j and integrating over the domain S gives a residual error which when set to zero and combined with orthogonality conditions

$$\int_S \phi_i \nabla^4 \phi_i dS = \int_S \phi_i \frac{\rho \omega_i^2}{D} \phi_i dS, \quad \int_S \nabla^4 \phi_i \phi_j dS = 0, \int_S \phi_i \phi_j dS = 0,$$

and the assumption that R_t can be modeled as proportional damping gives the n ordinary differential equations

$$\begin{aligned} &\int_S \phi_j^2 dS(\rho \omega_j^2 \eta_j + \rho \ddot{\eta}_j) = f(\sum_{i=1}^{n} \eta_i \int_S \phi_i dS \int_S \phi_j dS + \int_S \phi_j dS z S_h) - \\ &R_t \int_S \phi_j^2 dS \dot{\eta}_i + [F \phi_j]_{\substack{r=r_0 \\ \theta=\theta_0}} . \end{aligned} \tag{2.9}$$

Additionally, substituting the summation expression for w into Equation 2.8 gives

$$M_h \ddot{z} = f(\sum_{i=1}^{n} \eta_i \int_S \phi_i dS + S_h z) S_h - R_h \dot{z} , \tag{2.10}$$

$$f = \frac{-\gamma P_0}{V}. \qquad (2.11)$$

Equations 2.9 and 2.10 are solved for the case the case of n = 2 with

$$\phi_1 = I_0(b_{01})J_0(b_{01}r) - I_0(b_{01}r)J_0(b_{01}),$$
$$\phi_2 = (I_1(b_{11})J_1(b_{11}r) - I_1(b_{11}r)J_1(b_{11}))\mathrm{Cos}(\theta),$$

with $b_{01} = 1.015\pi$ and $b_{11} = 1.468\pi$ for a clamped circular plate [81]. This yields, in general, three coupled ordinary differential equations, but considering the antisymmetric nature of ϕ_2, the following equations result:

$$\int_S \phi_1^2 dS(\rho\ddot{\eta}_1 + R_1\dot{\eta}_1 + \rho\omega_1^2\eta_1) = f((\int_S \phi_1 dS)^2\eta_1 + \int_S \phi_1 dS z S_h) + [F\phi_1]_{\substack{r=r_0 \\ \theta=\theta_0}},$$
$$\int_S \phi_2^2 dS(\rho\ddot{\eta}_2 + R_2\dot{\eta}_2 + \rho\omega_2^2\eta_2) = [F\phi_2]_{\substack{r=r_0 \\ \theta=\theta_0}}, \qquad (2.11)$$
$$M_h\ddot{z} = f(\eta_1\int_S \phi_1 dS + S_h z)S_h - R_h\dot{z},$$

Solution of Equations 2.11 completely define the motion of the flexible plate in the model and the motion of the air mass. It is noteworthy that, due to the antisymmetry of ϕ_2, η_2 does not influence the motion of the air mass, z.

2.1.2 Continuous Model Acoustic Pressure Prediction

Given that the motion of the flexible plate is known as a function of frequency, an expression for acoustic pressure resulting from this pressure can be formulated under special circumstances. Following a well-known derivation in reference [82], the sound pressure on one side of an otherwise rigid wall of infinite expanse at a distance R from a point source in the wall is

$$p = j\omega\rho_0 \frac{q}{2\pi R} e^{-jkR}, \qquad (2.12)$$

where ρ_0 is ambient density, q is source strength defined as the velocity of the source times its area, and k is wavenumber in the acoustic medium. If a large number of point sources are located in the wall, a summation of their individual contributions provides the expression for total pressure at some observation point on one side of the wall

$$p = \frac{j\omega\rho_0}{2\pi} \sum \frac{q_i}{R_i} e^{-jkR_i}, \qquad (2.13)$$

where q_i and R_i are individual source strengths and distances from the observation point respectively. In the case of the flexible plate of the acoustic cavity, each elemental area dS has an out-of-plane velocity equal to $\dot{w}$ where w has been uniquely determined by solution of Equations 2.11. Each elementary area dS can be thought of as a point source embedded in the wall with strength $dq = \dot{w}(S,t)dS$. Using this relation and converting the summation in Equation 2.13 into an integral over the active area of the plate, the Rayleigh integral results

$$p_t = \frac{j\rho_o\omega}{2\pi} \int_S \frac{\dot{w}e^{-jkR}}{R} dS, \qquad (2.14)$$

where p_t is the total pressure at the observation point due to the movement of the flexible plate and R is the distance from the elemental area dS to the observation point as shown in Figure 2.2. It is important to remember that the

active area of the plate must be surrounded by an infinite rigid wall or baffle for this integral to be valid.

The expression for R which is valid in the nearfield is given by

$$R = ((x_1 - x_0)^2 + (y_1 - y_0)^2 + (z_1)^2)^{\frac{1}{2}},$$

where the coordinates with subscript 0 mark the midpoint of dS and those with subscript 1 mark the observation point. It was necessary to formulate the expression to be valid in the nearfield since at the acoustic frequencies of interest, nearfield radiation is significant.

The acoustic pressure at the observation due to the air mass movement in the vent was computed as a simple equivalent source

$$p_h = j\omega\rho_o \frac{S_h \dot{z} e^{-jkr_h}}{2\pi r_h},$$

where r_h is the distance from the center of the vent to the observation point. SPL is then determined for a given observation point and frequency, ω, by treating p_l and p_h as same frequency sources [1]

$$\overline{p_T^2} = \overline{p_l^2} + \overline{p_h^2} + 2\overline{(p_l p_h)}\ , \quad SPL = 10Log\left[\frac{\overline{p_T^2}}{p_{ref}^2}\right], \qquad (2.15)$$

The solution of Equations 2.11 and 2.15 give the SPL at any point in the acoustic field in front of the baffled acoustic cavity for a given force input level at a given frequency.

2.2 Discrete Model of Low Frequency Plate/Cavity Function

A discrete model of the system was sought to open the problem up to more complicated substructures and boundary conditions where an exact or approximate continuous solution does not necessarily exist. One such complication considered was the addition of piezoceramic sensors and actuators into the problem. These make the stiffness of the plate discontinuous. Other potential complications include varying plate shapes, end conditions, and anisotropy. The discrete formulation allowed the use of powerful finite element modeling to solve the homogeneous plate problem and get eigenvalues and eigenvectors to uncouple the complete system problem.

2.2.1 Structural/Piezoelectric/Cavity Equations

The discrete model is made up of three distinct phases. A cross section showing this is shown in Figure 2.3. The sensors and actuators are piezoceramic materials which are piezoelectric materials. The substructure is made of a structural material, a special case of the piezoelectric material with no electrical properties. The acoustic cavity consists of an air spring and an entrained air mass. This model of the acoustic cavity is only valid under the previously stated restrictions on the cavity dimensions. The complete energy for the acoustic cavity includes kinetic energy (T), potential energy (U), and electrical energy (W_e), respectively. In particular,

$$
\begin{aligned}
T &= \int_{V_P} \tfrac{1}{2}\rho_P \dot{\mathbf{w}}^T \dot{\mathbf{w}} dV_P + \int_{V_S} \tfrac{1}{2}\rho_S \dot{\mathbf{w}}^T \dot{\mathbf{w}} dV_S + \frac{1}{2} m_h \dot{z}^2, \\
U &= \int_{V_P} \tfrac{1}{2}\mathbf{S}^T \mathbf{T} dV_P + \int_{V_S} \tfrac{1}{2}\mathbf{S}^T \mathbf{T} dV_S + \frac{1}{2}\beta(\Delta V)^2, \qquad (2.16) \\
W_e &= \int_{V_P} \tfrac{1}{2}\mathbf{E}^T \mathbf{D} dV_P,
\end{aligned}
$$

where $\dot{\mathbf{w}}$ is a vector of velocities of the piezoceramic and structural materials, $\dot{z}$ is the velocity of the air mass, ρ_p and ρ_s are the volume densities of the piezoelectric and structural materials, **S** and **T** are material strain and stress vectors, **E** is the vector of the electric field, **D** is the vector of electrical displacements, β is an effective spring constant for the air spring, and ΔV is the change in volume of the air cavity due to displacement of the plate and the air mass.

In Appendix A, a generalized form of Hamilton's principle is used with the energy expressions to derive finite elements for the piezoelectric, substructure, and air spring portions of the acoustic cavity. On assembling the elements, the details of which are also in Appendix A, we get the global equations of the complete system as

$$\begin{aligned}
&[\mathbf{m}_p + \mathbf{m}_s]\ddot{\mathbf{w}} + [\mathbf{k}_s + \mathbf{k}_{uu}]\mathbf{w} = -\Theta_A \mathbf{v}_A + \beta \mathbf{m}(\mathbf{m}^T\mathbf{w} + S_h z), \\
&\mathbf{m}_h \ddot{z} + \beta S_h{}^2 z = -\beta S_h \mathbf{w}^T \mathbf{m}, \qquad (2.17) \\
&\mathbf{v}_S = \frac{\Theta_S{}^T \mathbf{w}}{C_S},
\end{aligned}$$

To find a solution for Equations 2.17, the left hand side of the first equation is set to zero so that

$$[\mathbf{m}_p + \mathbf{m}_s]\ddot{\mathbf{w}} + [\mathbf{k}_s + \mathbf{k}_{uu}]\mathbf{w} = \mathbf{0}. \qquad (2.18)$$

This equation considers only the structural properties, the stiffness and the mass, of the substructure and the piezoceramic sensors and actuators. Presuming the material properties are available, a finite element model can

be constructed to get the eigenvalues and eigenvectors of the problem, $\phi_1,\phi_2,\phi_3,...\phi_n$ and $\omega_1,\omega_2,\omega_3,...\omega_n$. In a completely analogous fashion to the continuous model, a series solution to the problem is assumed, $\mathbf{w} = \Phi\eta$, where Φ is an m x n matrix in which the n columns are eigenvectors which are of dimension m which is the number of nodal degrees of freedom in the finite element model. Substituting the assumed solution into the first of Equations 2.17 gives

$$\mathbf{M}\Phi\ddot{\eta} + \mathbf{K}\Phi\eta = -\Theta_A\mathbf{v}_A + \beta\mathbf{m}(\mathbf{m}^T\Phi\eta + S_h z), \qquad (2.19)$$

where $\mathbf{M} = \mathbf{m_p}+\mathbf{m_s}$ and $\mathbf{K} = \mathbf{k_p}+\mathbf{k_s}$. Multiplying Equation 2.19 by Φ^T gives

$$\Phi^T\mathbf{M}\Phi\ddot{\eta} + \Phi^T\mathbf{K}\Phi\eta = -\Phi^T\Theta_A\mathbf{v}_A + \Phi^T\beta\mathbf{m}(\mathbf{m}^T\Phi\eta + S_h z), \quad (2.20)$$

and assuming the eigenvectors were mass orthonormalized gives

$$\mathbf{I}\ddot{\eta} + \omega^2\eta = -\Phi^T\Theta_A\mathbf{v}_A + \mathbf{S}\eta + \mathbf{W}z, \qquad (2.21)$$

where $\mathbf{S} = \Phi^T\beta\mathbf{m}\mathbf{m}^T\Phi$, $\mathbf{W} = \Phi^T\beta\mathbf{m}S_h$, I is an n x n identity matrix, and ω^2 is an n x n diagonal matrix of squared eigenvalues from the homogeneous problem. Analogous to Equation 2.9 in the continuous case, Equation 2.21 represents, in general, n coupled equations.

2.2.2 State Space Formulation

Also analogous to the continuous model, under special circumstances, Equations 2.21 reduce in complexity significantly. Considering again the case of the first two plate modes as an approximate

solution and considering one actuator and proportional damping gives two coupled equations

$$\begin{aligned}\ddot{\eta}_1 + \xi_1\omega_1\dot{\eta}_1 + \omega_1^2\eta_1 &= \Theta_1 v_A + S_{11}\eta_1 + S_{12}\eta_2 + W_1 z,\\ \ddot{\eta}_2 + \xi_2\omega_2\dot{\eta}_2 + \omega_2^2\eta_2 &= \Theta_2 v_A + S_{21}\eta_1 + S_{22}\eta_2 + W_2 z,\end{aligned} \tag{2.22}$$

where $\Theta_1 = \Phi_1^T\Theta_A$, $\Theta_1 = \Phi_2^T\Theta_A$, $\xi = 2\zeta$ and ζ is the damping ratio. Additionally, the second of Equations 2.17 with an added proportional damping coefficient C_h gives a third coupled equation

$$\ddot{z} + \frac{C_h}{m_h}\dot{z} - \frac{\beta S_h^2}{m_h} z = -\frac{\beta S_h}{m_h}\eta^T\mathbf{Y} = \frac{Y_1}{m_h}\eta_1 + \frac{Y_2}{m_h}\eta_2,$$

where $\mathbf{Y} = \Phi^T\mathbf{m}$. If the second plate mode can be assumed to be symmetric, the following set of three equations result

$$\begin{aligned}\ddot{\eta}_1 + \xi_1\omega_1\dot{\eta}_1 + \omega_1^2\eta_1 &= \Theta_1 v_A + S_{11}\eta_1 + W_1 z,\\ \ddot{\eta}_2 + \xi_2\omega_2\dot{\eta}_2 + \omega_2^2\eta_2 &= \Theta_2 v_A,\\ \ddot{z} + \gamma_h\dot{z} - \frac{\beta S_h^2}{m_h} z &= \frac{Y_1}{m_h}\eta_1,\end{aligned} \tag{2.23}$$

where $\gamma_h = \frac{C_h}{m_h}$. Here, as in the continuous case, the second plate mode is not coupled to the air mode or the first plate mode.

A state space model may be formulated for Equations 2.23 to simplify solution of the problem and to simplify the investigation of active control. The state variables are defined as

$$\mathbf{x} = \begin{Bmatrix} \eta_1 \\ \eta_2 \\ z \\ \dot{\eta}_1 \\ \dot{\eta}_2 \\ \dot{z} \end{Bmatrix},$$

Equations 2.23 then take the form

$$\dot{\mathbf{x}} = \mathbf{A}\mathbf{x} + \mathbf{B}\mathbf{V}_A \tag{2.24}$$

where

$$\mathbf{A} = \begin{bmatrix} 0 & 0 & 0 & 1 & 0 & 0 \\ 0 & 0 & 0 & 0 & 1 & 0 \\ 0 & 0 & 0 & 0 & 0 & 1 \\ S_{11} - \omega_1^2 & 0 & W_1 & -\xi_1\omega_1 & 0 & 0 \\ 0 & -\omega_2^2 & 0 & 0 & -\xi_2\omega_2 & 0 \\ \dfrac{V_1}{m_h} & 0 & \dfrac{-S_h^2\beta}{m_h} & 0 & 0 & -\gamma_h \end{bmatrix}, \quad \mathbf{B} = \begin{Bmatrix} 0 \\ 0 \\ 0 \\ \Theta_1 \\ \Theta_2 \\ 0 \end{Bmatrix}$$

The third of Equations 2.17 is used to get the output matrix of the state space model. Assuming only one sensor, the equation gives

$$v_S = \frac{\Theta_S^T \Phi \eta}{C_S}.$$

Assuming the two term series solution leads to $v_S = \mathbf{C}\mathbf{x}$, where

$$\mathbf{C} = \left\{ \frac{\Theta_S{}^T \Phi_1}{C_S} \quad \frac{\Theta_S{}^T \Phi_2}{C_S} \quad 0 \quad 0 \quad 0 \quad 0 \right\}.$$

2.2.3 Comparison of Actuator Models

The treatment of the piezoceramics can be compared to another model of a segmented piezoceramic actuator for structural control formulated by Dimitriadis, Fuller, and Rogers [36]. This model seems to be the most widely used in other references including [47, 48, 50, 53, and 64]; however, no direct experimental verification of the model could be found. In this approach, an analytical expression is derived for the excitation of an isotropic rectangular plate by surface mounted, rectangular piezoceramic actuators. These actuators are mounted symmetrically about the neutral axis and are electrically 180 degrees out of phase to produce bending moments in the plate. The output of the model is the displacement of the plate due to a time varying input voltage into the piezoceramic actuator. In order to compare the models, magnitudes of the transfer functions between piezoceramic actuators and the displacement at a point on a clamped rectangular plate are shown in Figures 2.4 and 2.5. The plates used to generate these figures are identical except that the plate in the first figure has a relatively high modulus, 100 GPa, which is around one half the modulus of steel, and the plate in the second figure has a relatively low modulus, 0.69 GPa, which is the modulus of sitka spruce in its lowest modulus direction. A damping ratio of 3% was assumed for both modes in both models to give a good comparison representative of a lightly damped structure. These figures illustrate that the agreement between the models is reasonable for the high modulus plate, but it was unacceptable for the low modulus plate. Details of this comparison are

given in Appendix B. In order to study this trend in more detail, a series of numerical tests were performed where the amplitude of the first mode coefficients were compared for plates of varying modulus and the same thickness as the original test. The results, shown in Figure 2.6, establish a trend of increasing error with decreasing plate modulus.

It is believed that the reason for the error between the two models lies in a violation of one or both of the linked assumptions made, in the model by Dimitriadis, Fuller, and Rogers, that the piezoceramic actuators create a spherical surface of curvature and that the solution obtained for an infinite piezoceramic applies to a segmented piezoceramic. In a relatively low modulus plate, the relatively high modulus piezoceramic would represent a marked discontinuity making these assumptions seem unreasonable. Since these assumptions were not necessary in the discrete model, it is probably more accurate. The discrete approach is also much more general since it is applicable to any substructure which can be modeled using a finite element code. This is in contrast to the Dimitriadis, Fuller, and Rogers approach which is limited to cases where an exact or approximate solution exists. Complications such as mixed boundary conditions, stiffeners and plate anisotropy might preclude this approach altogether but would require no changes in the approach to the discrete model.

2.2.4 Discrete Model Acoustic Pressure Prediction

To get the resulting pressure from the movement of the baffled plate in response to a voltage input into the actuators, we start by considering the expression for pressure as a result of a piston baffled by a wall

$$p = -\frac{\rho_0}{2\pi}\frac{\ddot{w}S}{R}e^{-jkR}, \qquad (2.25)$$

where $\ddot{w}$ is the acceleration of the piston and R is the distance from the middle of the piston to the observation point. This equation is valid if the dimensions of the piston do not exceed $\frac{\lambda}{4}$ of the sound being considered [83].

If the displacement of the piston is known as a function of an input voltage which is driving the piston, it may be expressed as a transfer function

$$H_w(s) = \frac{W(s)}{V(s)},$$

where W(s) is the Laplace transform of the displacement and V(s) is the Laplace transform of the voltage. H_w is easily related to the acceleration transfer function H_a by

$$H_a(s) = s^2 H_w(s), \qquad (2.26)$$

Setting s=jw and substituting $k = \frac{\omega}{a_0}$, a transfer function relating pressure to input voltage into the piston can then also be defined using Equation 2.25 as

$$H_p(\omega) = -\frac{\rho_0 S}{2\pi R} e^{-j\frac{\omega R}{a_0}} H_a(\omega).$$

For a collection of k adjacent pistons whose motion is all controlled by the same input voltage, the overall transfer function can then be defined as

$$H_p(\omega) = -\frac{\rho_0}{2\pi}\sum_{i=1}^{k}\frac{S_i e^{-j\frac{\omega R_i}{a_0}}}{R_i}H_a^i(\omega), \qquad (2.27)$$

where H_a^i is the transfer function for each piston with respect to the input voltage.

This analogy can be directly applied to the discrete model of the acoustic cavity. The transfer function relating the averaged displacement of the plate and the air mass to the input voltage is readily available from the state space model. To obtain the plate transfer functions, the averaged out-of-plane displacements for each mode can be found using a modified output matrix

$$\bar{\mathbf{C}}_i = \left\{\overline{\Phi_1} \quad \overline{\Phi_2} \quad 0 \quad 0 \quad 0 \quad 0\right\},$$

where $\overline{\Phi_1}$ and $\overline{\Phi_2}$ are averaged out of plane displacements over a selected area of the discretized plates which meets the criteria that it's largest length is less than one quarter wavelength of the sound being considered. The transfer function of averaged out-of-plane displacement is then defined as

$$H_w(s) = \mathbf{C}(s\mathbf{I} - \mathbf{A})^{-1}\mathbf{B}, \qquad (2.28)$$

where the **A** and **B** matrices are the same as in Equation 2.24. The air mass can be treated as an additional piston and its displacement transfer function can be obtained using

$$\mathbf{C}_h = \{0 \quad 0 \quad 1 \quad 0 \quad 0 \quad 0\}.$$

The sum of the contributions of the plate and the air mass give the overall pressure transfer function.

2.3 Analytical Model Summary

A spatially continuous structural/acoustic model of a clamped, circular plate backed by a rigid, vented cavity was developed. A Rayleigh integral was used to predict acoustic pressure resulting from both symmetric and antisymmetric plate modes. Pressure resulting from the movement of air in and out of the vent was also included in the model. A spatially discrete structural/acoustic model of a clamped, rectangular plate backed by a rigid, vented cavity was also developed. The discrete approach allows solution of complicated problems such as anisotropic plates and plates with varying end conditions using FEM. This approach was also shown to be well suited to the incorporation of piezoceramic sensors and actuators into the model. The piezoceramic modeling approach was compared to a spatially continuous formulation and found to agree well when the plate substructure had a relatively high modulus. The spatially continuous model underpredicted the actuator effectiveness as compared to the discrete model, when the plate was relatively soft. A discretized form of the Rayleigh integral was used to derive a transfer function between the voltage applied to a piezoceramic actuator mounted on the plate and the resulting acoustic pressure due to movement of the structure and air in the vent. This result, along with modal superposition, yielded a state space model of low enough order to be suitable for control design.

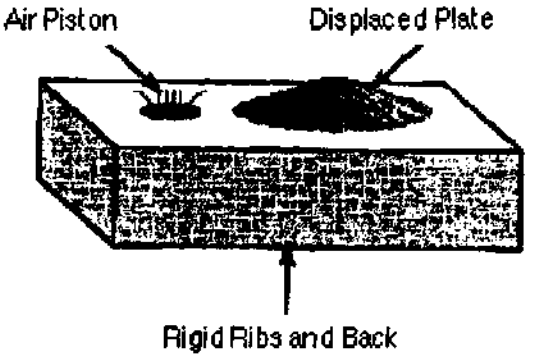

Figure 2.1- Acoustic cavity model

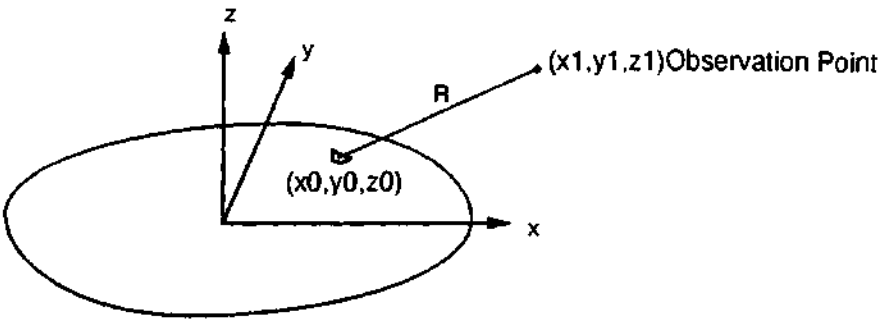

Figure 2.2 - Relation of observation point to flexible plate

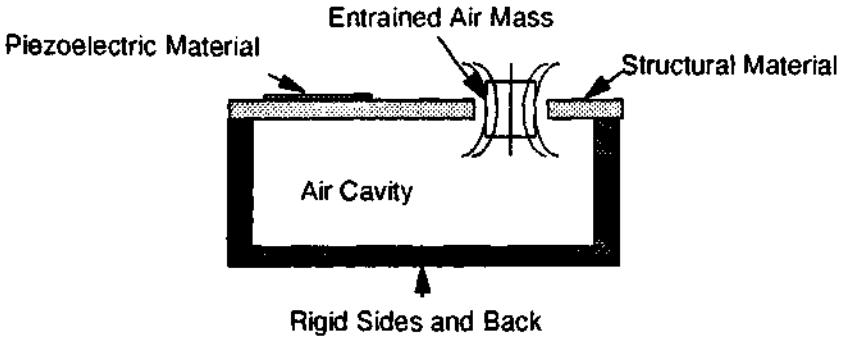

Figure 2.3 - Model of acoustic cavity for energy formulation

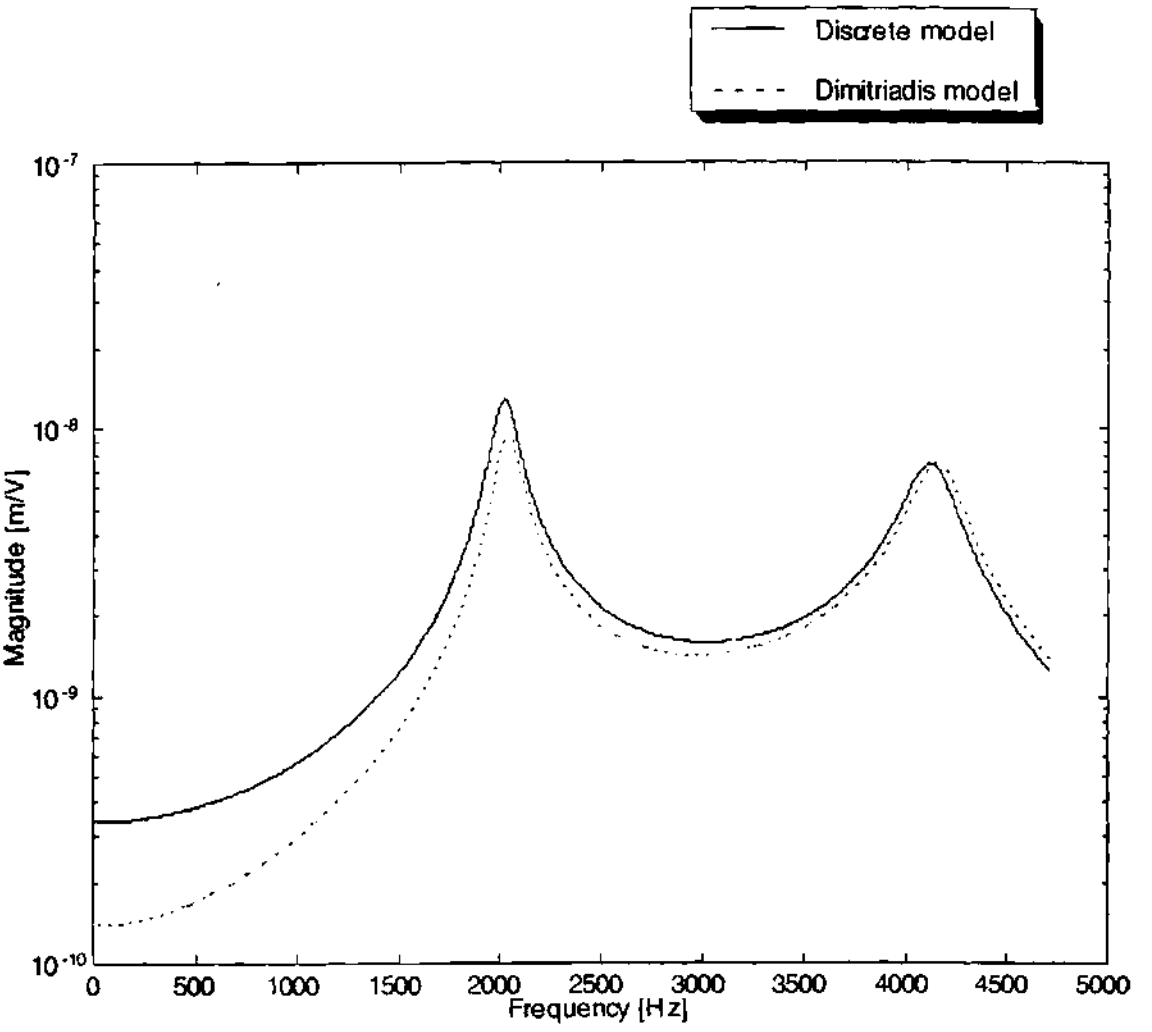

Figure 2.4 - Comparison of transfer functions for high plate modulus

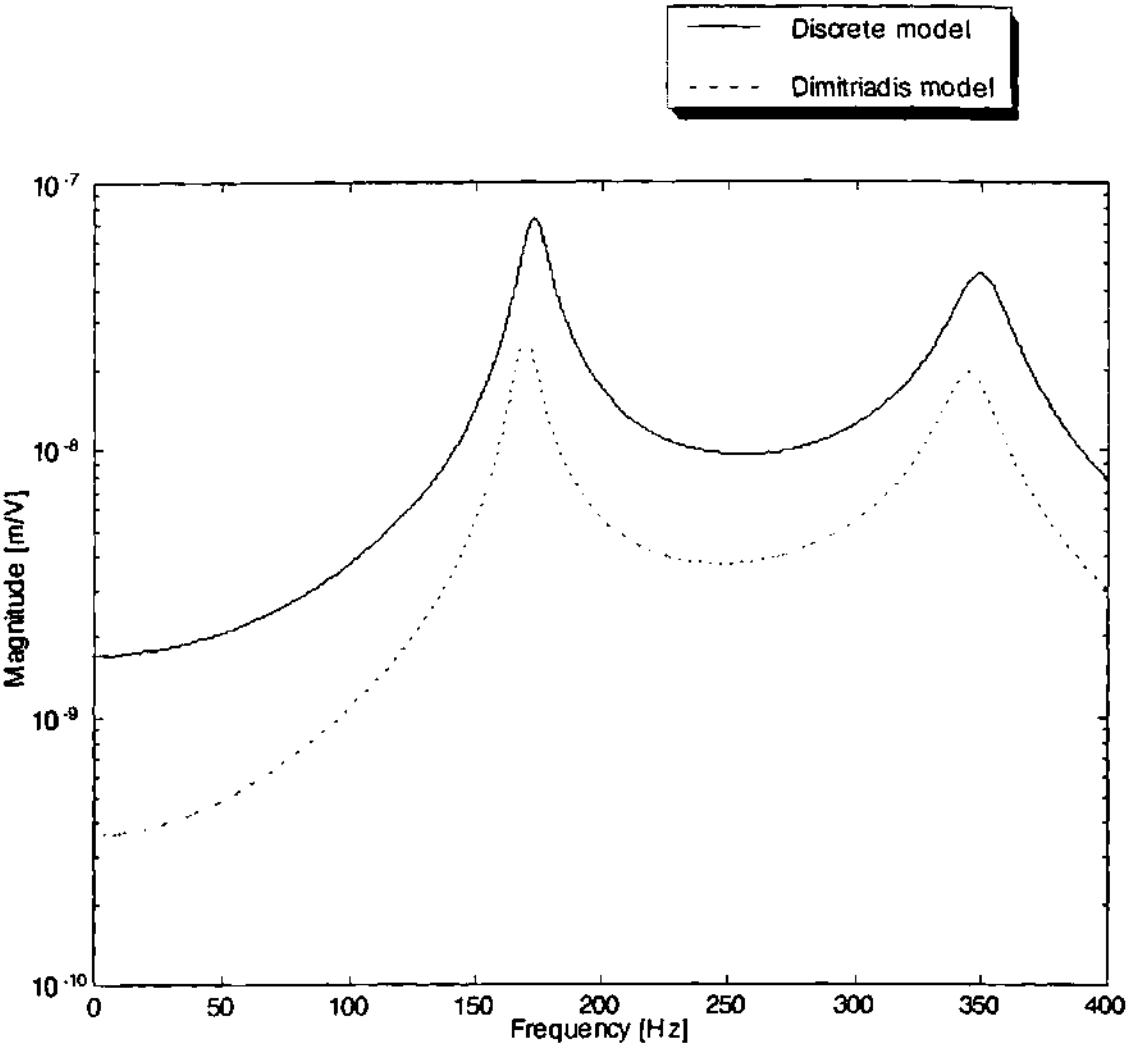

Figure 2.5 - Comparison of transfer functions for low plate modulus

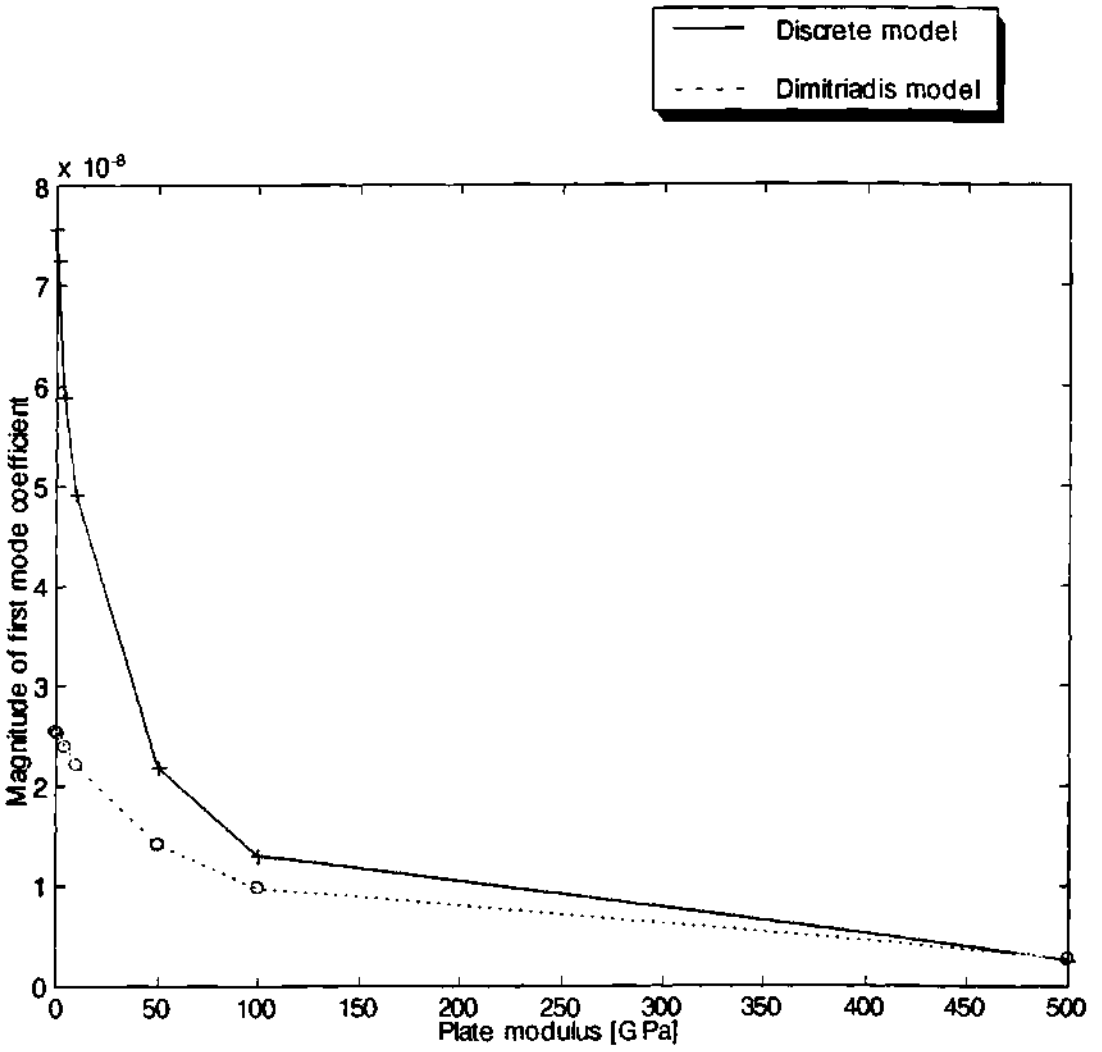

Figure 2.6 - Comparison of first mode coefficients for varying plate modulus

CHAPTER III

CONTROL APPROACHES

The next topic considered is how to force the acoustic response of a system to behave in a desired manner. Using the sensors and actuators incorporated in Chapter 2, active control can be used to modify the system's acoustic response. Section 3.1 looks at control objectives and how to achieve them. The related topic of sensor and actuator placement is covered in Section 3.2. Both pole placement using state feedback control and classical frequency response-based methods are investigated in Section 3.3 and Section 3.4. A relationship is established between a target acoustic plant and a target structural plant using transfer functions in Section 3.5.

3.1 Control Objectives

The objective of active control, in this study, will be to modify the system's structural dynamics so that its acoustic response matches that of a target system that displays a desired acoustic response. This concept will be called acoustic replication. The idea has been developed somewhat for steady state disturbances using model-based feedforward control by Clark and Fuller [50]. In this instance, a desirable acoustic response was silence. The present study differs in two important ways. First, the disturbance to the

system is a transient excitation. Second, the desired acoustic response has suppressed as well as enhanced acoustic amplitude.

In the most general case of acoustic control using smart structures or other direct structural actuation, the controller formulated for a vibration objective usually does not match a controller formulated for an acoustic noise objective. This is because at a given frequency, the structural vibration displacement is made up of a combination of many structural modes and a vibration controller typically is formulated with the goal of changing the magnitude of the overall displacement. The acoustic pressure resulting from the vibration depends on both the magnitude and the relative phase of the modal components making up the overall displacement, so an acoustic controller might change both magnitude and relative phase, or just magnitude or just relative phase. Considering the example of suppression of farfield radiated sound from a vibrating structure, the feedforward controller formulated to minimize acoustic radiation off resonance tends to adjust the relative phase of the structural modal components making up the vibration, without necessarily changing their amplitude, so that the sound is not radiated into the farfield. The structure becomes a less efficient far field sound radiator when an appropriate control is implemented. This process has been coined modal restructuring [37]. This is in contrast to a vibration controller, which would typically be formulated to reduce the amplitude of the vibration.

For the special case of modification of the damping, frequency, and the related amplitude of a specific structural/acoustic mode, or several structural/acoustic modes, the vibration control objective may be directly related to the acoustic control objective. Pressure prediction methods

developed in Chapter 2 can then be used to verify the effects in the acoustic field. This direct relationship is evident on reexamination of Equations 2.43, 2.44 and 2.45

$$H_w(s) = \mathbf{C}(s\mathbf{I} - \mathbf{A})^{-1}\mathbf{B}, \tag{2.45}$$

$$H_a(s) = (s)^2 H_w(s), \tag{2.43}$$

$$H_p(\omega) = -\frac{\rho_0}{2\pi}\sum_{i=1}^{k}\frac{S_i e^{-j\frac{\omega R_i}{a_0}}}{R_i}H_a^i(\omega). \tag{2.44}$$

Examining the pressure transfer function in Equation 2.44, we can define a structural/acoustic mode as a local maximum in the pressure transfer function corresponding to the structural mode. The relationship between the maxima in the structural transfer functions and the maxima in the pressure transfer function are determined by the numerators of Equation 2.44. A maximum of the structural transfer function may go completely unnoticed in the acoustic field dependent on the position of the microphone and the radiation efficiency of the structural mode corresponding to the maximum. Radiation efficiency is usually defined in terms of far-field radiation since, at relatively high frequencies, the near field is limited to a space very close to the source and the observer is located in the far field. At relatively low frequencies, however, it is conceivable that the observer may be located at a point where near-field acoustics are significant. In relation to this work, it is important to note that the radiation efficiency of a structural mode, when excited at the

corresponding resonant frequency, is determined by the mode shape, which determines the numerators of Equation 2.44.

It is evident that damping and frequency of a given structural mode are reflected in the structural transfer function by the determinant of $(s\mathbf{I} - \mathbf{A})$. This gives the denominator of the structural transfer functions. This is also shown by Equations 2.43 and 2.44, with $s = j\omega$, to be the denominator of the pressure transfer function which determines the damping and frequency of the acoustic/structural mode. For instance, decreasing the damping of a structural mode will result in decreased damping in the corresponding structural/acoustic mode. If the control does not change the corresponding mode shape of the structure, the only parts of Equation 2.44 that would change are the denominators of $H_a^i(\omega)$ which are common. This will also result in an increase in the magnitude of the structural/acoustic mode due to the decreased damping.

In this research, all control objectives can be broken down into changes in damping and frequency of structural/acoustic modes which force the controlled system to match the desired acoustic response. This makes it possible to use feedback control approaches that have been developed extensively for active vibration control to directly modify the dynamics of the structure. Since the control objective is to tailor the frequency response, as opposed to attenuate, most optimal control methods do not apply. This is because optimal control performance criteria are usually directed at minimizing vibration. Only three references could be found which investigated smart structure actuation in conjunction with feedback control to suppress a transient response [46, 53, 56]. No references could be found that used active control to tailor a frequency response including suppression as

well as enhancement of structural/acoustic modes. For this objective, pole placement using state feedback and one classical frequency response-based control filter are investigated.

3.2 Sensor and Actuator Placement

Before exploring specific control methods, it is important to consider sensor and actuator location issues. We start with the general equation for the system with one sensor and one actuator given by

$$L[\mathbf{w}(x,y,z)] = L_A[v_A],$$

where L is the differential operator which determines the homogeneous equation of motion, $\mathbf{w}(x,y,z)$, for the distributed parameter system and L_A couples the voltage, v_A, applied to the piezoceramic actuator to the motion in the distributed parameter system. The operator L_A depends on location as well as other structural properties of the system. We also have the general equation for the voltage generated in the sensor as

$$v_S = L_S[\mathbf{w}(x,y,z)].$$

Here, L_S couples the motion of the system to the voltage generated in the sensor, v_S, and also depends on location as well as other structural properties of the system.

Given a location for both the sensor and actuator, we can characterize the system by its transfer function between the sensor and actuator. For the discrete model derived in Chapter 2, this transfer function is defined by

Equation 2.45 where **C** is a vector realization of L_S and **B** is a vector realization of L_A. If we revisit the definitions of the elements of **C** and **B** we see that

$$C_i = \frac{\Theta_S{}^T \Phi_i}{C_S}, \quad B_i = \Phi_i{}^T \Theta_A. \tag{3.1}$$

In both cases, the quantities are proportional to the summation of the products of the forces generated at the nodes of the piezoceramic material, represented by Θ_S in the sensor and Θ_A in the actuator, and the modal displacements at the same nodal degrees of freedom. The forces are completely dependent on the properties of the piezoceramic material whereas the contribution due to the modal displacements depends on where the piezoceramic is located in the system. If the sensor or actuator is placed in a bad position with respect to a given mode shape, that mode might be completely unobservable or uncontrollable. For example, this is the case when a piezoceramic is placed symmetrically about a nodal line in an antisymmetric mode shape [36]. On the other hand, there are optimum locations of sensors and actuators where the components of **B** and **C** are maximized. Large quantities of **B** and **C** reduce the need for voltage gain in both the actuator and sensor for a given control objective.

In the analytical plate problem, we can use the results of Dimitriadis, Fuller, and Rogers [36] as a guide for placement of actuators. Looking again at Equation B.3 given by

$$\int \phi_i^2 dA(\ddot{\eta}_i - \omega_i^2 \eta_i) =$$

$$\frac{C_0 \varepsilon_{pe}}{\rho}\left[\int_{y_1}^{y_2}\left(\frac{\partial \phi_i}{\partial x}_{|x=x_1} - \frac{\partial \phi_i}{\partial x}_{|x=x_2}\right)dy + \int_{x_1}^{x_2}\left(\frac{\partial \phi_i}{\partial y}_{|y=y_1} - \frac{\partial \phi_i}{\partial y}_{|y=y_2}\right)dx\right].$$

The corresponding state space model with 2n states is

$$\dot{\mathbf{x}} = \mathbf{A}\mathbf{x} + \mathbf{B}v_A$$

where

$$\mathbf{A} = \begin{bmatrix} \mathbf{0} & \mathbf{I} \\ \omega^2 & \mathbf{0} \end{bmatrix}, \quad \mathbf{B} = \frac{C_0 d_{31}}{t\rho}\begin{Bmatrix} 0 \\ \vdots \\ 0 \\ T_1 \\ T_2 \\ \vdots \\ T_n \end{Bmatrix}.$$

In this case, **0** is an n x n matrix of zeros **I** is an n x n identity matrix ω^2 is the n x n diagonal matrix of modal resonant frequencies. Furthermore,

$$\mathbf{x} = \begin{Bmatrix} \eta_1 \\ \eta_2 \\ \cdot \\ \cdot \\ \eta_n \\ \dot{\eta}_1 \\ \dot{\eta}_2 \\ \cdot \\ \cdot \\ \dot{\eta}_n \end{Bmatrix}, \quad T_i = \frac{\int_{y_1}^{y_2} \left(\frac{\partial \phi_i}{\partial x}_{|x=x_1} - \frac{\partial \phi_i}{\partial x}_{|x=x_2} \right) dy + \int_{x_1}^{x_2} \left(\frac{\partial \phi_i}{\partial y}_{|y=y_1} - \frac{\partial \phi_i}{\partial y}_{|y=y_2} \right) dx}{\int_A \phi_i^2 dA}.$$

It is evident that the factor $\frac{C_0 d_{31}}{t\rho}$ is dependent on piezoceramic electrical properties, relative thicknesses and elastic moduli of both the piezoceramic and the structure. Once the plate and the actuator are selected, these are fixed. The coefficients T_i, however, represent the difference of slopes of each mode shape measured at opposing sides of the piezoceramic actuator. This quantity is maximum when the related curvature is at a maximum. Comparison of a sum of the x and y curvature associated with each mode shape will give local maximums for a square actuator. Other summations can be derived based on the intended shape and orientation of the actuator. A good location for an actuator to control several modes of a plate would be a location where there is an overlap of regions of high curvature for each mode.

In an experimental implementation of the control problem, it may not be possible to model the structure to a level that would provide satisfactory locations for sensors and actuators. An innovative way to find potentially good locations is to do a modal survey that evaluates potential locations directly. This can be done by first finding an out-of-plane location that has high modal contributions from the modes to be controlled by doing a

traditional modal survey using out-of-plane sensors and actuators. This will be the position where an out-of-plane actuator such as a shaker or an impulse hammer will be applied. Structural response with respect to a force input, at this location, can then be measured at candidate sensor and actuator locations on the structure by measuring a transfer function between a piezoceramic sensor that has the same size and properties as the piezoceramic actuator that will be used to control the structure and the out-of-plane actuator. The transfer functions measured at several locations on the structure can then be compared with respect to magnitude at the frequencies corresponding to the modes to be controlled. Those transfer functions corresponding to an optimal location will have the highest response at the modal frequencies of interest. This, in turn, corresponds to high values in the **C** matrix. Optimal locations for the sensor used in this modal survey will also be optimal locations for the actuators. This results from the reciprocity of the structural problem since good sensor positions at measuring out-of-plane motion will also be good actuator positions at creating out-of-plane motion. This reciprocity is especially evident on examining Equation 3.1. At a given location, if the sensor is the same size as the actuator, $\Theta_S = \Theta_A$ and the individual elements of **B** are directly proportional to the individual elements of **C** at a given location.

3.3 State Variable Control Using Pole Placement

Once optimal sensor and actuator positions have been selected and using the state space model developed in Chapter 2, the method of control design known as pole placement can be implemented. Since the state variables are not directly available as output in the model, it is necessary to

construct an observer which has an estimate of the state variables as its output. The state variables are then multiplied by a control gain matrix, **K**, and fed back to the original plant along with an additional disturbance signal **Fv**. A schematic of the state space control process is shown in Figure 3.1. It has been shown [84] that for a plant that is controllable, it is possible to construct a control signal that moves the open loop plant's poles to a desired stable location when the control loop is closed.

The equations which are represented by Figure 3.1 are

$$\begin{aligned} \dot{\mathbf{x}} &= \mathbf{Ax} + \mathbf{Bu}, \\ \mathbf{y} &= \mathbf{Cx}, \end{aligned} \tag{3.2}$$

$$\dot{\hat{\mathbf{x}}} = \mathbf{A_c}\hat{\mathbf{x}} + \mathbf{Ly} + \mathbf{Bu}, \tag{3.3}$$

$$\mathbf{u} = \mathbf{Fv} - \mathbf{K}\hat{\mathbf{x}}, \tag{3.4}$$

where Equations 3.2 are the original state space model equations, Equation 3.3 is the observer equation and Equation 3.4 is the feedback equation and $\mathbf{A_c} = \mathbf{A}\text{-}\mathbf{LC}$. These can be combined as in reference [85] to form the closed-loop system

$$\begin{Bmatrix} \dot{\mathbf{x}} \\ \dot{\hat{\mathbf{x}}} \end{Bmatrix} = \begin{bmatrix} \mathbf{A} & -\mathbf{BK} \\ \mathbf{LC} & \mathbf{A_c} - \mathbf{BK} \end{bmatrix} \begin{Bmatrix} \mathbf{x} \\ \hat{\mathbf{x}} \end{Bmatrix} + \begin{bmatrix} \mathbf{BF} \\ \mathbf{BF} \end{bmatrix} \mathbf{v}, \tag{3.5}$$

which has closed loop eigenvalues given by the roots of the equation

$$\begin{vmatrix} \mathbf{I}\lambda - \mathbf{A} & \mathbf{BK} \\ -\mathbf{LC} & \mathbf{I}\lambda - \mathbf{A_c} + \mathbf{BK} \end{vmatrix} = 0.$$

This can be rearranged to give the equation

$$\begin{vmatrix} \mathbf{I}\lambda - \mathbf{A} + \mathbf{BK} & \mathbf{BK} \\ \mathbf{0} & \mathbf{I}\lambda - \mathbf{A_c} \end{vmatrix} = 0, \tag{3.6}$$

which, in turn, gives the equation

$$|\mathbf{I}\lambda - \mathbf{A} + \mathbf{BK}| \bullet |\mathbf{I}\lambda - \mathbf{A_c}| = 0. \tag{3.7}$$

Equations 3.5-3.7 illustrate the separation principle. The state space control pole placement problems can be divided into two separate problems. The selection of **L** determines the position of the n eigenvalues of the observer. If the original system is detectable, it is always possible to find an **L** which gives the desired eigenvalues of $\mathbf{A_c}$. Equation 3.7 illustrates that the n eigenvalues of the closed loop plant can then be specified separately. Stability is guaranteed if the observer poles and the closed loop plant poles are stable. Recognizing this, an observer can be designed which gives an estimate of the states, and a controller can then be designed as if all the states were measured [85].

Proceeding with the control problem, the poles of the closed loop transfer function are given by the roots of the equation

$$|\mathbf{I}\lambda - \mathbf{A} + \mathbf{BK}| = 0, \tag{3.8}$$

which has n variables k_1, k_2...k_n. The left hand side of Equation 3.8 can be set equal to

$$(\lambda - s_1)(\lambda - s_2)...(\lambda - s_n), \qquad (3.9)$$

where $s_1, s_2 ... s_n$ are the desired pole locations. Collecting the coefficients of λ and setting them equal to zero gives n equations to solve for the values of k which achieve the desired pole locations.

For a single-input, single-output system, the closed loop plant of the state variable feedback system can be obtained as in reference [85] as

$$\frac{y(s)}{v(s)} = \frac{b(s)d(s)}{a(s)[d(s)+e(s)]+b(s)q(s)}, \qquad (3.10)$$

where $d(s)=|sI - A_c|$, $q(s)=K(sI - A_c)^{-1}L|sI - A_c|$, $e(s)=K^{-1}(sI - A_c)^{-1}B|sI - A_c|$ and the remaining terms b(s) and a(s) are defined by the open loop transfer function as

$$\frac{b(s)}{a(s)} = C(sI - A)^{-1}B. \qquad (3.11)$$

An effective control filter which can be compared to those that will be obtained from the classical frequency response-based methods can be derived by taking the transfer function in Figure 3.1 between the plant output y and the control input u. This is given as

$$C_e = \frac{-q(s)}{d(s)+e(s)}. \qquad (3.12)$$

This gives the function which multiplies the output of the open loop transfer function and is fed back to the open loop plant input if the external disturbance v is set to zero.

3.4 Classical Frequency Response-Based Control

There are a large number of control filters that can be used to achieve a desired control objective analytically. When it comes to practical experimental implementation, this number decreases markedly. There is a relatively simple second order control filter, a low pass filter which has also been called a positive position feedback (PPF) filter, that has been used successfully in feedback control problems primarily to actively increase damping in structures [35, 86-88]. A schematic of the filter connected in a feedback loop with the structural plant is shown in Figure 3.2 where $\mathbf{H} = \mathbf{C}(s\mathbf{I} - \mathbf{A})^{-1}\mathbf{B}$. Simulated control using the low pass filter will be demonstrated in Figures 3.4 and 3.5, using the state space model developed in Chapter 2 for the low modulus plate as the structural plant.

The low pass filter has a transfer function

$$C_{LPF}(s) = \frac{\omega^2}{(s^2 + 2\zeta\omega s + \omega^2)}, \qquad (3.13)$$

where ω is the filter resonance and ζ is the filter damping coefficient. It's magnitude and phase relationships are shown in Figure 3.3. This filter is used in active damping applications primarily when there is one or a band of closely spaced modes that are in phase with each other. The resonance frequency of the filter is tuned to match that of the mode or band of modes and the damping of the filter can be further adjusted to avoid influencing

other modes in the transfer function. In Figure 3.4, the filter is tuned to the second plate mode resonance, at 350 Hz, and used to increase damping in the mode by feeding back a sensor signal to the actuator, which is 90 degrees out of phase with the structural vibration. If the phase relationship of the filter is shifted by 180 degrees, the same filter decreases damping in the mode as in Figure 3.5. This 180 degree phase shift can be obtained in the actual system by adding an inverting amplifier directly before the control filter in Figure 3.1.

3.5 Control Approach Summary

An experimental procedure was introduced for finding good actuator positions for control of structural/acoustic modes. This procedure was based on the reciprocity between measured in-plane motion at a candidate actuator location due to an out-of-plane excitation and measured out-of-plane motion at the excitation location due to in-plane actuation at the candidate position. Pole placement and a classical frequency response-based method were developed for control objectives that involved changing damping and frequency of structural/acoustic modes, including intentional enhancement as well as suppression.

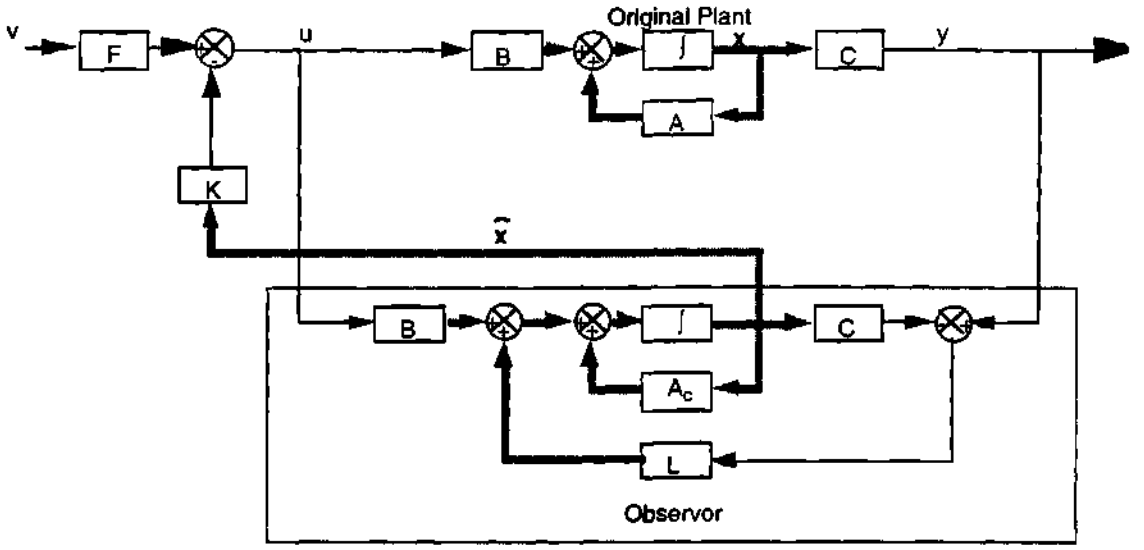

Figure 3.1- State space control schematic

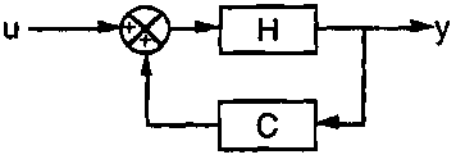

Figure 3.2- Classical control schematic

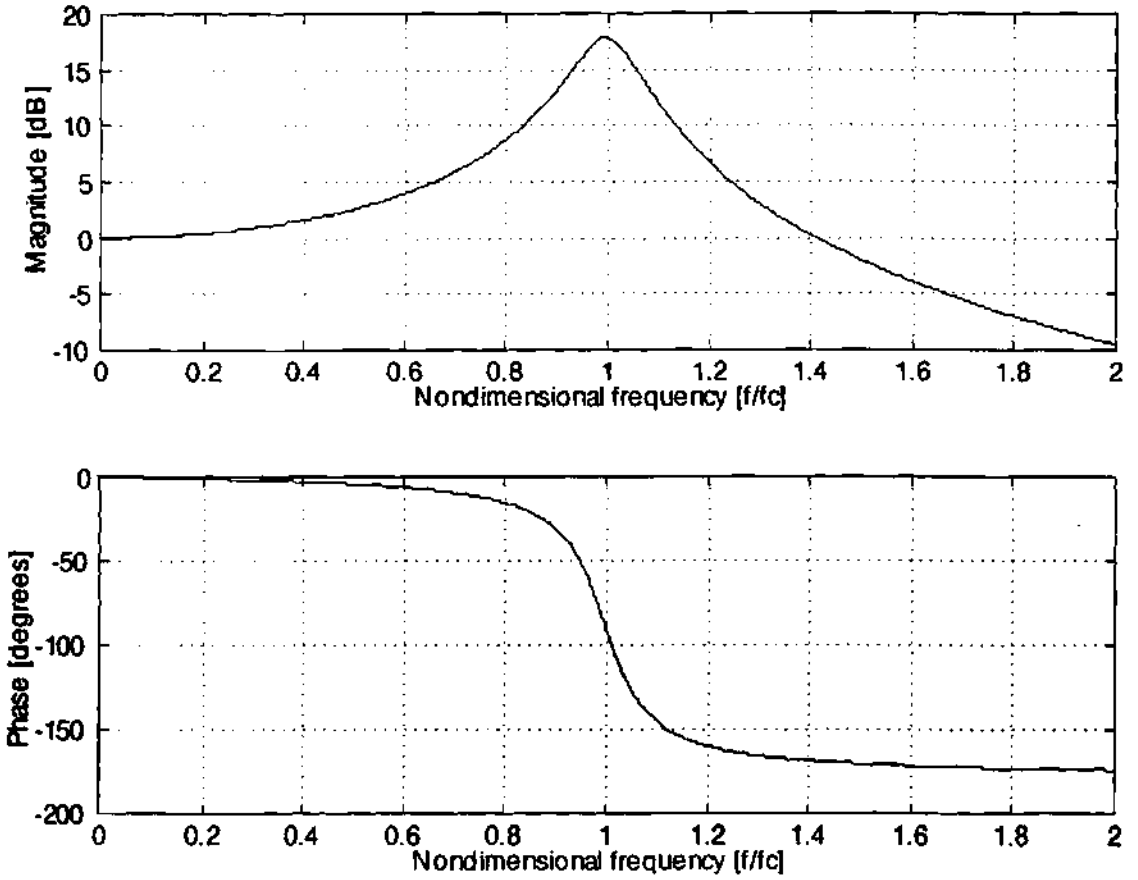

Figure 3.3 - Magnitude and phase of low pass filter

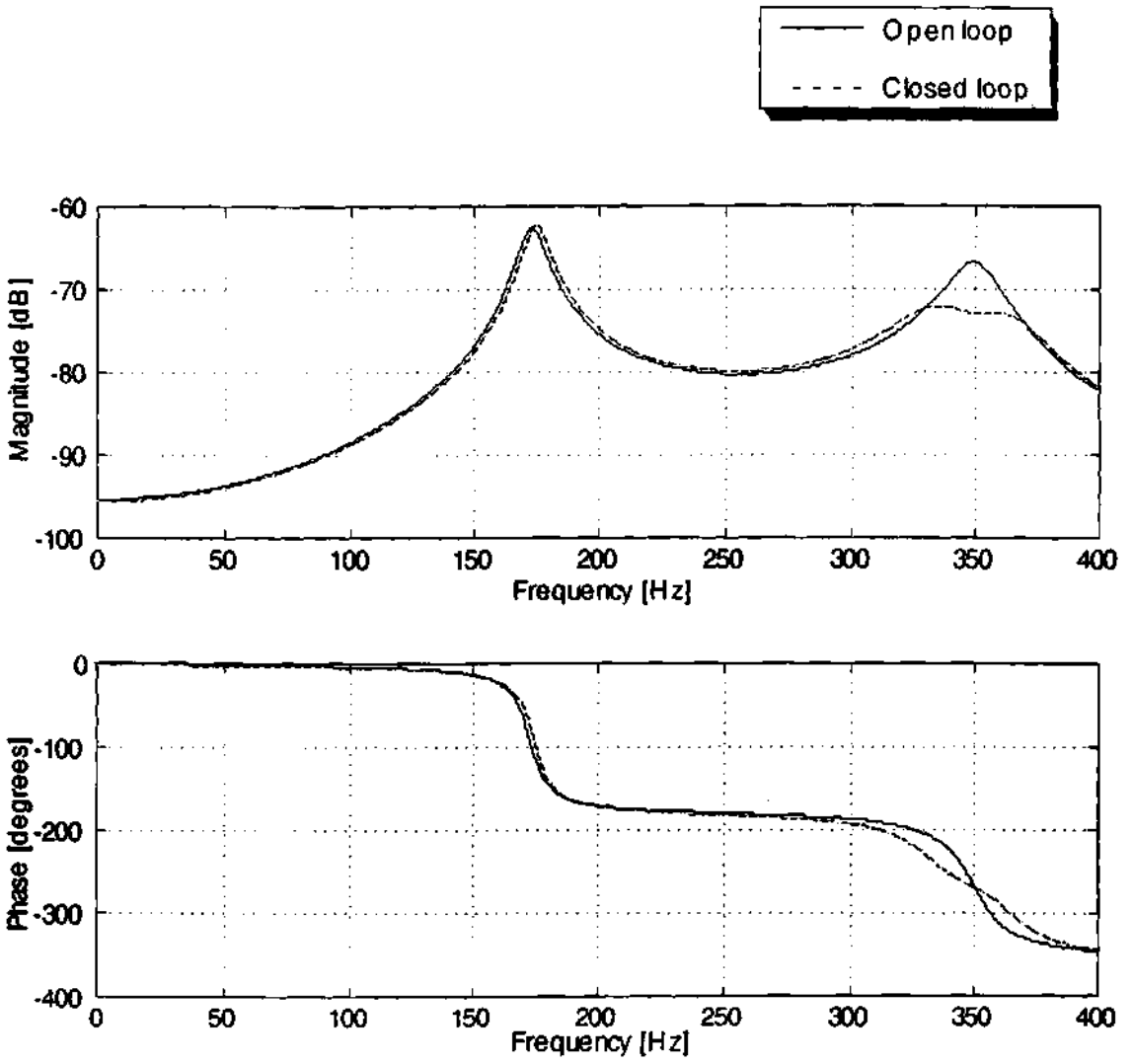

Figure 3.4 - Damping increases when loop is closed

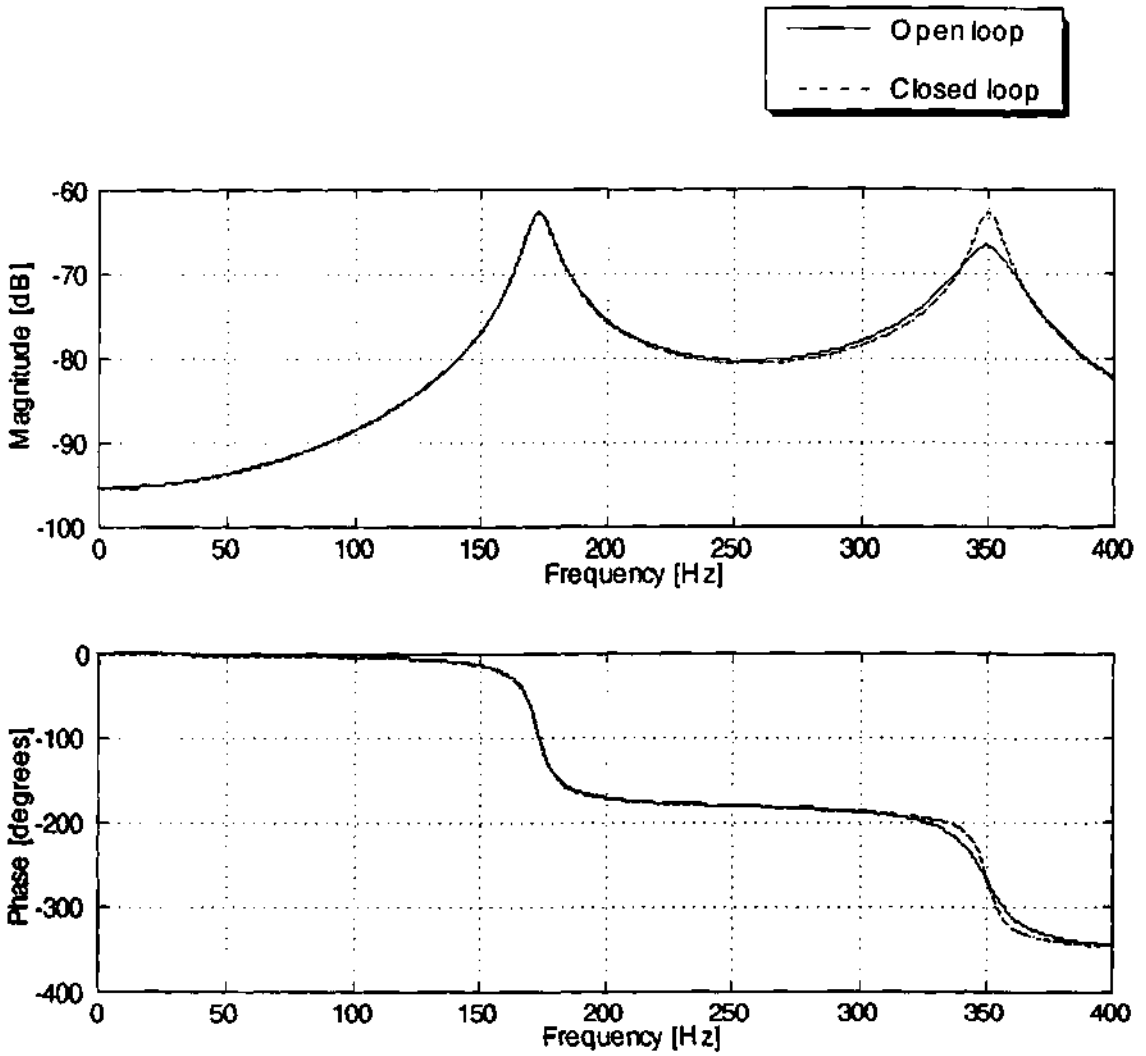

Figure 3.5 - Damping decreases when loop is closed

CHAPTER IV

APPLICATION TOWARD ACOUSTIC GUITAR

The previous chapters have developed the theory for active modification of the acoustics produced by a vented, cavity-backed panel using active control and piezoceramic sensors and actuators. One potential application is the acoustic guitar. This instrument displays the structural/acoustic behavior modeled, and research has been done to quantify specific frequency response characteristics which differentiate instruments of very high quality. In addition, the guitar is exceptionally suited as a test specimen. The flat top plate is responsible for most of the sound produced in the low frequency region, and it is extremely amenable to the incorporation of piezoceramic sensors and actuators. Finally, a test specimen was relatively inexpensive and readily available from the manufacturer. In this chapter, the continuous and discrete models are used to predict the passive guitar acoustic behavior due to a shaker and piezoceramic actuator input, respectively (Section 4.1). Some specific control objectives are gleaned from the aforementioned previous research for implementation on the test guitar, and the discrete model is used to demonstrate both state variable control and classical frequency response-based control (Section 4.2). The experimental control validation is then performed including open- and closed-loop structural and acoustic control results (Section 4.3).

4.1 Validation of Theoretical Models

Several geometric and frequency response-based measurements were taken from the guitar test specimen as inputs into the models. The guitar used was a relatively inexpensive model, a Fender Gemini II folk guitar. Figure 4.1 shows the guitar nomenclature and geometry. The continuous model was useful because it provided a closed-form solution to predict the passive behavior of the guitar in response to a shaker input. The goal of the discrete model was to also predict passive behavior of the guitar but primarily to study open and closed-loop control behavior, since this model included piezoceramic sensors and actuators.

4.1.1 Common Measurements

An initial modal survey was done using a Genrad model 2515 computer-aided test system to extract experimental mode shapes. A PCB 086C20 impulse hammer was used at 35 locations with a PCB 303A03 accelerometer in a location that was expected to have a significant participation from both structural modes. The accelerometer location was location 17 in Figure 4.2 which shows all locations used in the modal survey. The accelerometer weighed 2 grams, which was considered negligible compared to the mass of the guitar top plate. In all experimental measurements on the guitar body, the guitar was immersed to the ribs in sand to fix the motion of the back and ribs [72]. The first three modes in the initial modal analysis were the air mode at 108 Hz, the first plate mode at 206 Hz and the first antisymmetric plate mode at 377 Hz. The first two plate mode shapes that resulted are shown in Figure 4.3. In this particular guitar, the antisymmetric mode does not clearly conform to the standard (0,1) plate

mode or (1,0) plate mode identified by previous researchers in folk guitars [72], but the procedure for modeling an antisymmetric mode is similar in any case. This antisymmetric mode is acoustically important in this guitar as will be evident in its contribution to the measured SPL. The movement of the top plate at the air mode frequency was almost identical to the first plate mode but at a much lower amplitude.

Since a shaker input force applied to the guitar body was necessary to create an easily measurable SPL, an additional modal survey was done to verify that the mode shapes of interest did not change significantly under different forcing conditions. This modal survey was done using a Bruel and Kjaer type 4810 mini-shaker as the input force and the same accelerometer at the 35 measurement locations. The shaker was attached to the guitar near an antinode of the 2nd plate mode to insure its contribution in the measured transfer functions (position 18 in Figure 4.2). The first three mode shapes were virtually identical to the initial modal survey, although the frequencies shifted somewhat due to the added mass and stiffness of the shaker shaft and the force transducer. The air mode shifted up to 110 Hz while the first and second plate modes shifted down to 186 Hz and 344 Hz, respectively. A typical accelerance transfer function is shown in Figure 4.4. The accelerance transfer function is defined as the Fourier transform of the acceleration of the structure at the measurement point divided by the Fourier transform of the force input to the structure at the excitation point.

Inputs to the continuous and discrete models from physical measurements on the guitar were ρ, V, S_h, $r_{h,\ and}$ t. Parameters that were dependent on ambient conditions were γ, ρ_0, P_0, and a_0. Additionally, the measured values ω_h', ω_1', ω_2', ξ_h', ξ_1', and ξ_2' were taken from the

experimentally obtained accelerance transfer function using Modal-plus software by SDRC. Finally, the angle of the nodal line of the second plate mode is at an angle θ with respect to the symmetric line of the guitar. This was also determined experimentally from the initial modal survey and input into the model. Physical measurements used to derive model inputs are recorded in Table 4.1.

The assumption, in the models, that the cavity dimensions were less than $\lambda/2$ was violated for the antisymmetric plate mode since the longest cavity dimension of 0.50 meters was greater than the 0.49 meter value of $\lambda/2$, corresponding to the antisymmetric plate mode frequency of 344 Hz. This violation was allowed based on further investigation of the restriction. The $\lambda/2$ limit was imposed to avoid the first cavity resonance that occurs in an ideal duct at this frequency. The guitar body is not an ideal duct but has a varying geometry. Measurements of the first duct resonance made on a Martin D28 folk guitar, which is similar in geometry and has the same longest cavity dimension as the guitar under test, showed that the first duct resonance did not occur until 383 Hz. Additionally, even though the Martin D28 guitar had an antisymmetric plate mode shape that closely matched the pressure variation in the first cavity resonance, the coupling was considered weak [72]. In the case of the guitar under test, the mode shape of the antisymmetric mode is markedly different from that of the cavity resonance and occurs at a lower frequency than the actual duct resonance frequency, so coupling was ignored.

4.1.2 Continuous Model

As in the continuous model description in Chapter 2, an equivalent, clamped circular isotropic plate was used to model the motion of the lower bout of the guitar. The actual boundary conditions on the guitar lower bout are somewhere between clamped and simply supported but reasonable agreement between experiment and theory has been shown by past researchers using the clamped condition [75]. Figure 4.5 shows shape functions for the assumed plate. These can be compared to the actual measured mode shapes in Figure 4.3. Lower bout movement is thought to be responsible for most of the sound output of the guitar in the low frequency range. This type of movement, for low frequency function, has been verified experimentally [68, 74]. Depending on the type of guitar, the back plate may also have significant motion in lower frequency function. This can easily be included in the transfer function analysis by considering it as a plate in the same manner as the lower bout. However, prediction of SPL would require a different approach. This research considers only top plate motion. The experimental verification accounted for this by imposing a fixed boundary condition on the back.

The diameter of the equivalent isotropic plate was determined by averaging the widest point of the lower bout with the distance from the bottom of the guitar to the bottom of the rose. It was assumed that the undamped natural frequency, ω_2, was equal to the measured value of the ω_2' since the second plate mode has low damping and is not well coupled to the air mass. The first plate undamped natural frequency is then derived using the relationship for a circular isotropic plate of $\omega_1 = \omega_2 {}^{1.015^2}/_{1.468^2}$ [81]. The values for R_1 and R_2 were also assumed to be equal to the measured values of R_1'

and R_2' where $R = \rho\omega\xi$. After substitution of the measured parameters, numerical solution of Equations 2.11 gave the accelerance transfer function shown in Figure 4.6. This corresponds to the accelerometer and shaker positions used in the experimental measurement in Figure 4.4. The agreement between accelerance transfer functions was reasonable considering that no parameters were adjusted to match the two. The relative values of the peaks, with respect to each other, were consistent with experiment, and the way their relative contributions changed as a function of plate location was also consistent with experiment as witnessed by the similarities between the measured mode shapes and shape functions.

Pressure measurements were made in an anechoic facility with the guitar submerged up to the ribs in its sandbox and placed on a large wooden baffle. The dimensions of the anechoic facility, inside the foam, were approximately 5 m x 5 m x 6 m. The microphone used was built into a Tandy 33-2050 sound level meter. It's frequency response was flat from 32 to 10,000 Hz (± 3 dB). The guitar was excited by the suspended minishaker with the accelerometer and shaker fixed in favorable positions, 17 and 18 in Figure 4.2, respectively, to measure and excite the first and second plate modes as found in the second modal survey. Pressure was measured at observation points in front of the guitar using a microphone mounted on a tripod. Pressure level measurements were made as a result of input excitation by the shaker driven by an amplified pink noise source. The averaged transfer function with the microphone as the output and the minishaker attachment point force transducer as the input was computed. This gave the average pressure at the observation point for a given averaged

force input as a function of frequency. From this, SPL was computed for a 1 N force input to compare to predicted pressure values.

Figure 4.7 shows a schematic of the experimental setup used to measure sound pressure. Figure 4.8 shows the predicted SPL for a 1 N force input at each frequency from the solution of Equations 2.11 and the use of the Rayleigh integral developed in Chapter 2. Figure 4.9 is the measured SPL for an averaged 1 N force input at an observation point 50 cm above and 35 cm to the right of what was judged to be the center of the lower bout. The center of the lower bout was determined to be the point where the nodal line of the measured second plate mode crossed the guitar's plane of symmetry. This point is approximately halfway between locations 16 and 23 in Figure 4.2. The observation point was expected to have a pressure level contribution from both the first and second plate modes and the air mode. The measured SPL shows a mode slightly higher in frequency than the second plate mode at 381 Hz. This mode was also measured in the modal analysis but was not included in the model. Otherwise, the trends of the two SPL measurements match reasonably well.

4.1.2 Discrete Model

For the discrete model, a rectangular shape was selected for the equivalent plate representing the lower bout. This facilitated the incorporation of piezoceramic sensors and actuators since they are readily available in rectangular shapes. A location of the sensors and actuators was sought that coupled them well with the both the first and second plate modes. Using the criteria established in Chapter 3, a graph of first and second mode summed curvature magnitude from the approximate solution of Young [89] for the clamped, rectangular plate is shown in Figure 4.10. Without going

through a formal optimization process, the figure shows that the selected locations of the piezoceramics have a high contribution of summed curvature from both the first and second mode.

A finite element model was constructed to solve Equation 2.18, the details of which are left to Appendix C. Guitar model inputs which are specific to the finite element model are also in Appendix C. It was assumed, as in the continuous model that ω_2 and ξ_2 were equal to the experimentally measured values. A frequency independent value for the air mode damping was sought to allow the use of the state space formulation. To get the relationship between the measured parameters ω_1', ξ_2', ω_h', and ξ_h' and the corresponding equation parameters, the coupled oscillator approach of reference [73] was used as given by

$$\gamma_1' = \left[\frac{1+G}{2G}\right]\left\{\gamma_1 + \left[\frac{G-1}{G+1}\right]\gamma_h\right\},$$
$$\gamma_h' = \left[\frac{1+G}{2G}\right]\left\{\gamma_h + \left[\frac{G-1}{G+1}\right]\gamma_1\right\}, \qquad (4.1)$$

where $G = \dfrac{\omega_1'^2 - \omega_h'^2}{\omega_1^2 - \omega_h^2}$ and $\gamma = \xi\omega$. Upon entering the model inputs into the state space equations given in Section 2.2.2 and adding a gain of 100 before the actuator to represent an amplifier, the corresponding predicted transfer function is given in Figure 4.11.

4.2 Analytical Control Design

To demonstrate the feasibility of using active control to modify the acoustics of the guitar, some specific control objectives were formulated

based on the available literature. The pole placement method and the classical frequency response-based control method were then applied to the discrete model of the guitar including sensors and actuators to achieve the control objectives.

4.2.1 Control Objectives

As mentioned in Chapter 1, by far the most conclusive study relating guitar quality to specific factors in frequency response is reference [77]. In it, the single three most important factors which differentiated high quality instruments were all directly related to low damping in the (0,1) antisymmetric plate mode. Another important, potentially alterable factor was the damping in the air mode. This should be made high if possible. It was noted that both the air mode and the first plate mode should have higher damping, but that the peak level of the first mode should be high. Since damping and peak level are related, this advice may inspire two different objectives depending on the amount of material damping present in the first plate mode. If the material damping is large enough, the increase in peak level of the first plate mode due to a decrease in damping may be beneficial. If material damping is low, an increase in damping may be beneficial. Based on the advice from reference [77], four specific control objectives were formulated.

1. Decrease damping in second plate mode.
2. Decrease damping in second plate mode and increase damping in air mode.
3. Decrease damping in second plate mode and increase damping in air mode and first plate mode.
4. Decrease damping in first and second plate mode and increase damping in air mode.

Although the relative amounts of damping in these first three modes are extremely hard to control through passive means, they are controllable using active methods. Since the string input excitation to the guitar is transient and broadband, the problem is especially suited for the active feedback control methods developed in Chapter 3. In the stated control objectives, the amount of increase or decrease is somewhat arbitrary since specific target numbers are not given in the literature. For the pole placement method a decrease or increase of 20% will be sought and all four control objectives will be demonstrated. For the classical frequency response-based method, objective 1 will be demonstrated over a range dependent on control filter gain.

4.2.2 Analytical Control Simulation

The pole placement technique was carried out as described in Chapter 3 with sensor location, actuator location, and other state space parameters as in the discrete model of Section 4.1.1. Control objectives 1-4 were implemented by adjusting the real part, σ, of the poles without adjusting the imaginary part, ω. This had the desired effect of changing the damping without changing the damped natural frequency. For example, the relation between the damping ratio, ζ, and the parameters of the complex pole is

$$\zeta = \cos(\tan^{-1}(\frac{\omega}{\sigma})).$$

Using this relationship, the first control objective was meant by changing the location of the complex pole pair from -41.4±2159.3 to -33.2±2159.3. This corresponds to a decrease in damping ratio of 20%. The open and closed loop transfer functions using pole placement are shown in Figure 4.12. In addition, the corresponding effective control filter, as defined in Chapter 3, is

also shown in Figure 4.13. Control objectives 2-4 were realized in the same way. There predicted open and closed loop behavior are shown in Figures 4.14 - 4.16.

Using the classical frequency response-based methods, control objective 1 was implemented using the low pass filter as described in Chapter 3 to take away damping from a mode. This result is reproduced for varying gain values on the control filter in Figure 4.17 along with root locus plots for the varying gain values in Figure 4.18. The transfer function of the low pass filter, for the lowest gain in Figure 4.17, is shown in Figure 4.19. It is interesting to note that for the first control objective, both methods suggest the same form of control filter as can be seen by comparing Figures 4.13 and 4.19. Also, for all control objectives, as the 2nd plate mode decreases in damping, the real part of the pole gets closer to the right half plane in the root locus plot. This illustrates a limitation in the active control scheme. As the pole gets less damping, it is more likely to go unstable.

4.3 Experimental Control Validation

In order to verify the trend of the open and closed loop predictions, it was necessary to bond piezoceramic sensors and actuators onto the guitar top plate. Final sensor and actuator positions were found on the actual guitar after doing an additional modal survey with an in-plane sensor. The experimental control was implemented using both the pole placement and the classical frequency response-based design results on a digital signal processing (DSP) board and on a portable, battery-powered, control box.

4.3.1 Sensor and Actuator Location

The analytical model served as a rough guide for choosing sensor and actuator locations. It was necessary to further tailor the location, however, based on the true nature of the test specimen. The guitar top plate is not isotropic and of uniform thickness, although this approximation is a reasonable approximation to the first two out-of-plane mode shapes of the guitar. The guitar top plate is made up of a very thin, approximately 3 mm, wooden top plate with wooden stiffeners placed in an unsymmetric pattern beneath the top plate. This anisotropic behavior made it necessary to carry out a final modal survey to find good sensor and actuator locations. With the guitar in its sandbox using the same hammer described in the initial modal survey as an actuator at position 18 in Figure 4.2 to excite both the first and second plate modes, several transfer functions were taken at different sensor positions on the top plate as described for experimental sensor and actuator location in Chapter 3. PVDF was used, as a sensor in these transfer functions, because it senses in-plane motion in a similar fashion to the piezoceramics, but it is easily attached and removed using double sided tape. The differences in the geometry and structural properties of PVDF as compared to the piezoceramic sensors and actuators were ignored since neither material was expected to have a significant effect on the substructure mode shapes. As a result of this study, the locations shown in Figure 4.20 were selected since they each had the highest magnitudes in both the first and second mode. A 0.127 mm thick piezoceramic sensor, measuring 1.1 cm by 2.1 cm in its horizontal and vertical directions, and a 0.127 mm thick actuator, measuring 3.3 cm by 3.5 cm in its horizontal and vertical directions, were then bonded to the guitar top plate at the selected locations. Horizontal

and vertical directions are also with reference to Figure 4.20. Passive masses were attached to the guitar top plate to represent the shaker and the accelerometer masses which were present in the initial modal survey. The final open loop transfer function between the sensor and actuator location is shown in Figure 4.21 using a white noise input into the actuator and the piezoceramic as a sensor. This should only qualitatively be compared to the predicted behavior in Figure 4.11 since the actual experimental sensors and actuator were of a different size and thickness than the those modeled, and they were bonded in different locations.

4.3.2 Structural Control Results

It was not possible to apply the control filters designed using the model directly to the guitar test specimen due to differences in sensor and actuator size and properties, but it was possible to investigate their experimental implementation by allowing for an adjustable gain to compensate for these differences. The actual implementation of the effective control filters resulting from the pole placement method for control objectives 1 and 3 were implemented using a DS1102 DSP board from Dspace. This DSP board allows the user to load and execute a filter in the form of a transfer function programmed in Matlab software directly on hardware. The DSP board was also used to acquire data from the noise input and the sensor output for calculation of the open and closed loop structural transfer functions. The experimental setup for these measurements is shown in Figure 4.22.

The open and closed loop structural transfer functions using the effective control filter for control objective 1 is shown in Figure 4.23 for two different gain values. For this relatively simple control objective, the control

filter did perform acceptably. Open and closed loop structural transfer functions using the effective control filter for control objective 3 are shown in Figure 4.24 with the closed loop gain set to the same level as the higher gain in Figure 4.23. In this case, the damping of the second, antisymmetric mode is obviously reduced more than the damping of the air mode and the first plate mode are increased. This is due to the aforementioned discrepancies between the model and the actual experimental specimen. The relative amplitude ratios between the structural modes of the specimen and the structural modes in the model are different, so the controller formulated to influence more than one mode does not perform acceptably.

In addition to differences between the model and the test specimen already mentioned, a practical implementation of active control on the guitar would not be carried out with it submerged to the top plate in sand but with it being held by a guitar player. Recognizing that it is necessary to capture the actual behavior of the guitar under a more realistic boundary condition for further control design and simulation, it is useful to introduce the concept of transfer function modeling. A transfer function can be derived directly from sampled time records of a random noise disturbance and sensor outputs using the autoregressive moving average (ARMA) model [85]. This method is based on assuming an input-output relationship of the model as

$$y(k+1) = a_0 y(k) + a_1 y(k-1) + a_2 y(k-2) + \ldots + a_n y(k-n) + b_0 u(k+1) + b_1 u(k) + \ldots + b_p u(k+1-p) + v(k). \quad (4.2)$$

where y(i) are the outputs, u(i) are the inputs, and v(k) is a random noise term. The model parameters to be found, based on the sampled data, are

$$\theta = [a_0 \quad a_1 \quad \ldots \quad a_n \quad b_0 \quad b_1 \quad \ldots \quad b_p],$$

which transforms Equation 4.2 into

$$\begin{aligned} y(k+1) &= [y(k) \quad y(k-1) \quad \ldots \quad u(k+1) \quad u(k) \quad \ldots]\theta + v(k) \\ &= \mathbf{C}(k)\theta + v(k). \end{aligned} \tag{4.3}$$

Equations 4.3, can be combined at each time step to make one equation as

$$\begin{bmatrix} y(k+1) \\ y(k+2) \\ \cdot \\ \cdot \\ \cdot \\ y(k+N) \end{bmatrix} = \begin{bmatrix} C(k) \\ C(k+1) \\ \cdot \\ \cdot \\ \cdot \\ C(k+N-1) \end{bmatrix} \theta + \begin{bmatrix} v(k) \\ v(k+1) \\ \cdot \\ \cdot \\ \cdot \\ v(k+N-1) \end{bmatrix}. \tag{4.4}$$

Equation 4.4 can then be solved approximately using a least squares estimation procedure. The parameters, θ, are directly related to the discrete transfer function by the input-output relation in Equation 4.2 as

$$H(z) = \frac{b_0 + b_1 z^{-1} + \ldots + b_p z^{-p}}{1 - (a_0 z^{-1} + \ldots + a_{n-1} z^{-n})}.$$

The discrete transfer function can then be mapped into a continuous-time transfer function or left as a discrete-time model for digital control design.

An approximate transfer function was obtained using the ARMA model with a random noise input into the actuator while holding the guitar in a playing position. The associated experimental schematic is shown in Figure

based on Chapter 3, to decrease damping in the second mode. The transfer function of the filter is given by

$$\frac{GAIN \times 2.047x10^5}{s^2 + 153.4s + 5.849x10^6}.$$

The simulated closed loop result at values for GAIN of .035 and .05 are shown in Figure 4.28.

4.3.3 Acoustic Control Results

The next step was to design a portable, battery-powered, analog control filter based on the DSP results to facilitate acoustic tests and to provide a more realistic embodiment of an active acoustic guitar. Such a portable control filter was constructed. Its finished dimensions were 13 cm x 5 cm x 7 cm including four 9 volt batteries, and its schematic is shown in Figure 4.29. The resistor and capacitor values in the low pass filter came directly from the DSP board design. They are related to the filter damping and cutoff frequency by

$$\omega_c = \sqrt{\frac{1}{R1 \cdot R2 \cdot C1 \cdot C2}}, \quad \zeta = \sqrt{\frac{C2 \cdot [R1+R2]^2}{R1 \cdot R2 \cdot C1 \cdot 4}}.$$

The locations of R1, R2, C1, and C2 in the low pass filter are also shown in Figure 4.29. The open and closed loop structural and acoustic control results, using the portable filter, were then measured in anechoic tests similar to those earlier described, but with the piezoceramic actuator used as both the disturbance and the control actuator. The open and closed loop structural transfer function results are shown in Figure 4.30 . The open and closed loop acoustic transfer function results, with the microphone located 0.3 m above

position 1 in Figure 4.2, are shown in Figure 4.31. It is evident that closing the loop results in decreased damping in both the second antisymmetric structural mode and the corresponding structural/acoustic mode.

4.4 Acoustic Guitar Application Summary

Structural/acoustic control in a "smart" acoustic guitar was shown to be a means of favorably adjusting factors that ultimately determine quality. This was done by specializing the model and control approaches developed in Chapters 2 and 3 to the acoustic guitar. The continuous model was shown to be affective in predicting the passive structural and acoustic behavior of the acoustic guitar. The discrete model and the control approach allowed simulation and implementation of control objectives on a "smart" guitar that were highly correlated with guitar quality. Predictions of both open- and closed-loop structural and acoustic behavior were verified experimentally.

Table 4.1 Quantities from physical measurements used as model inputs

area density of plate	ρ	1.02 kg/m^2
cavity volume	V	1.75x10^{-2} m^3
area of vent	S_h	7.85x10^{-3} m^2
radius of vent	r_h	5x10^{-2} m
specific heat ratio	γ	1.4
ambient density	ρ_0	1x10^5 N/m^2
ambient pressure	P_0	1.29 Kg/m^3
ambient speed of sound	a_0	340 m/s
measured air mode frequency	ω_h	110 Hz
measured first plate mode frequency	ω_1	186 Hz
measured second plate mode frequency	ω_2	344 Hz
measured air mode damping ratio	ζ_h	0.036
measured first plate mode damping ratio	ζ_1	0.053
measured second plate mode damping ratio	ζ_2	0.019
2nd plate mode nodal line angle	Θ	45^0
radius of equivalent circular plate (continuous model)	r_S	1.75x10^{-1} m
thickness of plate (continuous model)	t	3x10^{-3} m

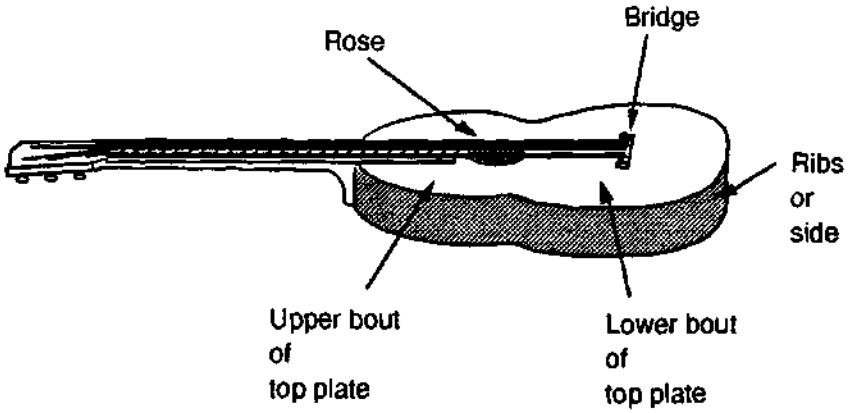

Figure 4.1 Guitar nomenclature and geometry

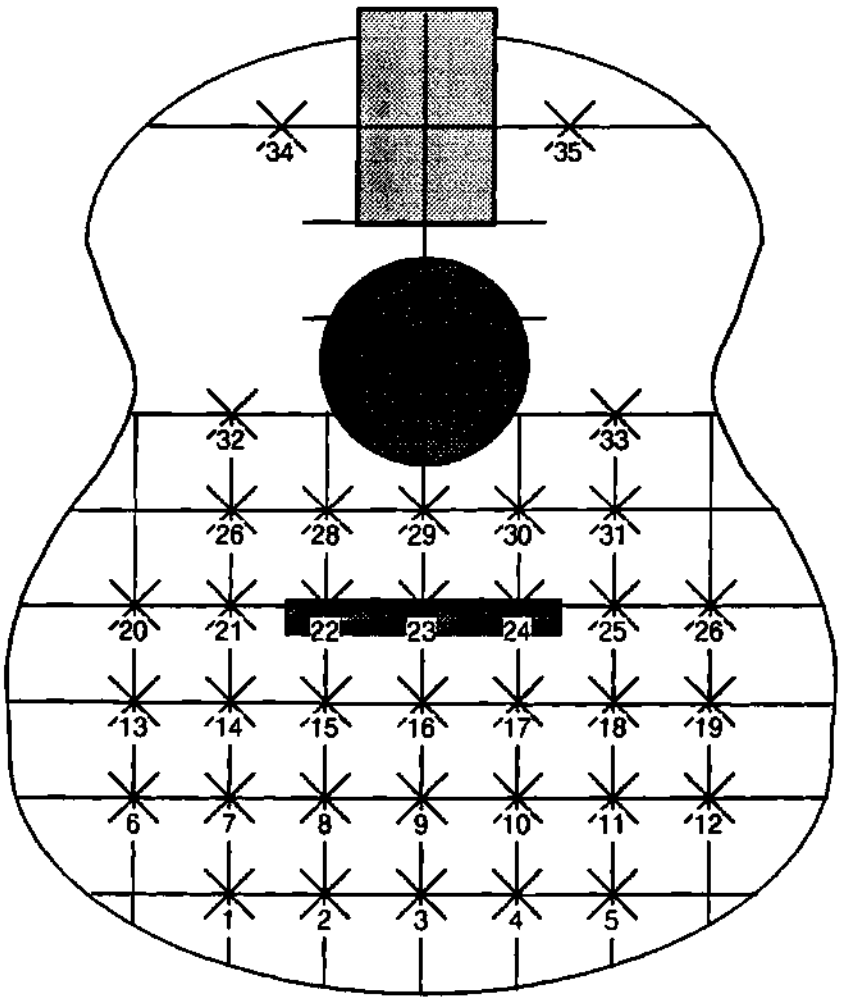

Figure 4.2 Guitar measurement locations (spacing between all grid lines is 5 cm)

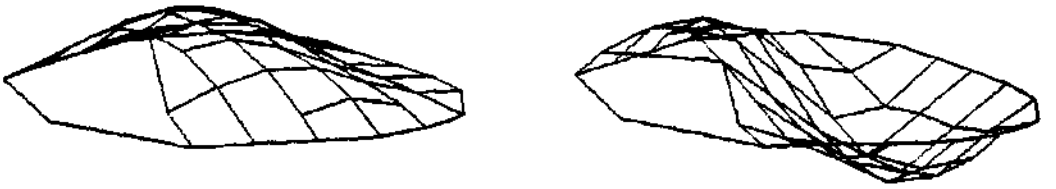

First mode Second mode

Figure 4.3 Measured mode shapes

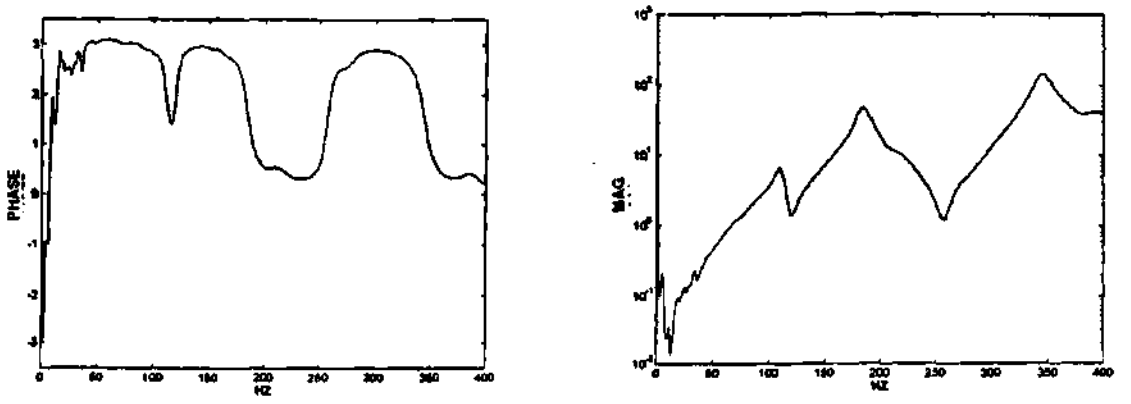

Figure 4.4 Measured accelerance transfer function

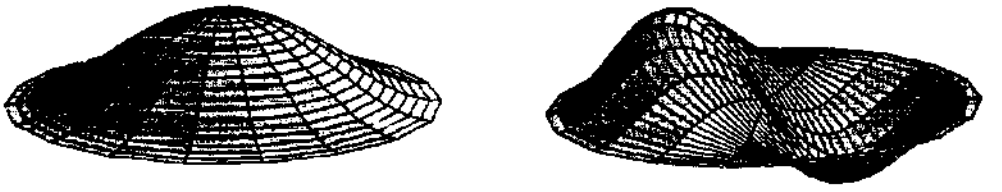

First mode Second mode

Figure 4.5 Shape functions of continuous model

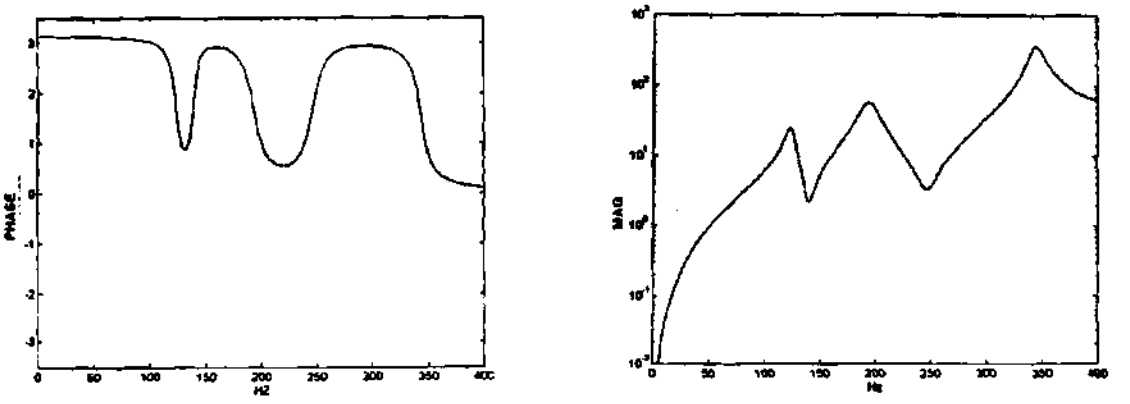

Figure 4.6 Predicted accelerance transfer function

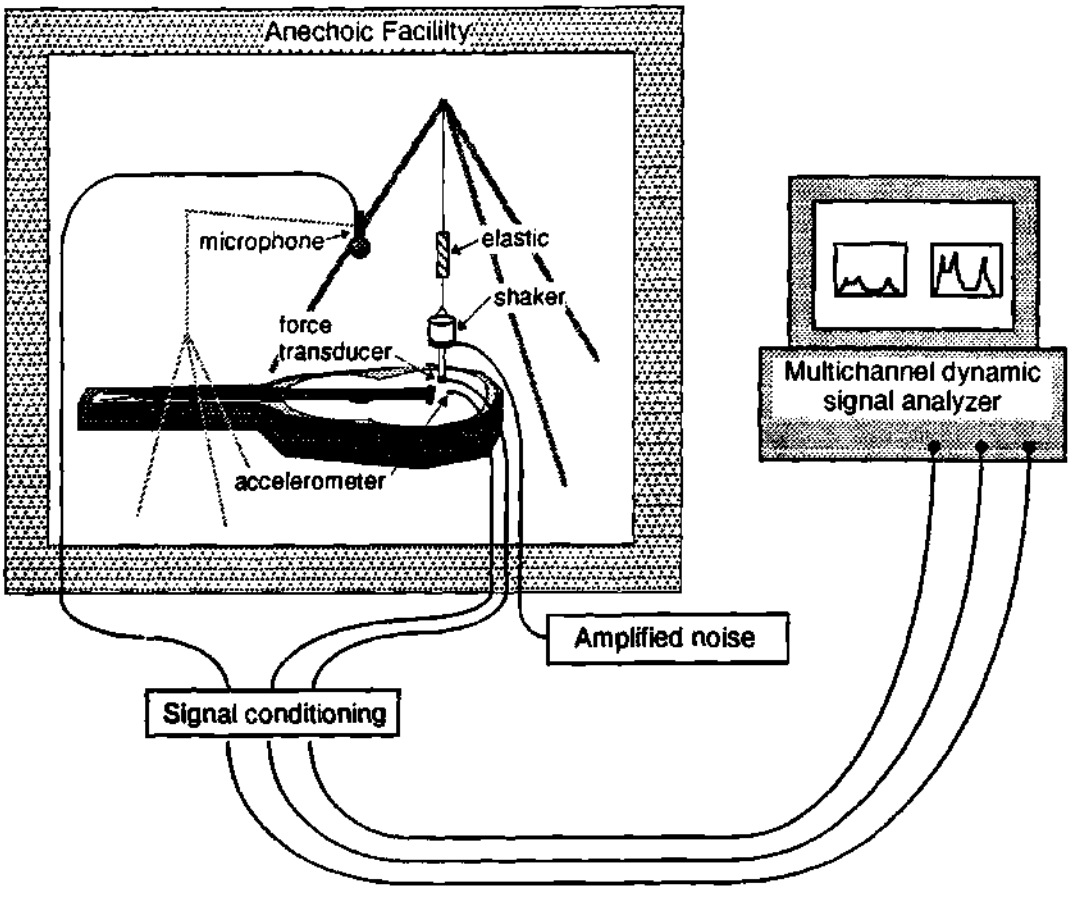

Figure 4.7 Experimental setup for measuring sound pressure

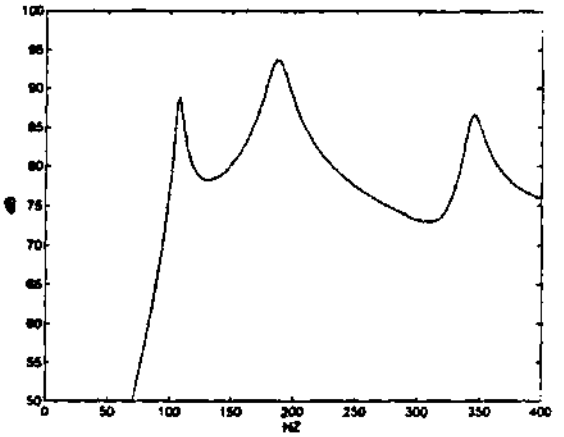

Figure 4.8 Predicted SPL

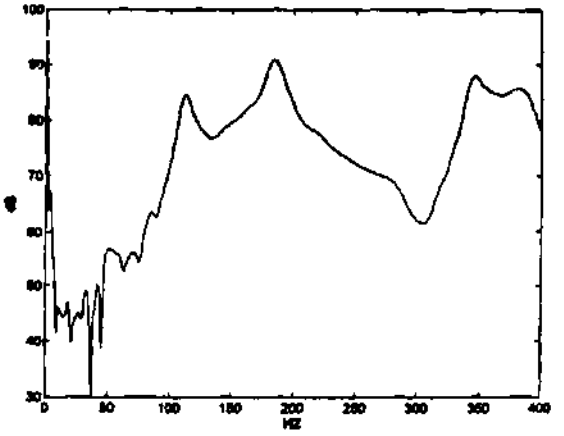

Figure 4.9 Measured SPL

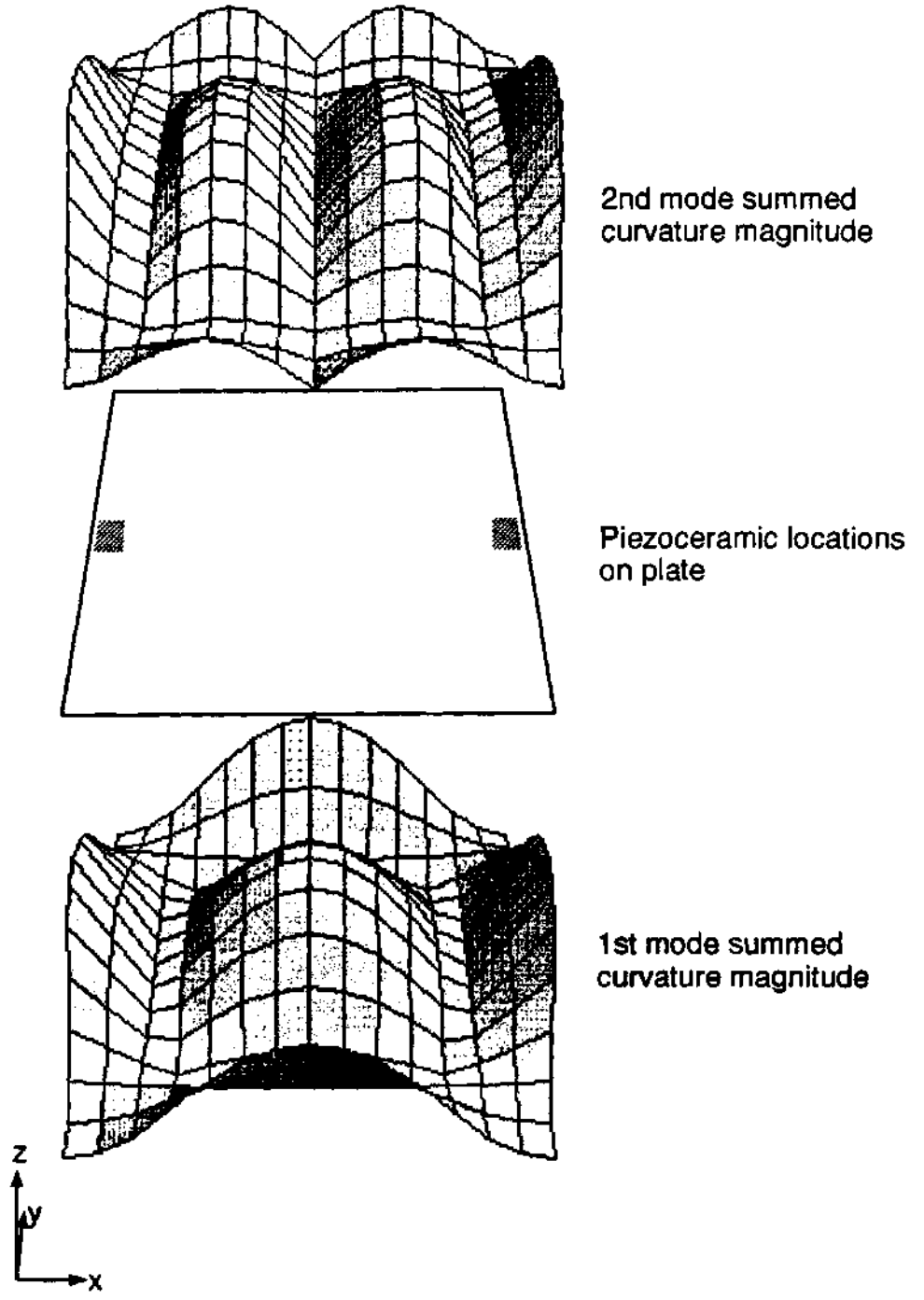

Figure 4.10 Piezoceramic location on plate for 1st and 2nd plate modes

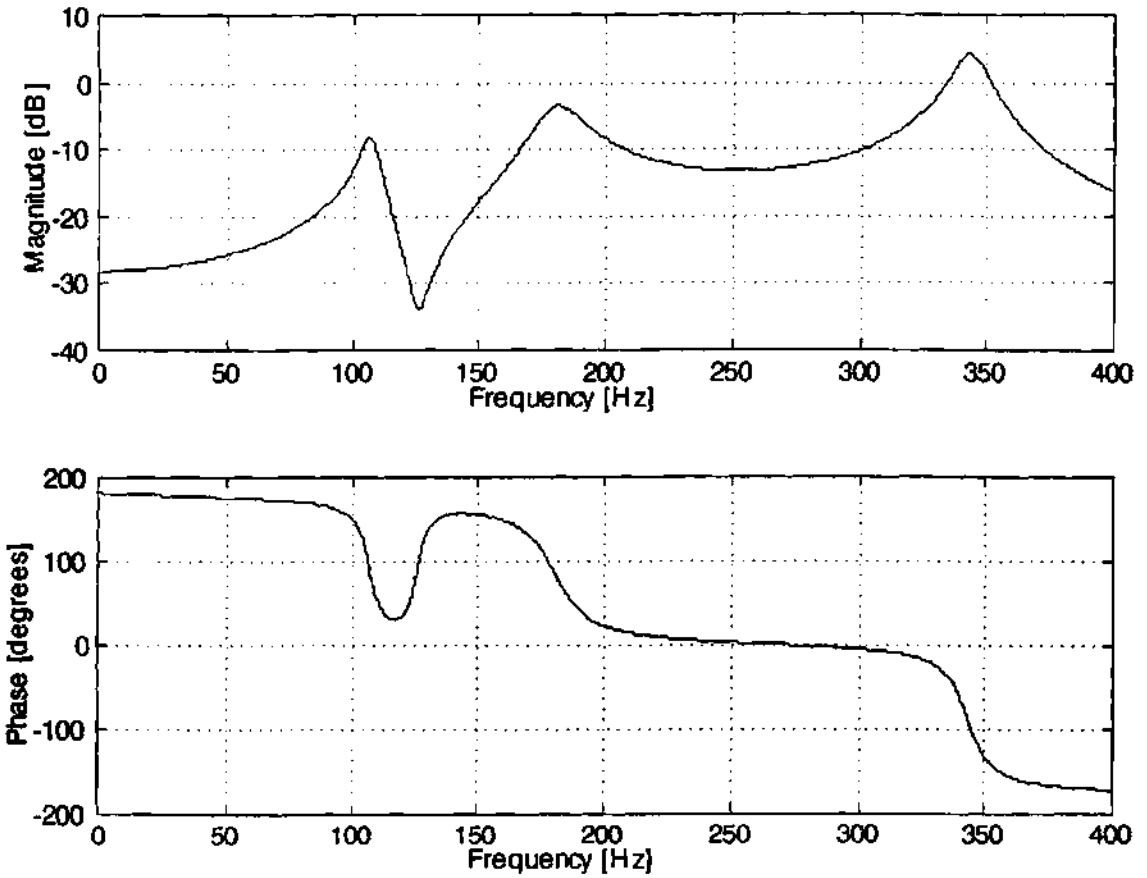

Figure 4.11 Predicted transfer function

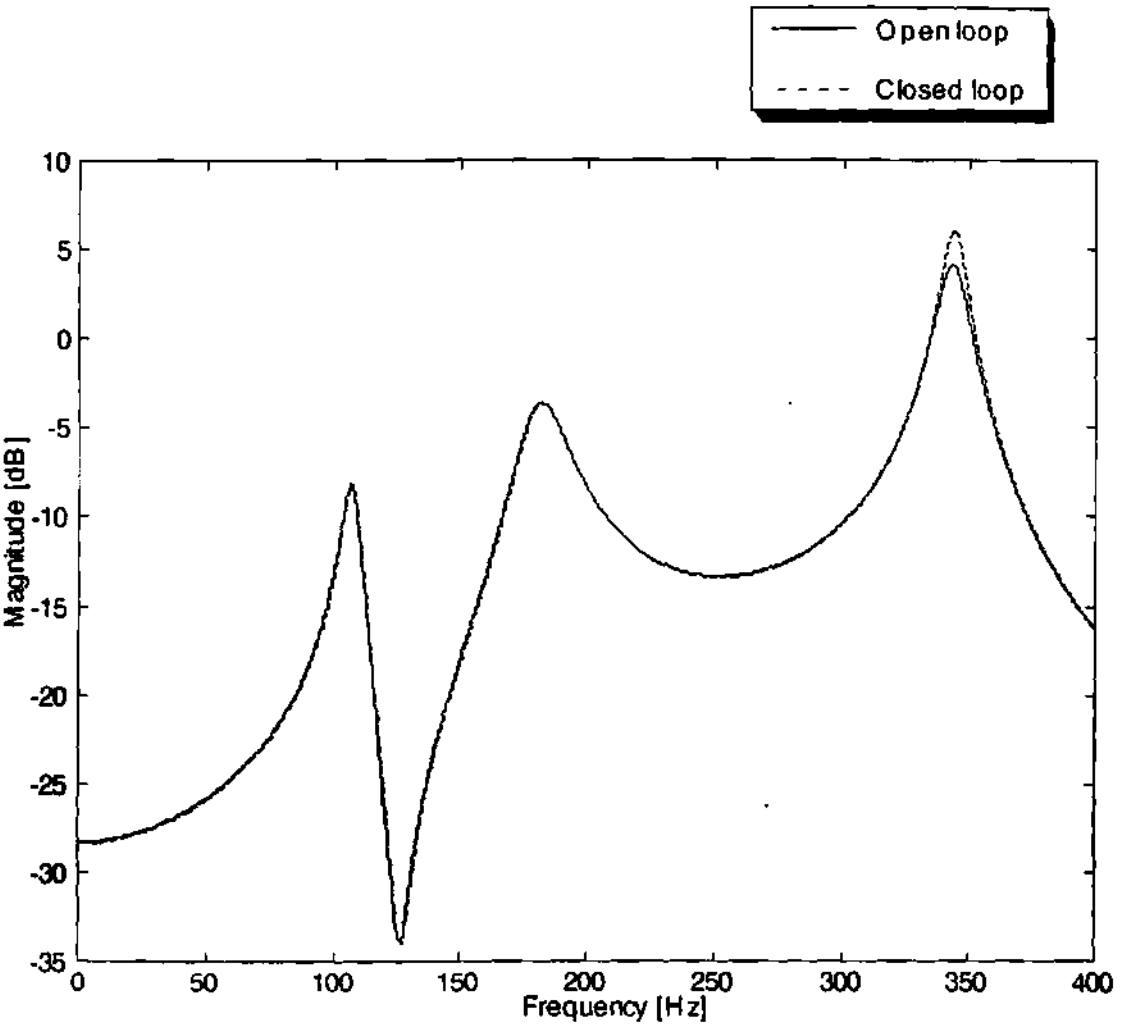

Figure 4.12 - Control objective number 1

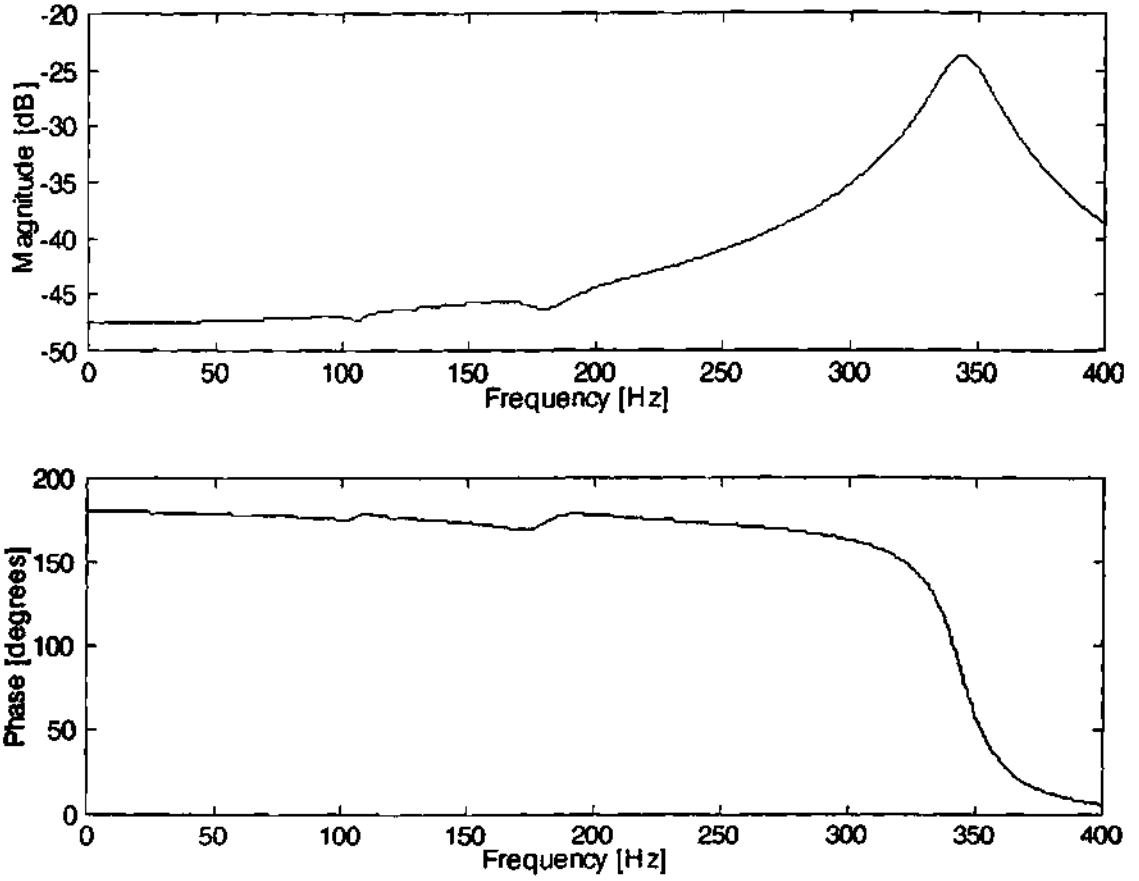

Figure 4.13 - Control objective 1 effective control filter

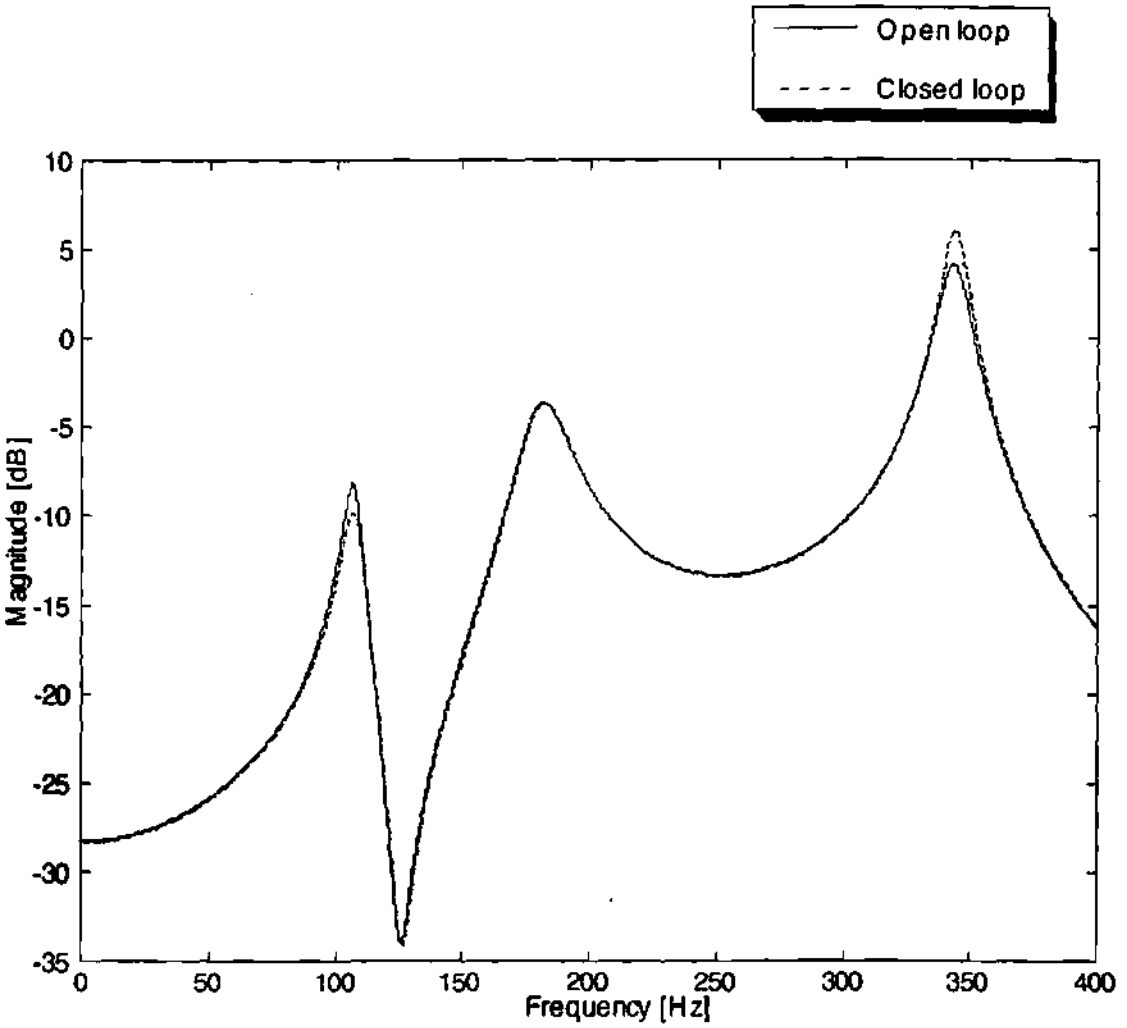

Figure 4.14 - Control objective number 2

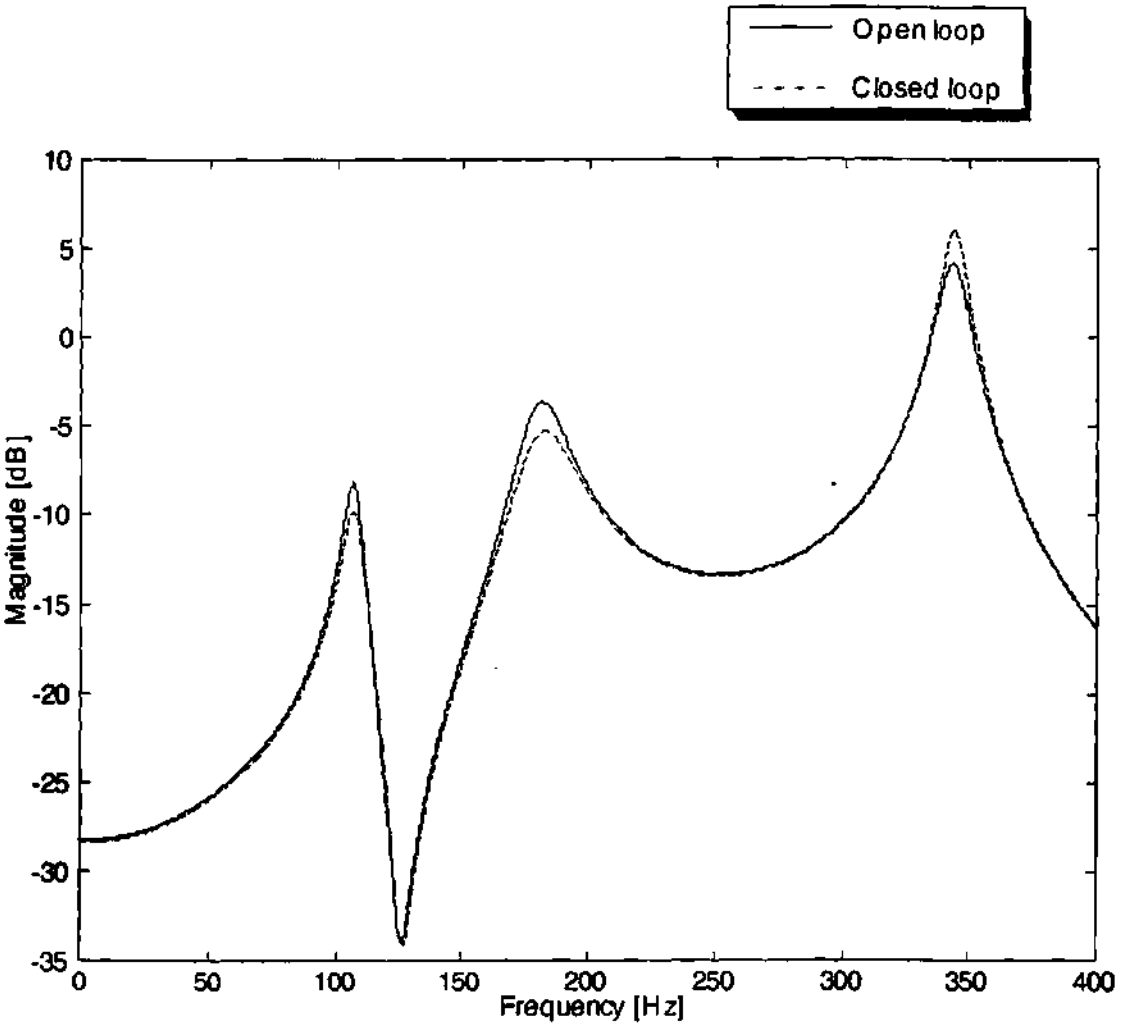

Figure 4.15 - Control objective number 3

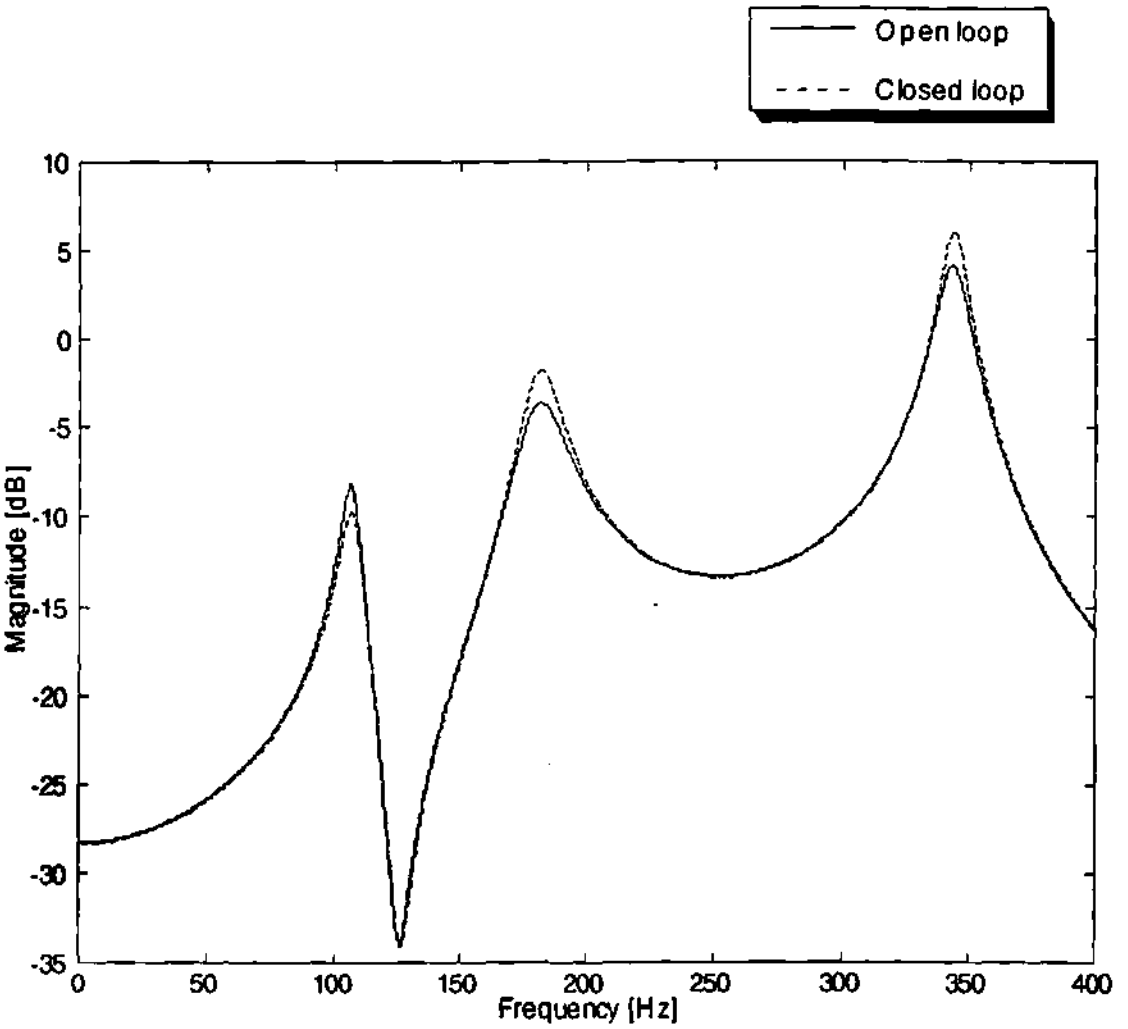

Figure 4.16 - Control objective number 4

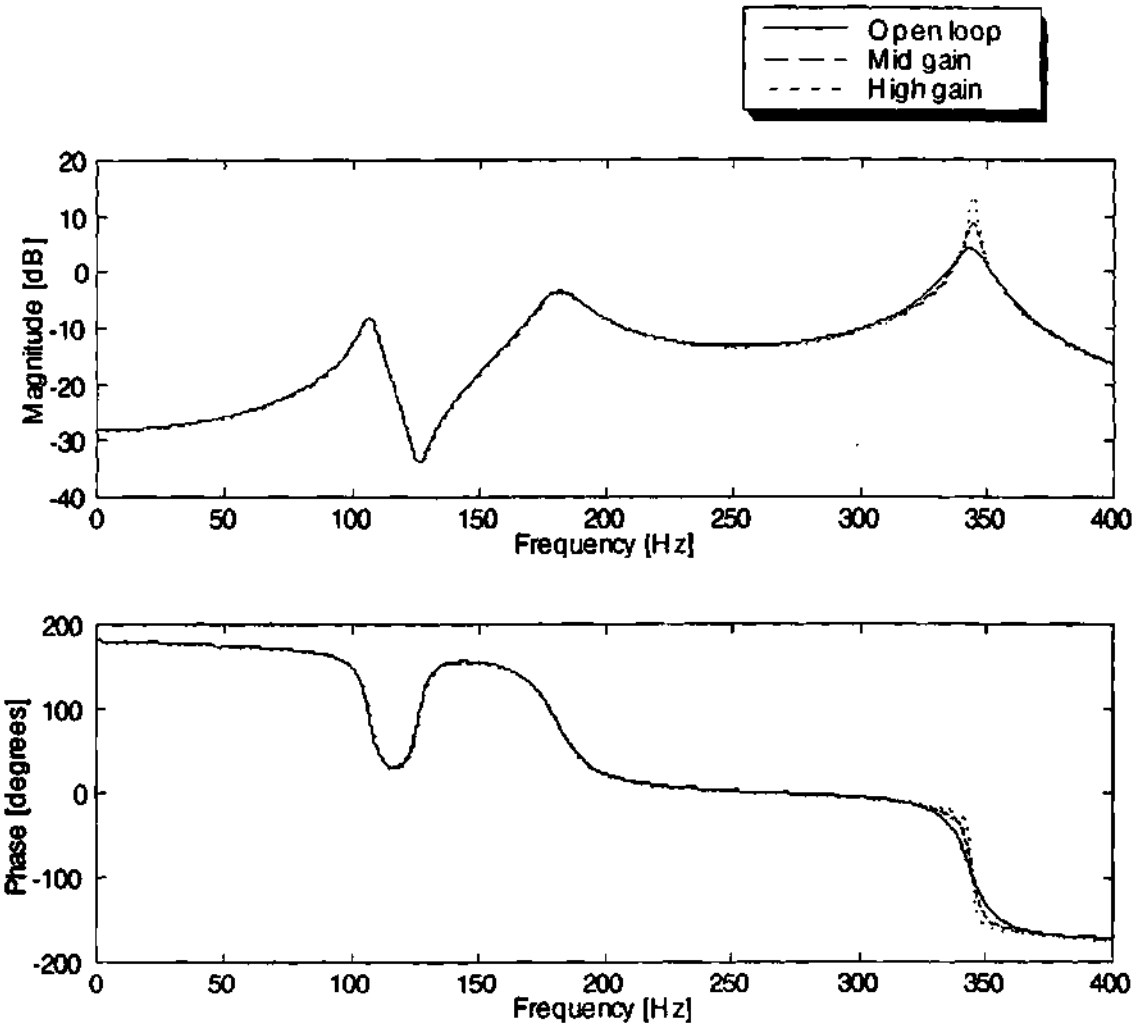

Figure 4.17 - Predicted closed loop transfer function with varying gain values

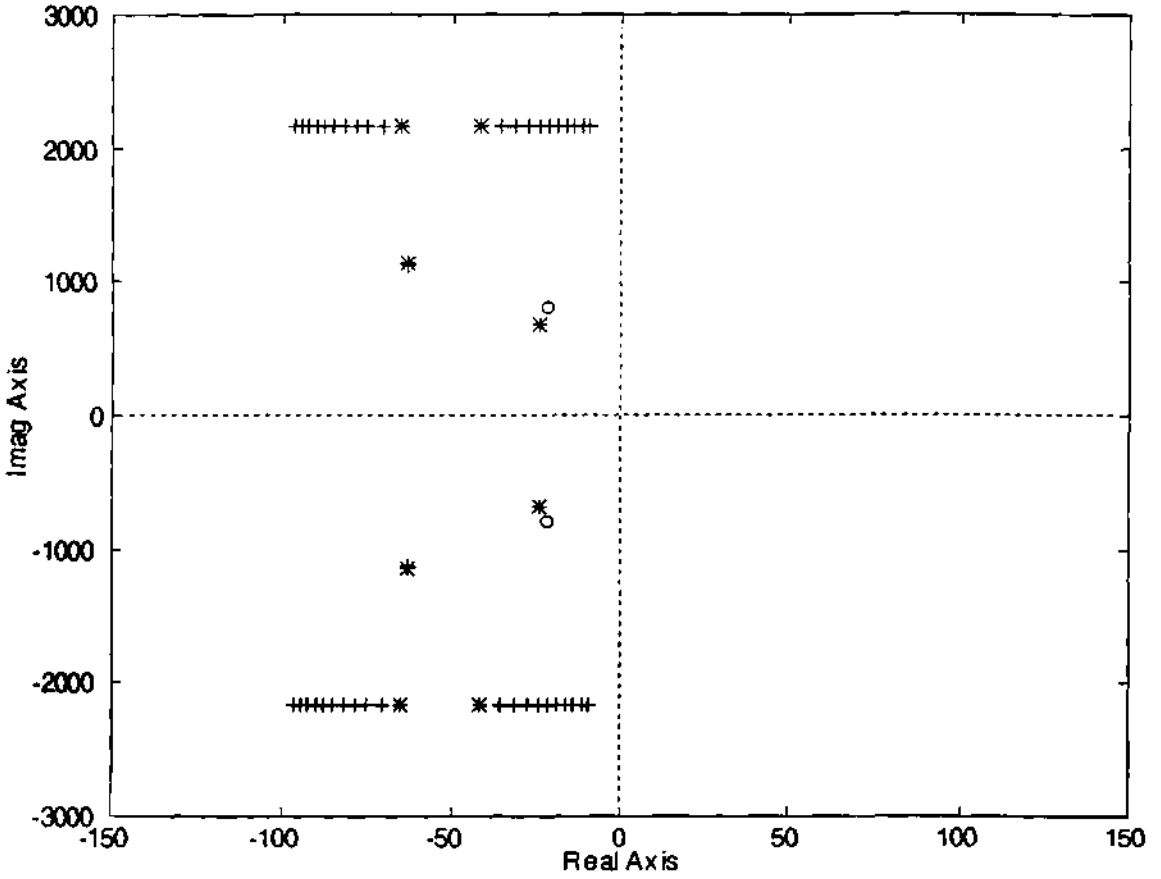

Figure 4.18 - Root locus using low pass filter

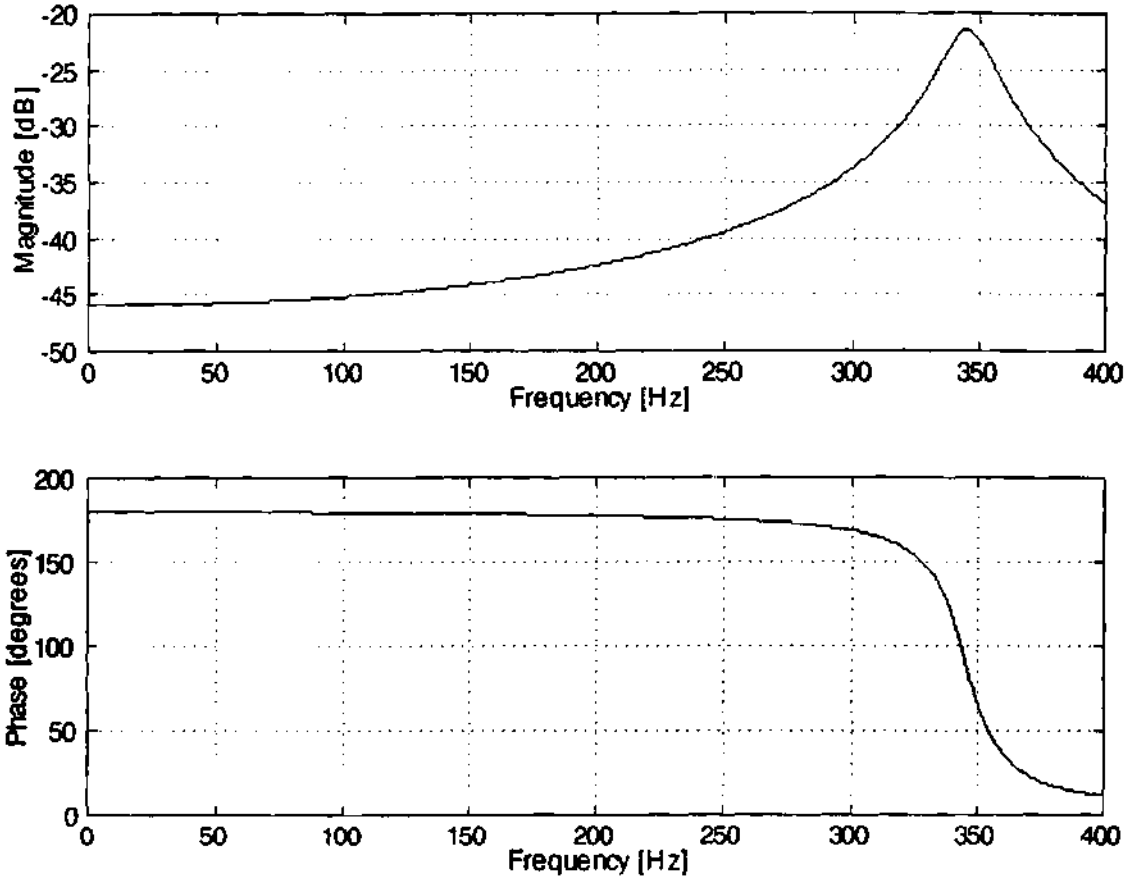

Figure 4.19 - Transfer function of low pass filter

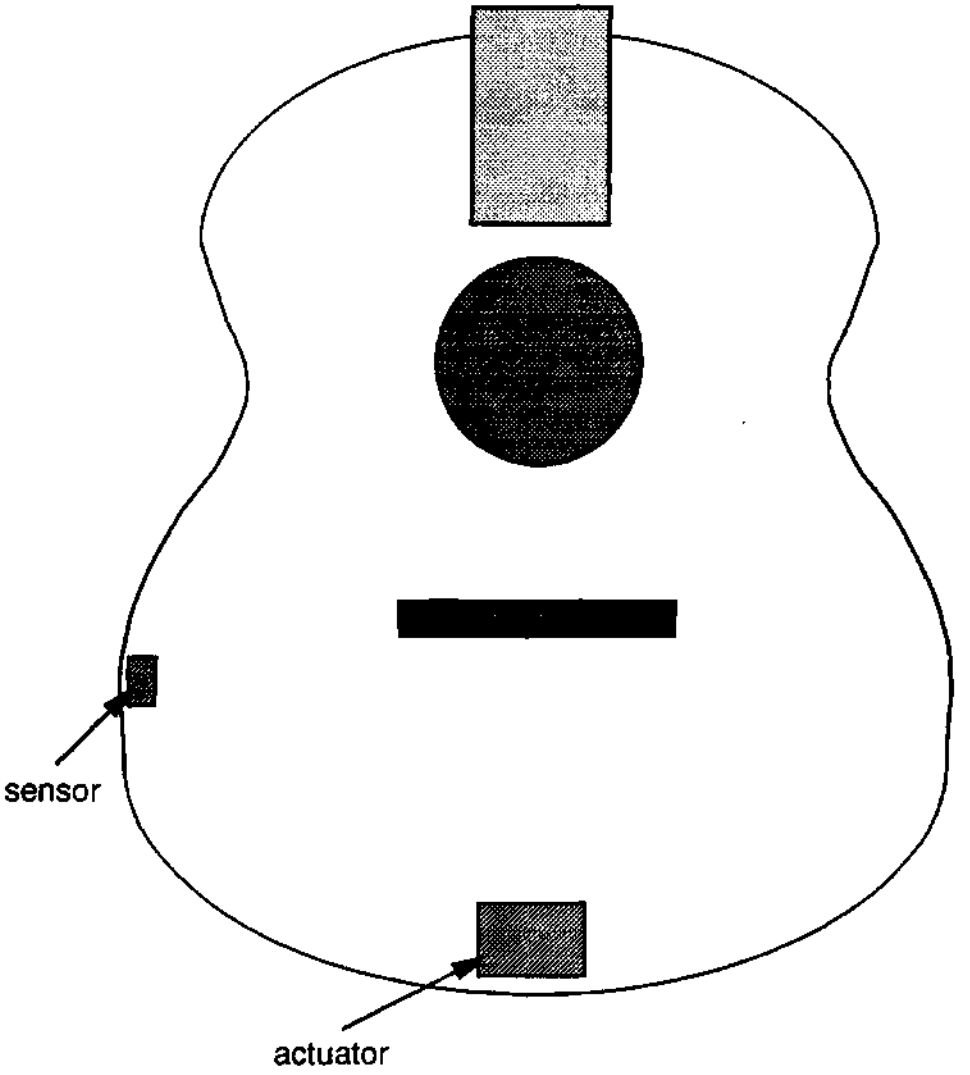

Figure 4.20 Final location of piezoceramic sensor and actuator

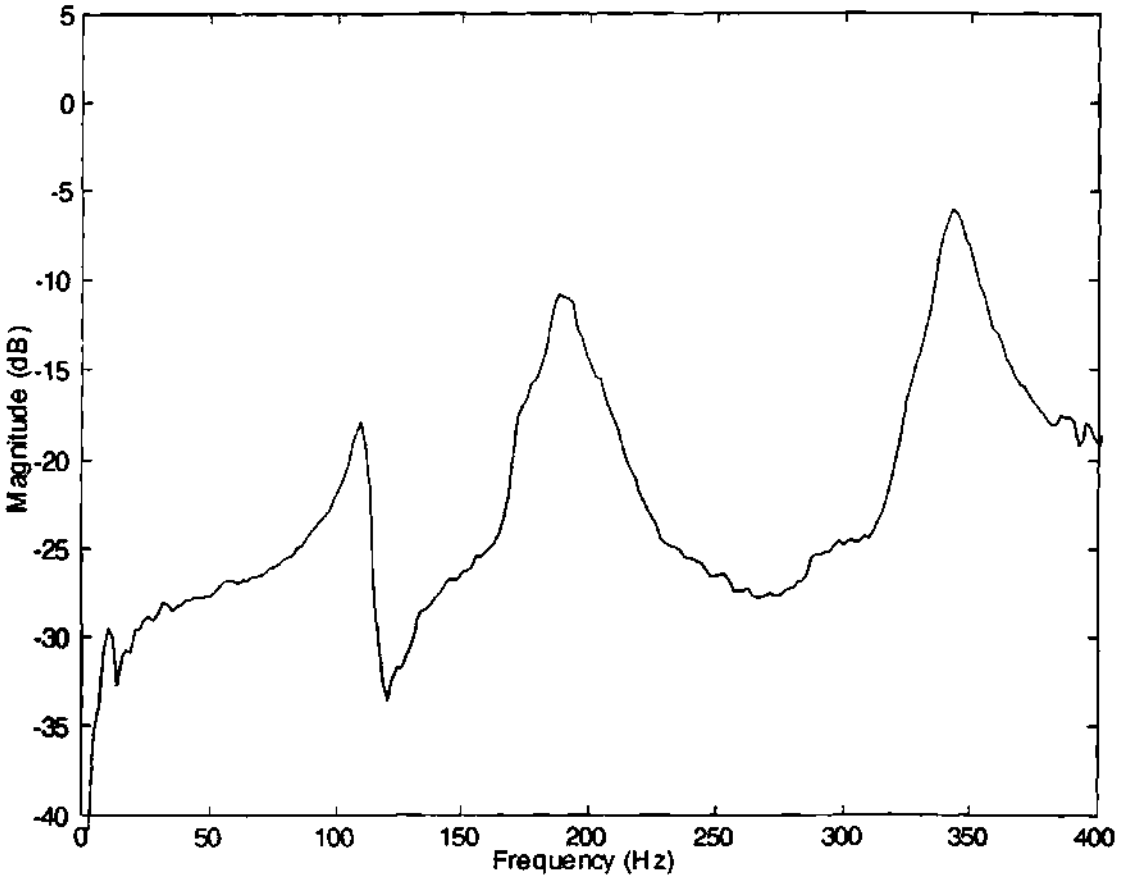

Figure 4.21 - Open loop transfer function with piezoceramic sensor and actuator

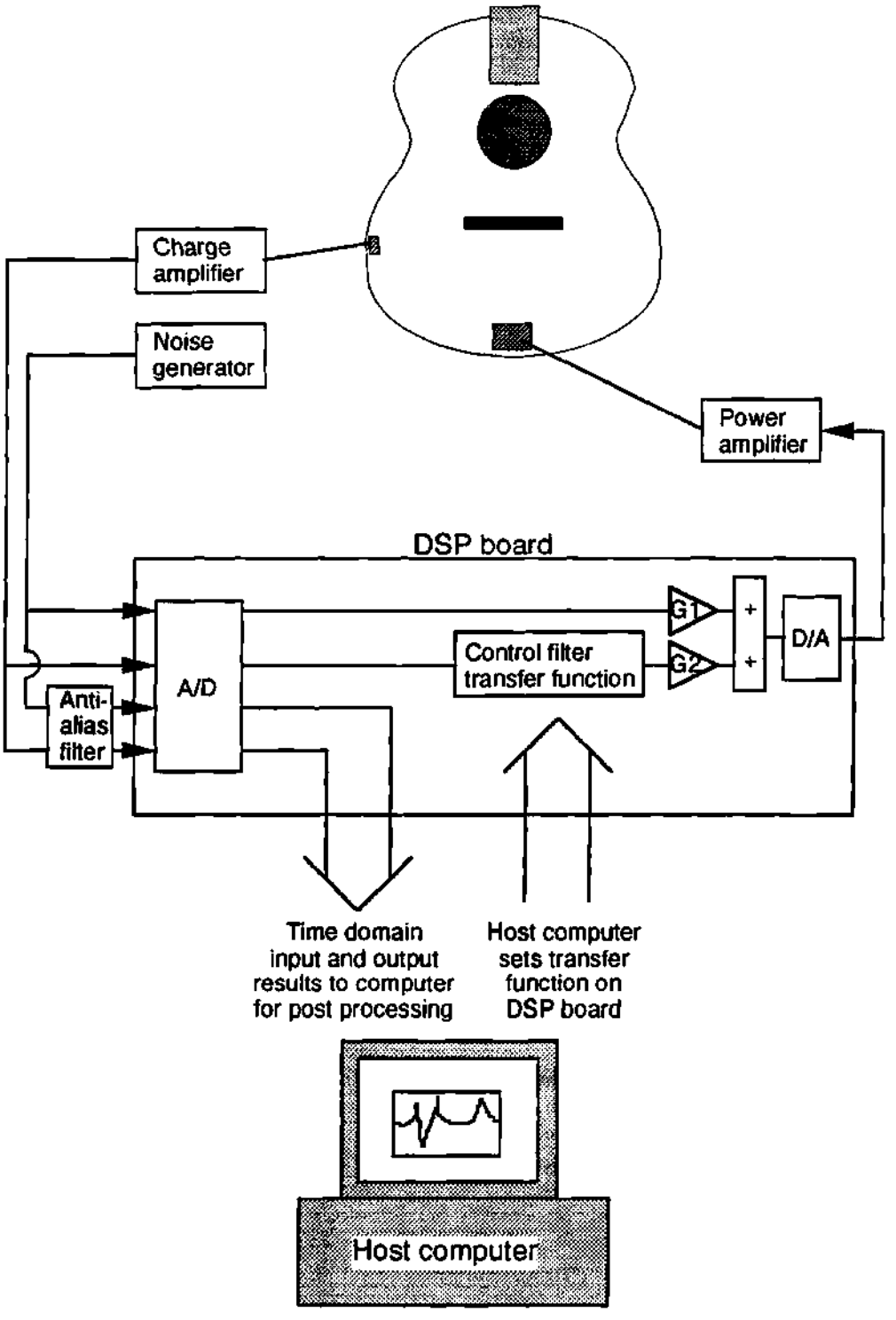

Figure 4.22 Experimental schematic for control using DSP board

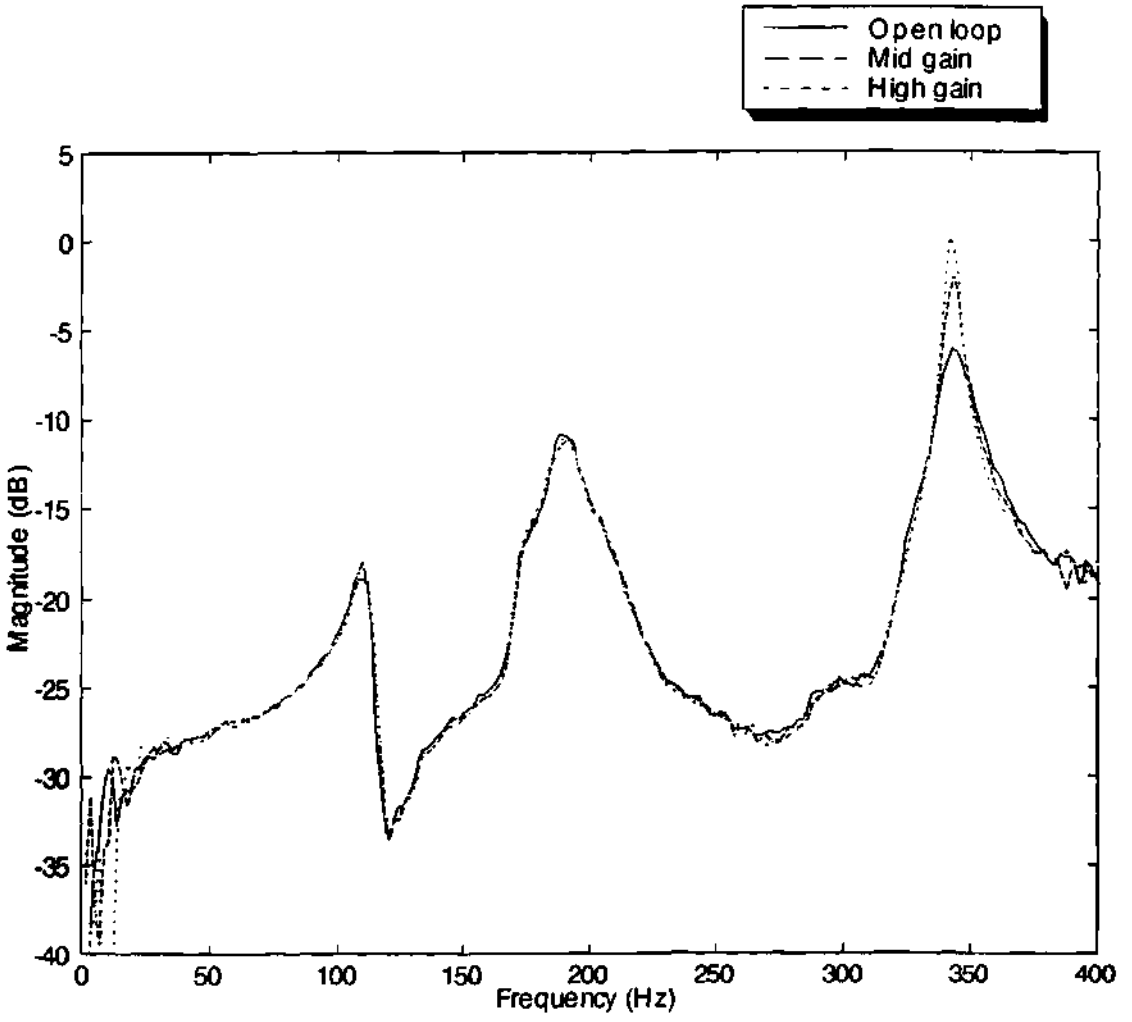

Figure 4.23 - Direct implementation of objective 1 with varying gain

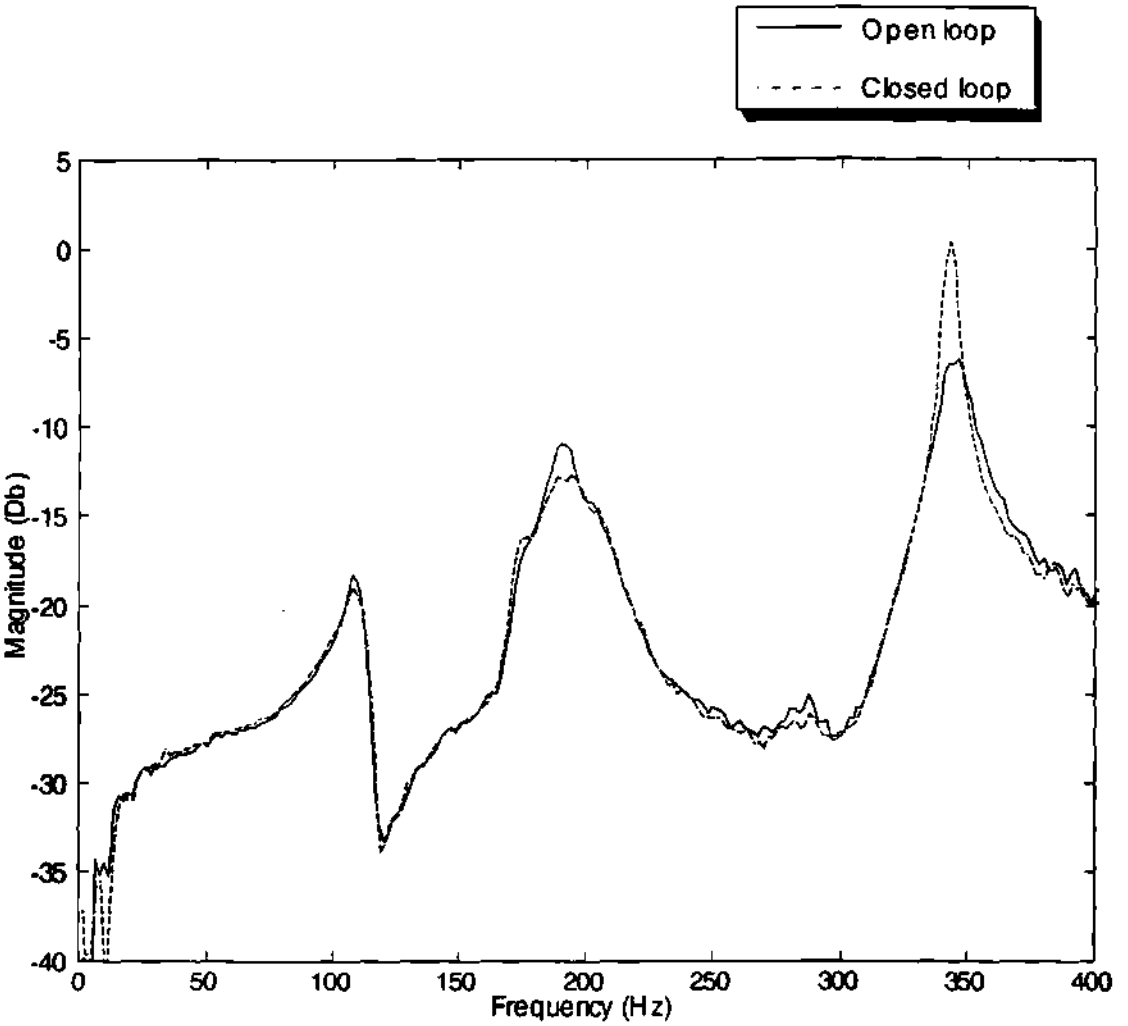

Figure 4.24 - Direct implementation of objective 3

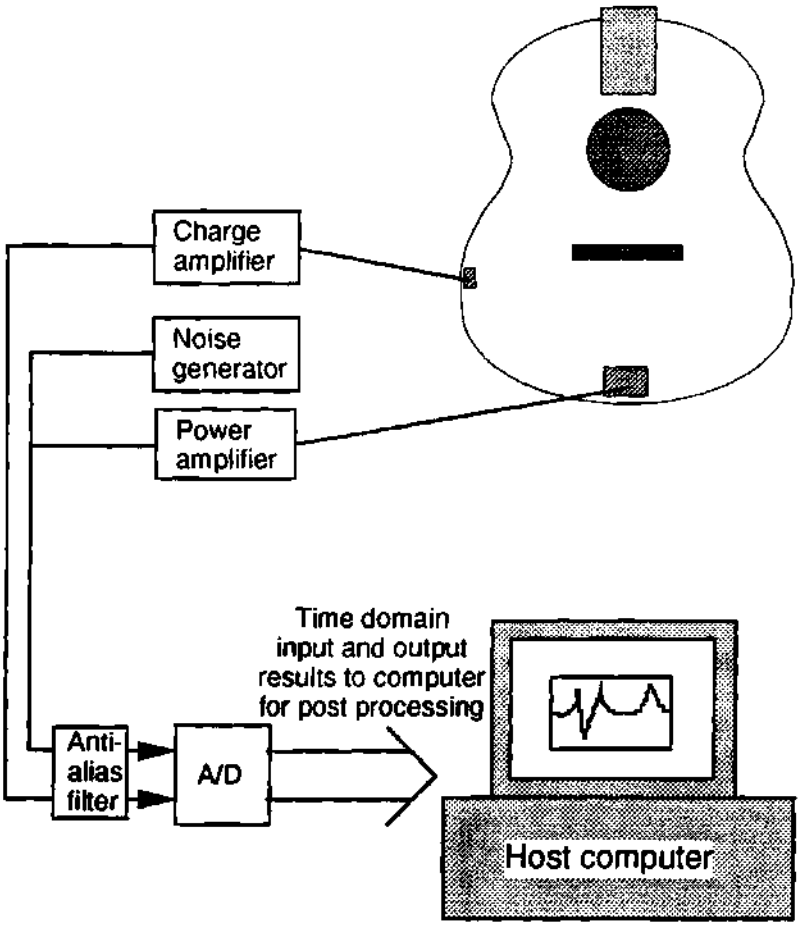

Figure 4.25 Experimental schematic for system identification

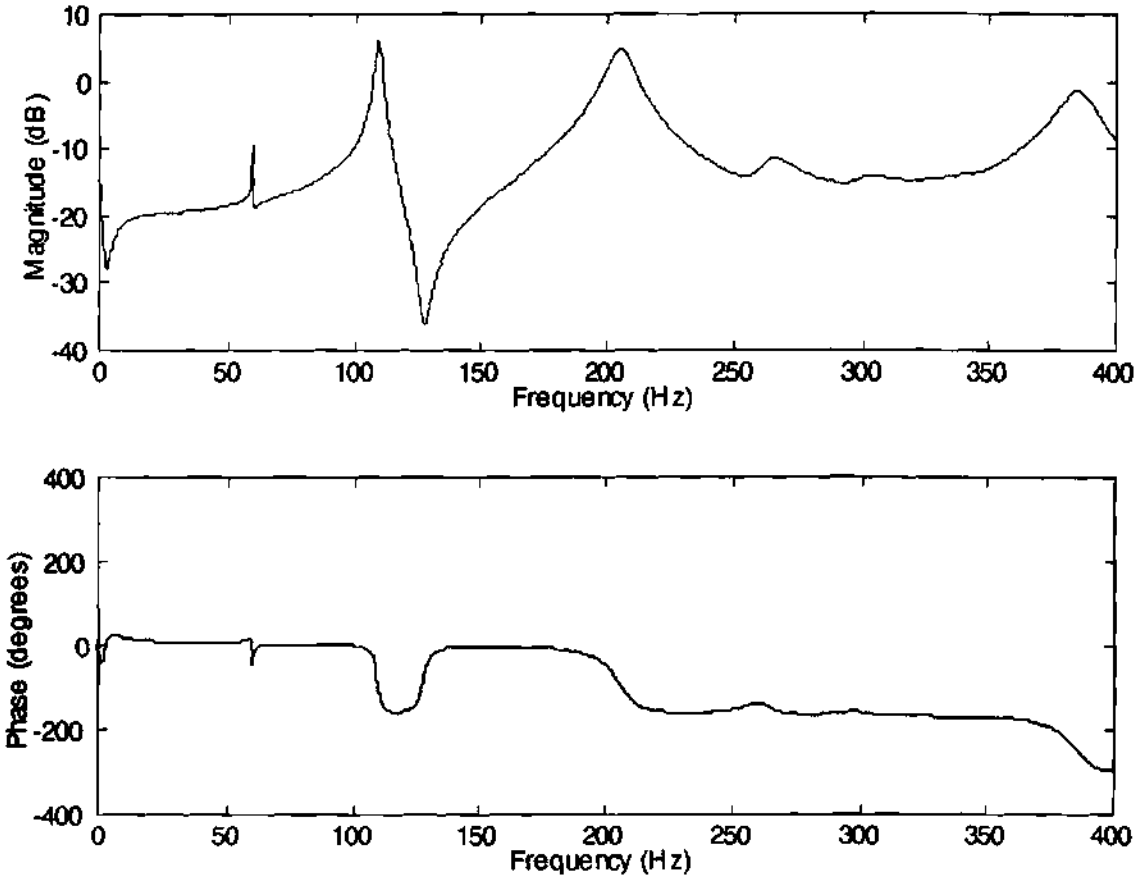

Figure 4.26 - ARMA model representation of transfer function

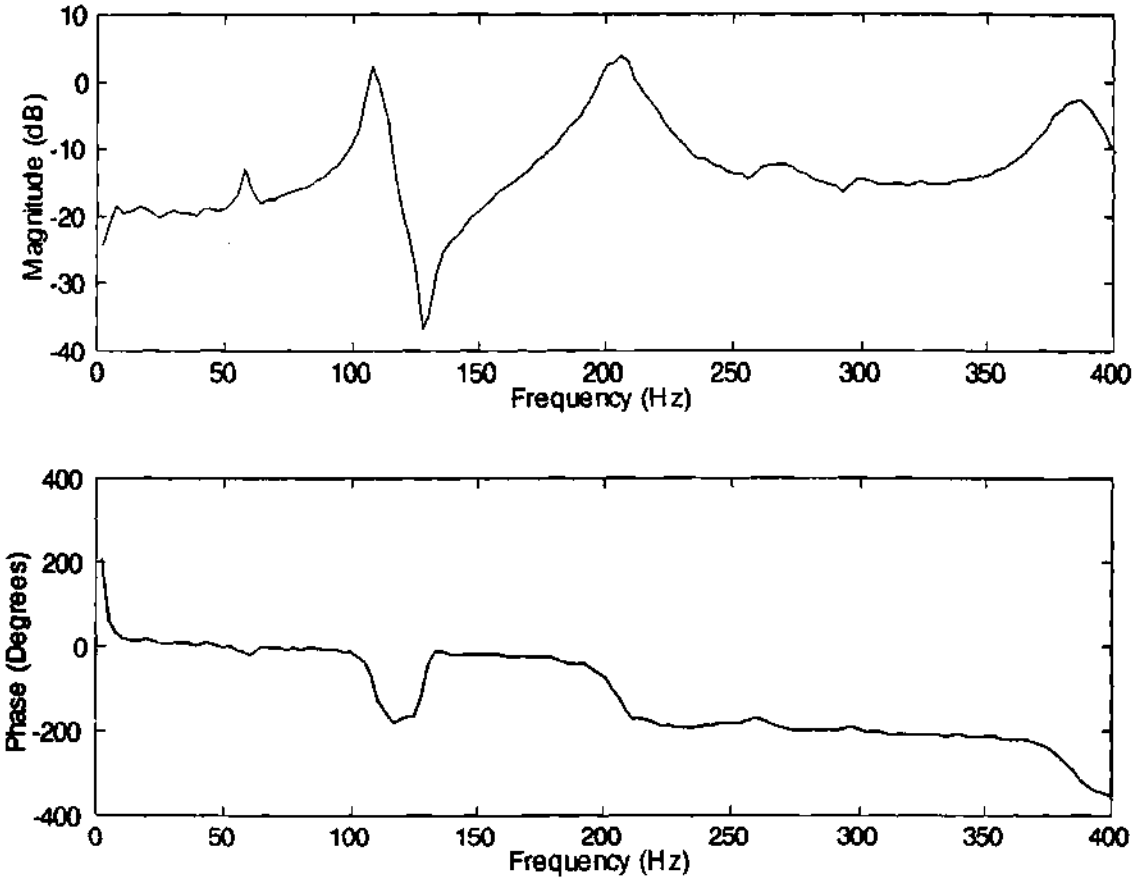

Figure 4.27 - FFT based measurement of transfer function

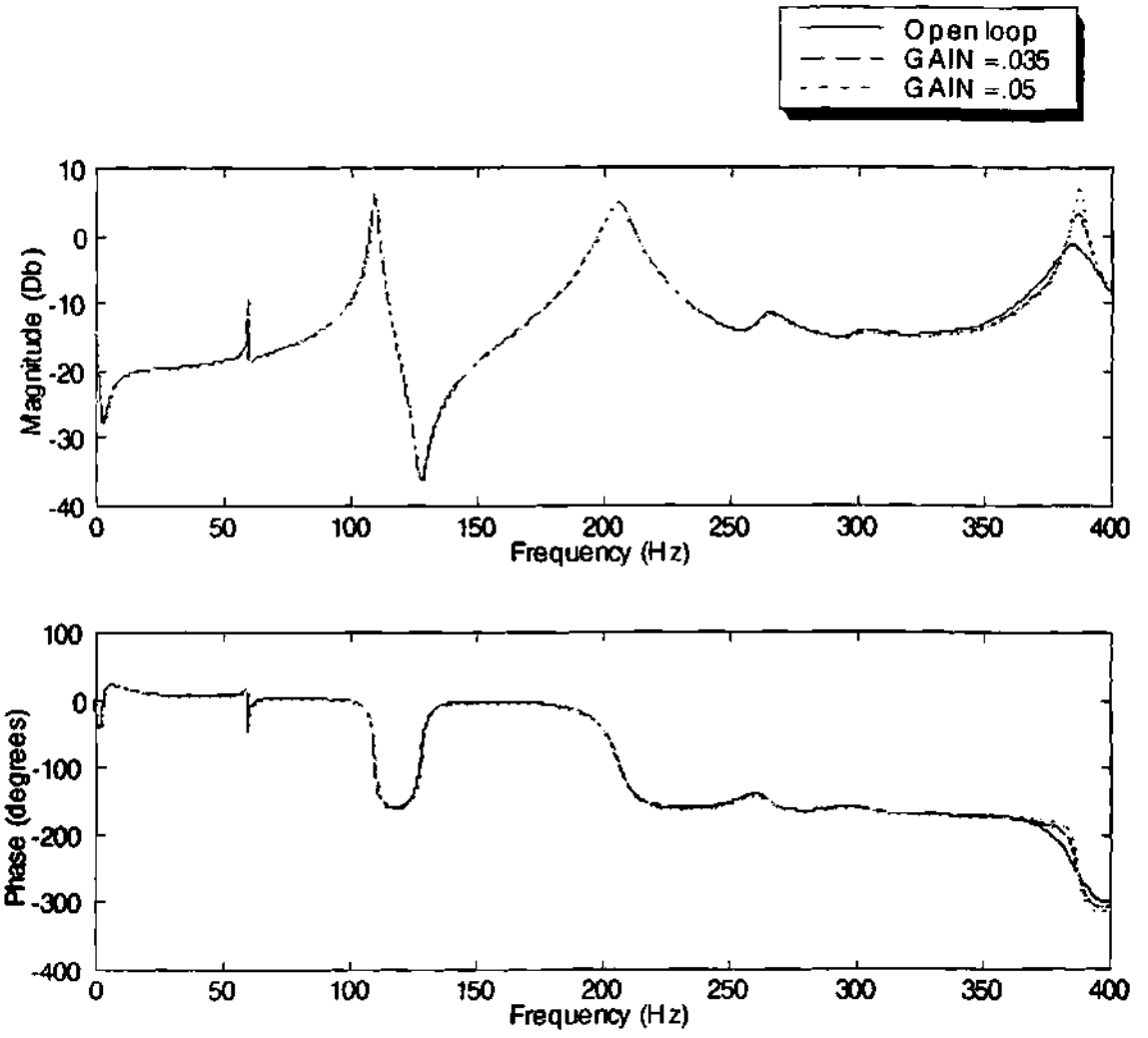

Figure 4.28 - Simulated implementation of objective 1 with varying gain

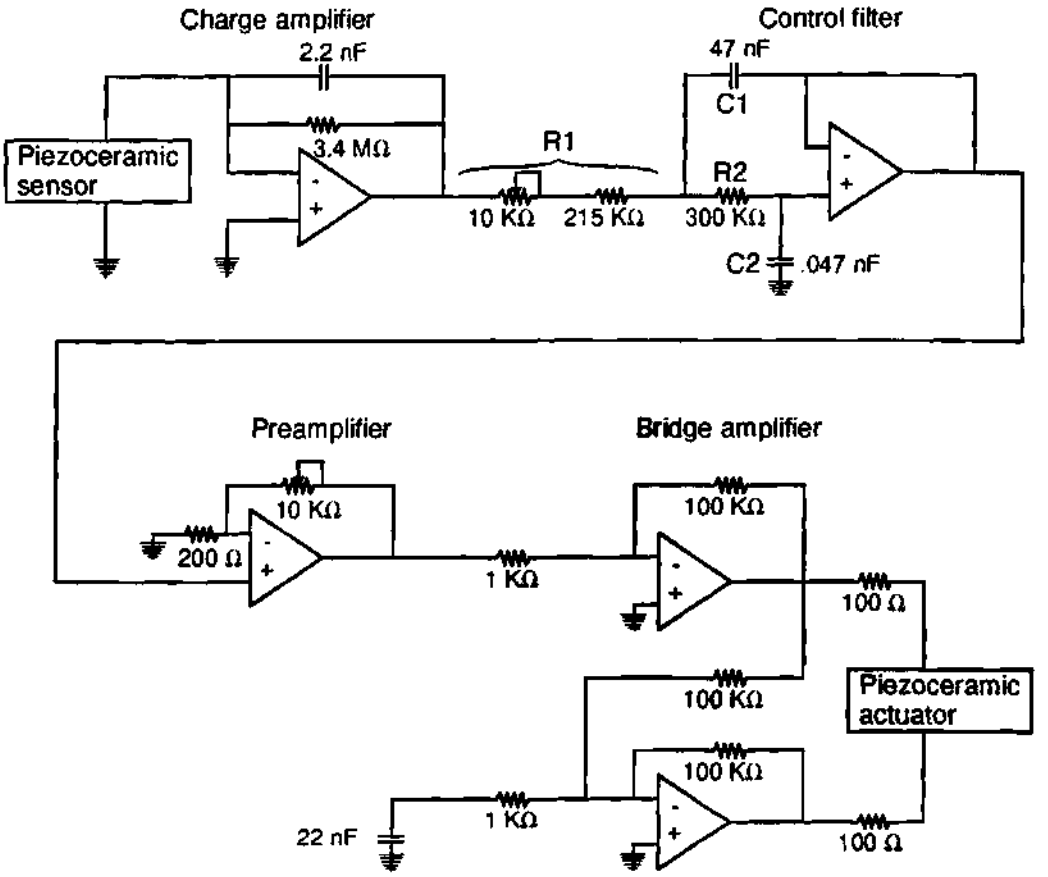

Figure 4.29 Schematic of portable control box

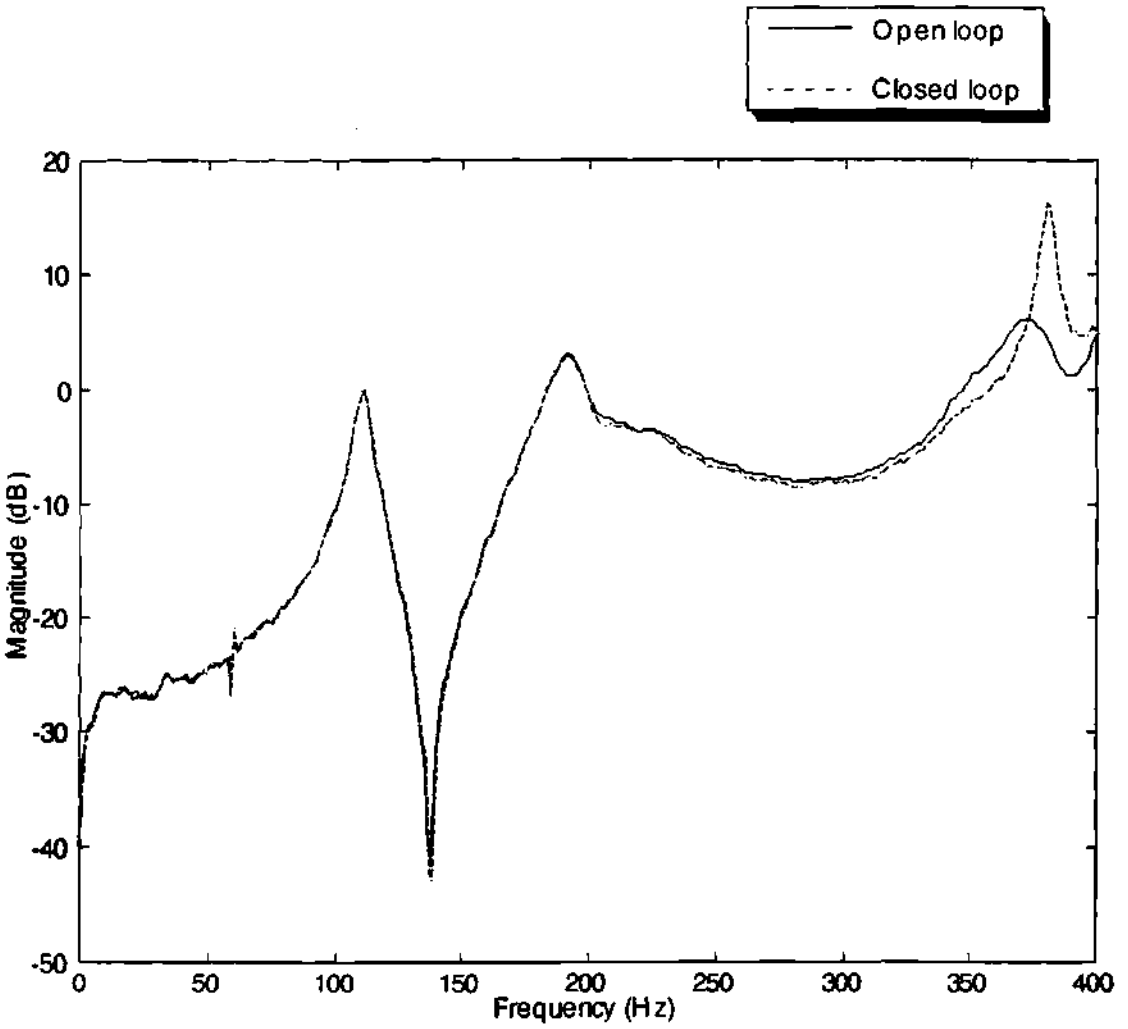

Figure 4.30 - Measured open and closed loop structural transfer function

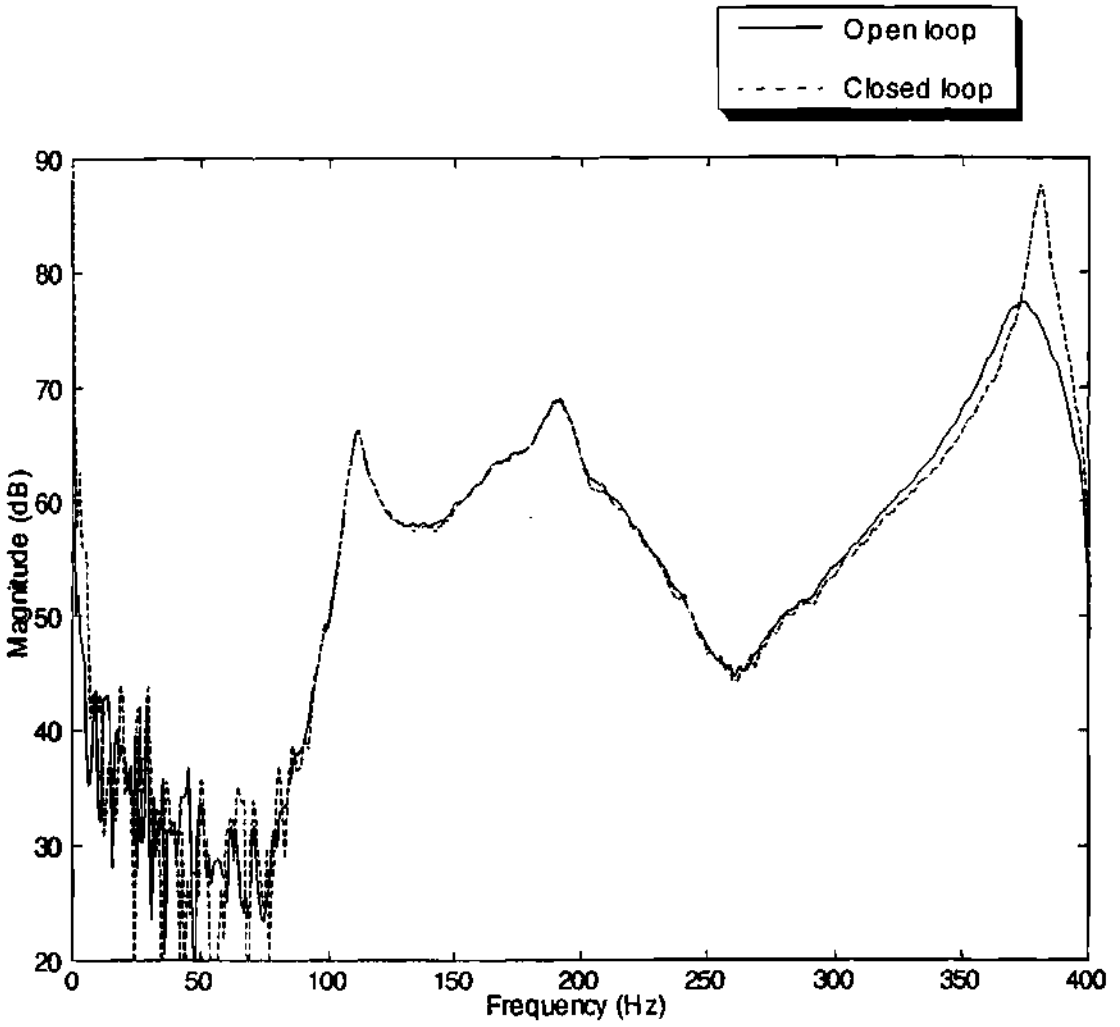

Figure 4.31 - Measured open and closed loop SPL

CHAPTER V

APPLICATION TOWARD COCKPIT PANEL

An aerospace example of a cavity backed plate is the cockpit or cabin of an aircraft. In this case, the flexible plate may be a window or structural panel. The primary issue, related to this research, is noise inside the aircraft that originates either through transmission through the flexible plate or through noise generation from the flexible plate induced by mechanical vibration. A secondary, but related, issue is noise generation by the plate directed outside the cavity toward a ground-based observer. Aspects of both issues can be examined within the constructs of the model developed in Chapters 2 and 3. In this chapter, the noise transmission issue is studied with the goal of suppressing transmitted noise using the classical frequency response-based control, and experimental verification is presented (5.1). The second issue of noise generation directed toward an observer is investigated with the goal of changing the acoustic signature that is produced by the vibrating plate received by an observer. This is done using the pole placement technique and predicted results are presented (5.2).

5.1 Noise Transmission Reduction

Noise transmission reduction using smart structural actuation or even direct structural actuation with feedback control is relatively new in the literature. The advantage to feedback control is the ability to control a broadband disturbance while the disadvantage is that more information must be known about the system as compared to an adaptive feedforward approach such as the LMS algorithm control [37]. Of the references that could be found using active techniques to control sound propagation into an enclosed cavity through a plate with smart structural actuation [54-59], only one looked at what could be considered a broadband disturbance, and no experimental papers on this topic could be found. The problem of broadband noise transmission reduction through a smart, rectangular cavity-backed plate [95] is considered here. The disturbance is assumed to be approximately plane so that the pressure, at a given time, is uniform over the plate. Within the framework of acoustic replication, the plate will be made to behave as a target plate that does not transmit the disturbance as well into the cavity. Stated as a control objective, this can be done directly by increasing the damping of the structural plate mode or modes that are responsible for the majority of the noise transmission. In this part of the study, the analytical model was used as a guide for placement of the sensors and actuators. Otherwise, the control design using the classical frequency response-based method was based on the measured transfer function.

With the assumption of a uniform pressure disturbance, the only modes expected to be excited in the plate were symmetric. This can be seen by looking back at the undamped, plate equation from Chapter 2 with a uniform external pressure disturbance as the only forcing term

$$D\nabla^4 w + \rho\ddot{w} = P_p. \qquad (5.1)$$

The coupling of the disturbance with the motion of the plate can be calculated by assuming a modal solution in an analogous fashion to the treatment of the continuous model in Chapter 2. First, a solution is assumed of the form $w = \sum_{i=1}^{n} \eta_i \phi_i$. This is substituted into Equation 5.1 and the equation is multiplied by ϕ_j, integrated over the domain of the plate and combined with the orthogonality conditions for the plate. The resulting equation is

$$\int_S \phi_j^2 dS(\rho\omega_j^2\eta_j + \rho\ddot{\eta}_j) = P_p \int_S \phi_j dS. \qquad (5.2)$$

From this result, only symmetric modes should be excited by the pressure disturbance since they make the integral term on the right hand side of Equation 5.2 nonzero. Further, of all the symmetric plate modes, only the first one has no nodal lines, meaning the entire plate surface has the same sign for z. This gives the largest value of the integral term on the right hand side of Equation 5.2. Based on this, the sensor and actuator position were selected using the summed curvature of the first mode only. The dimensions of the plate selected for the noise transmission experiment were: Lx = 0.5 m, Ly = 0.33 m, and thickness t = 3 mm. The plate was made of plexiglass material. The piezoceramic sensor and actuator positions, based on the first mode summed curvature results, are shown in Figure 5.1. All piezoceramic sensors and actuators used were 0.254 mm thick G1195. Piezoceramics 1-4 were 4.5 cm x 7 cm and 5-6 were 3 cm x 4.5 cm.

Initial transfer functions and control results were measured using the Genrad model 2515 dynamic signal analyzer with the plexiglass plate mounted in a wood frame and clamped to two cinder blocks as shown in Figure 5.2 which also shows the experimental schematic. The cinder block-wood frame combination was meant to simulate a clamped boundary condition for the plexiglass plate. The first transfer function was measured with piezoceramics 1-4 wired electrically in parallel and used as actuators with piezoceramic 5 used as a sensor. This corresponds to switch 1 in position "a" and switch 2 open in Figure 5.2. The result is shown in Figure 5.3. Since the transfer function was relatively simple, an approximate transfer function was formulated based on the estimated damping and frequencies of the poles in the measured transfer function. This approximate transfer function is

$$\frac{1x10^{15}}{s^6+204.2s^5+1.372x10^6s^4+1.576x10^8s^3+5.116x10^{11}s^2+1.707x10^{13}s+3.11x10^{16}}.$$

and is shown graphically in Figure 5.4. A low pass filter was designed with the goal of adding damping to the first pole. The transfer function of the low pass filter is

$$\frac{GAIN\times 7.589x10^4}{s^2+181.2s+7.589x10^4}.$$

The predicted control results, using the approximate transfer function, for varying GAIN values of 2 and 5 are shown in Figure 5.5. An analog control filter was built based on these results with a fine tuning adjustment for small

changes in frequency of the first mode. The filter was verified by closing the loop between actuator piezoceramics 1-4 and sensor piezoceramic 5 while using piezoceramic 6 as a white noise disturbance actuator. This corresponds to switch 1 in position "b" and switch 2 closed. The magnitude of the open and closed loop transfer functions between the disturbance actuator and the sensor are shown in Figure 5.6. Note that the actual open and closed loop transfer functions do not match those in Figure 5.5 since the transfer function is taken using a different actuator as the disturbance, but the suppression of the first mode is common to both figures.

The instrumented window was then bolted to the acoustic cavity. A gasket was included, between the window and the cavity, to insure a tight seal. The cavity is lined with acoustically absorbent material to suppress cavity resonances and to prevent transmission of sound at locations other than the plexiglass window. The inside dimensions of the cavity are 1.1 m long, 0.61 m deep, and 0.61 m high. A large loudspeaker was placed 0.3 m from the window to be used as a disturbance and a microphone was mounted inside the cavity to measure transmitted sound. This setup is shown in Figure 5.7. The electrical schematic of the control electronics is given in Figure 5.8. The loudspeaker was driven with a broadband noise source and the resulting sound pressure level was measured with the control loop on and off at the microphone location inside the box. The control filter cutoff frequency had to be tuned slightly to account for the shift of the first resonant frequency of the plate from 43.75 Hz to around 50 Hz. The resulting open and closed loop sound pressure levels as well as that of the noise directly in front of the loudspeaker source are shown in Figure 5.9. It is evident from the open loop result that assuming the first mode would be most heavily coupled

with a uniform pressure disturbance was valid since the vast majority of the sound is transmitted at the first mode frequency. The closed loop result shows that actively damping the first mode suppresses the noise transmitted by 9 dB at this frequency. Also, closing the loop accounts for an increase in the transmitted noise below the controlled resonance of a maximum of about 12 dB. However, even with the increase in amplitude that takes place below the resonance the level is still below the threshold of human hearing whereas the effect at the resonance frequency is to decrease an audible sound significantly [11].

5.2 Acoustic Signature Modification

There are also potential aerospace applications of acoustic replication where the control objective isn't necessarily silence. One reason for changing the acoustic signature of an aircraft might be to thwart efforts to recognize the aircraft based on that signature [90]. Another reason might be that the control effort involved in mimicking a relatively quiet aircraft could be less than that required for all out noise suppression. No references could be found that explored a control objective other than suppression of transmitted or radiated sound from a smart structure. The problem of changing, without necessarily suppressing, the predicted sound pressure level at a microphone position outside the acoustic cavity due to a mechanical excitation of the cavity-backed plate is considered here. The pole placement technique is employed to change the damping and the frequencies of the first and second plate modes.

The state space model for the plate used to illustrate acoustic signature modification was the same as that used for the discrete model plate

described in Appendix B. It was assumed that the cavity was not vented and that cavity modes were suppressed by acoustic lining in the cavity in the frequency range of interest. In lieu of an exact formulation of how panels or windows might be excited on an aircraft due to mechanical vibration, excitation of the plate was assumed to be due to an out-of-plane actuation source at the location shown in Figure 5.10. This excitation was assumed to vibrate the plate and cause sound to propagate away from the cavity where it is measured by a microphone at an observation point. An experimental schematic would look similar to Figure 5.7 except the plate would be excited by a shaker and the microphone would be outside the cavity.

The pole placement technique described in Chapter 3 was used to shift both the real and the imaginary part of the poles making up the structural/acoustic modes in a way that would obviously change the measured SPL due to the disturbance, the plate's acoustic signature. This was done by adjusting both the real part, σ, and the imaginary part, ω, of the poles. This had the desired effect of changing the damping and the damped natural frequency of the poles. The poles were changed from $-41.402\pm2159.33i$ and $-69.5\pm1032.55i$ to $-91.402\pm2284.99i$ and $-39.5\pm718.396i$ respectively. The predicted open and closed loop structural transfer function between the piezoceramic sensor and piezoceramic actuator are shown in Figure 5.11. The discretized version of the Rayleigh integral, as developed in Chapter 2, was then used to predict both the open and closed loop SPL due to a 1 N force input over the frequency range shown at a microphone location x= 1.17 m , y= 1.17 m, and z= 1 m with reference to the axes defined in Figure 5.10. The result is shown in Figure 5.12. The closed loop response shows a shift in maximum amplitude from the

second mode to the first mode due to a decrease in first mode damping and an increase in the second mode damping respectively. In addition the damped natural frequency of the first mode is shifted down and the second mode is shifted up.

5.3 Cockpit Panel Application Summary

The concept of acoustic replication was demonstrated to have potential application in reducing noise transmission into and modifying the acoustic signature of an aircraft cockpit. In the noise transmission reduction study, it was shown experimentally that actively increasing the damping of the first symmetric mode of a "smart" panel reduced broadband noise transmission by 9 dB near the resonant frequency of the symmetric mode. This was at the expense of an increase in noise transmission below the resonant frequency. In the acoustic signature modification study, it was shown analytically that it was possible to significantly change the acoustic signature of a "smart" panel using active structural/acoustic control.

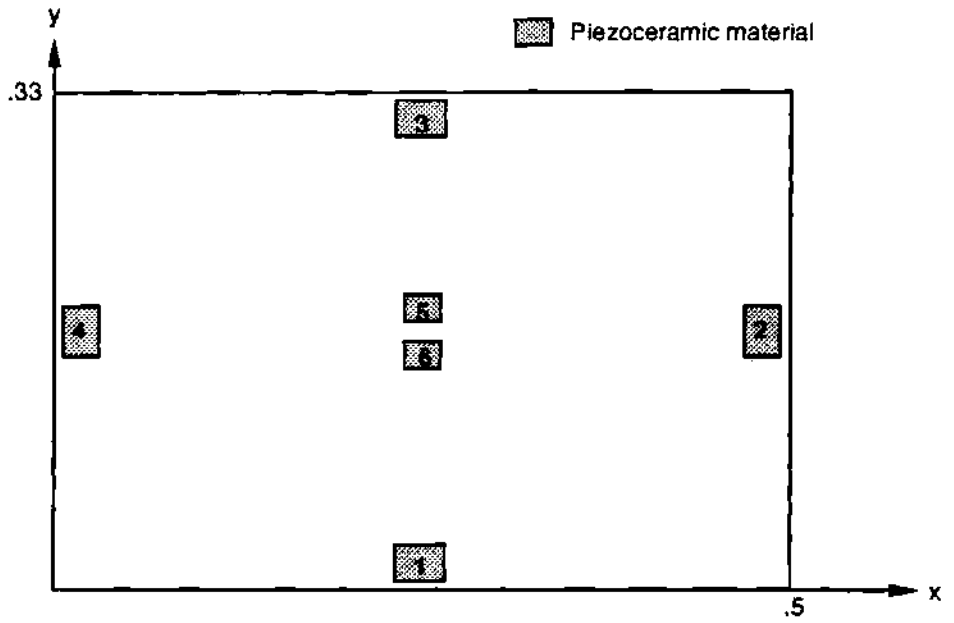

Figure 5.1 Sensor and actuator positions

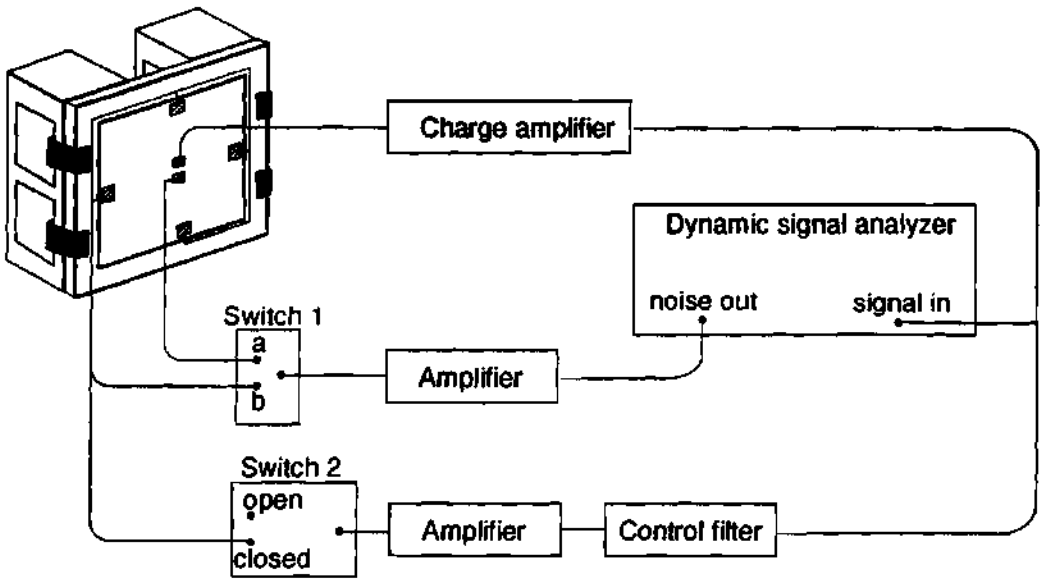

Figure 5.2 Experimental schematic for measuring initial transfer functions

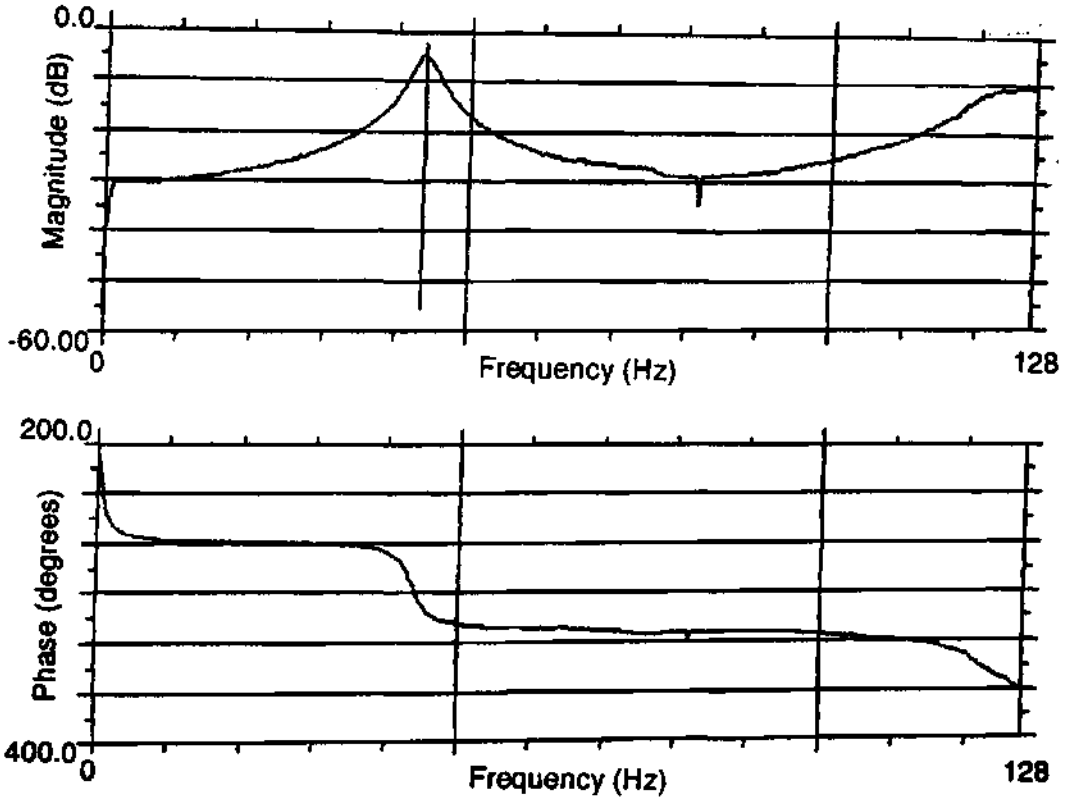

Figure 5.3 Measured transfer function between actuators 1-4 and sensor 5

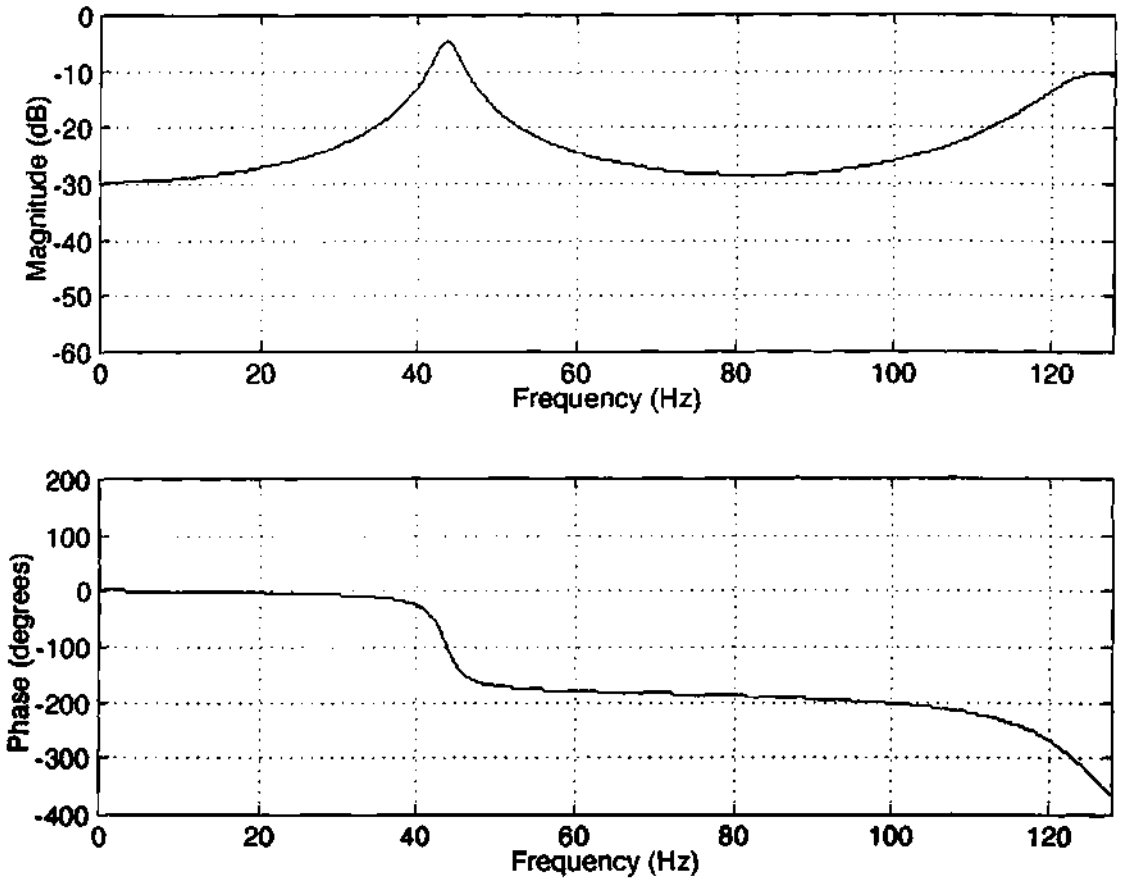

Figure 5.4 Approximate smart window transfer function

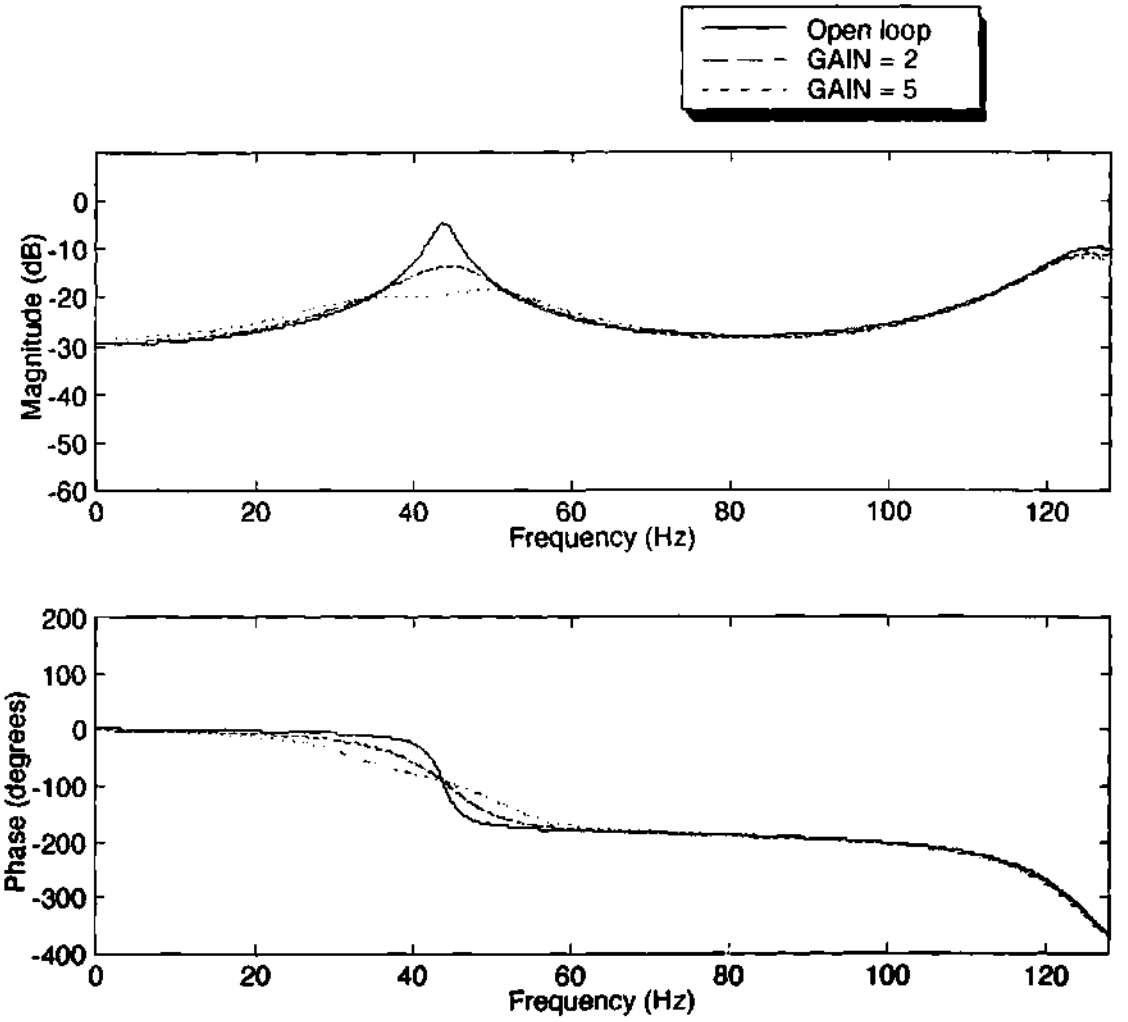

Figure 5.5 Predicted open and closed loop transfer function for varying gain values

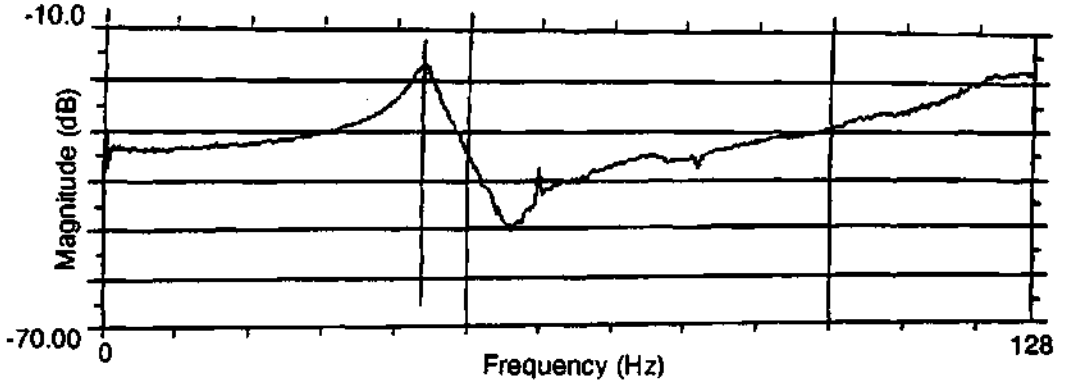

a. Open loop

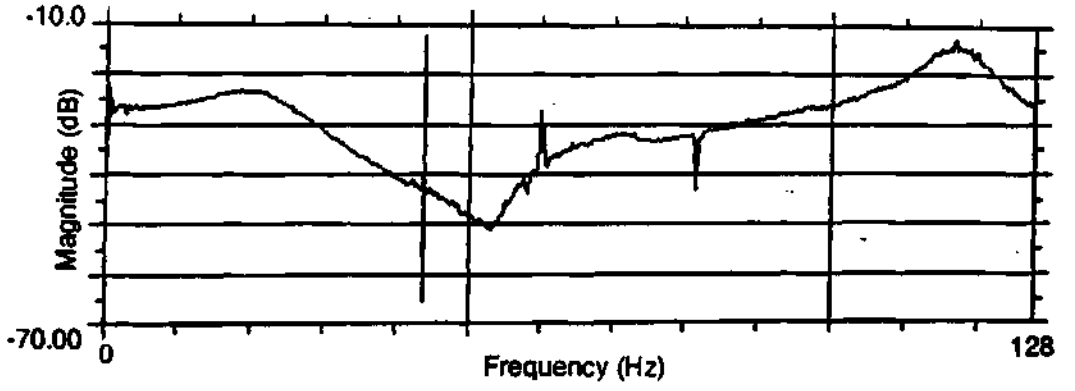

b. Closed loop

Figure 5.6 Measured open and closed loop transfer functions between actuator 6 and sensor 5

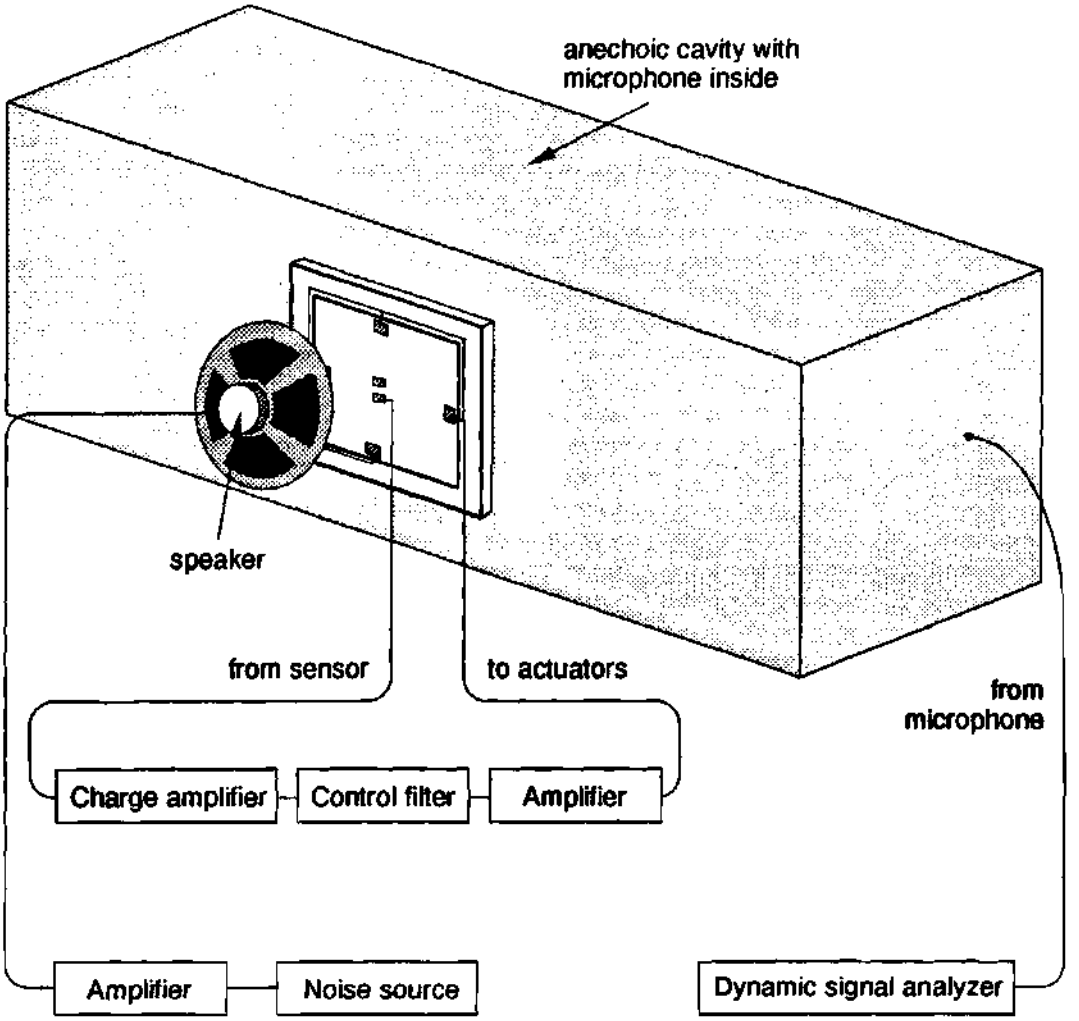

Figure 5.7 Noise transmission experimental schematic

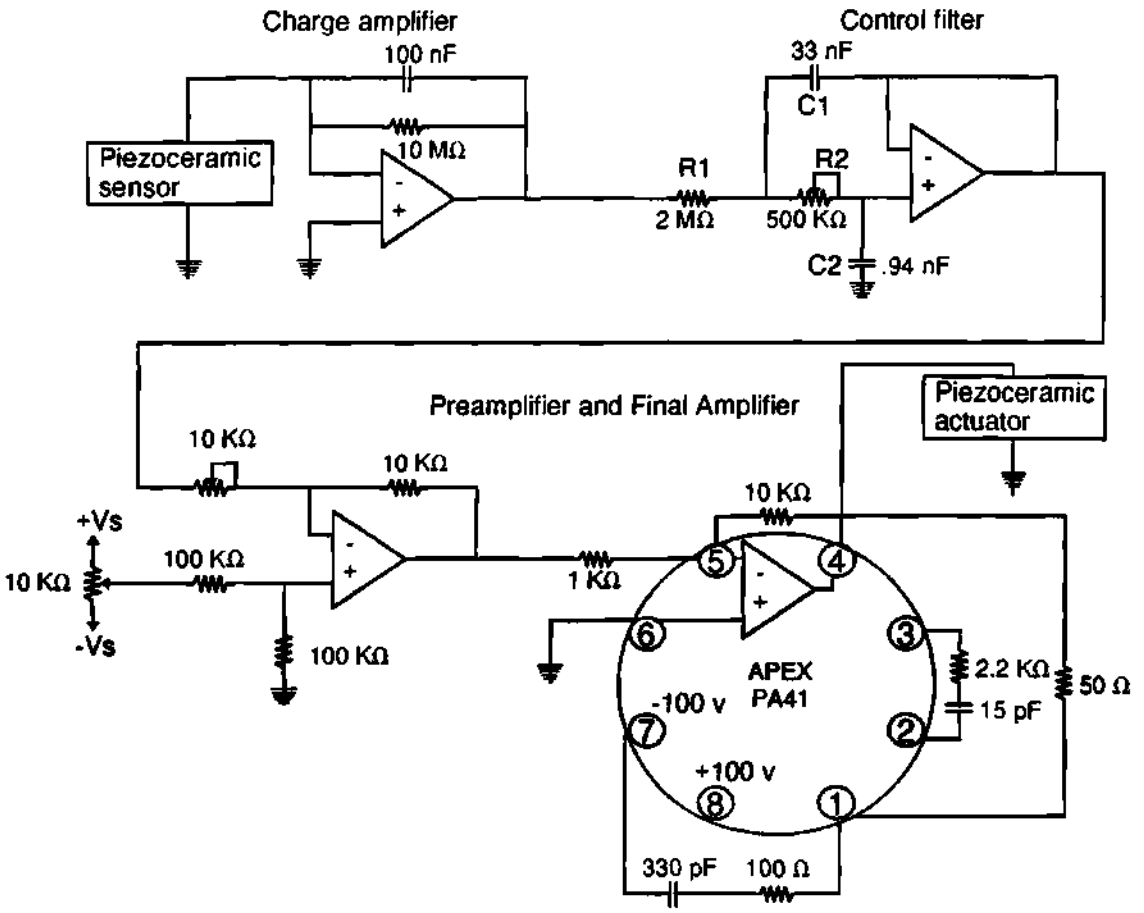

Figure 5.8 Schematic of control circuit for smart window

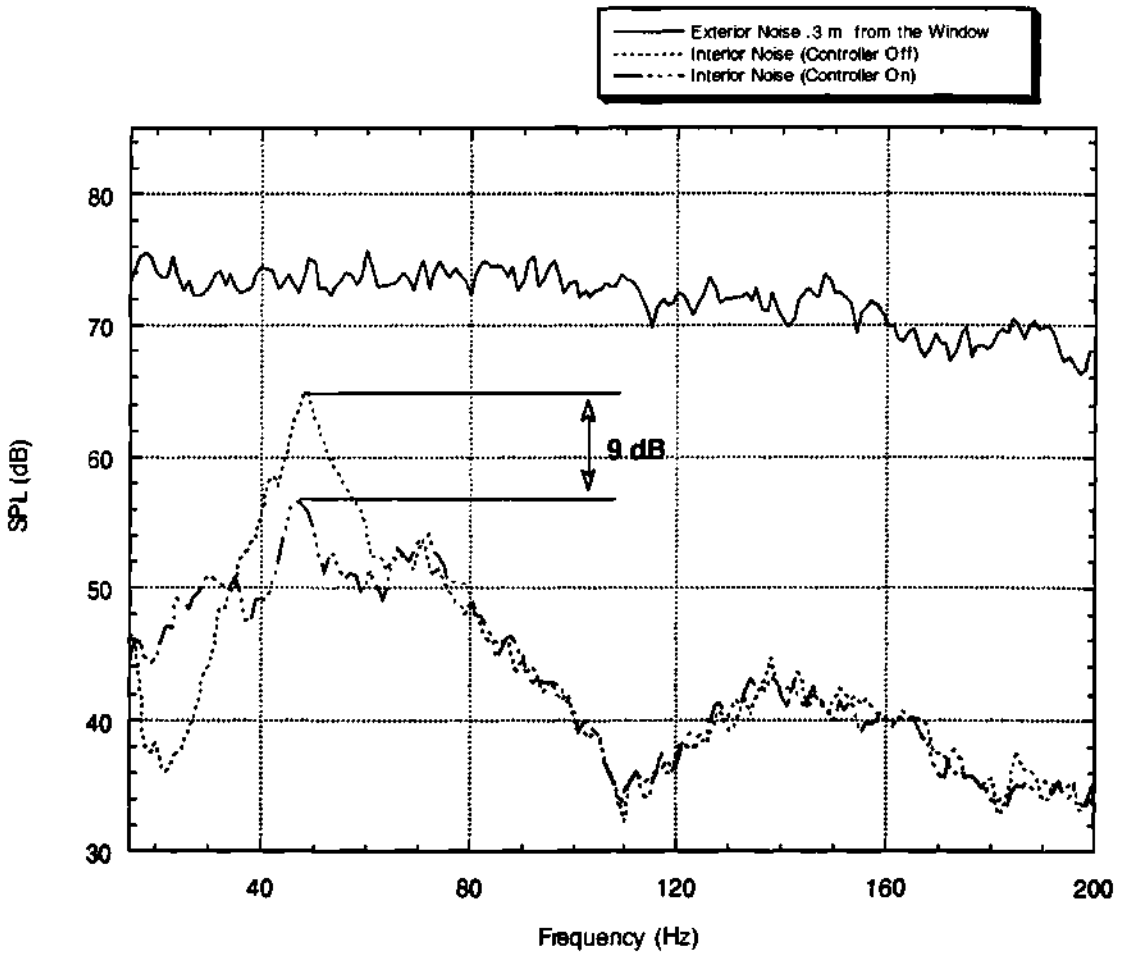

Figure 5.9 Noise transmission results

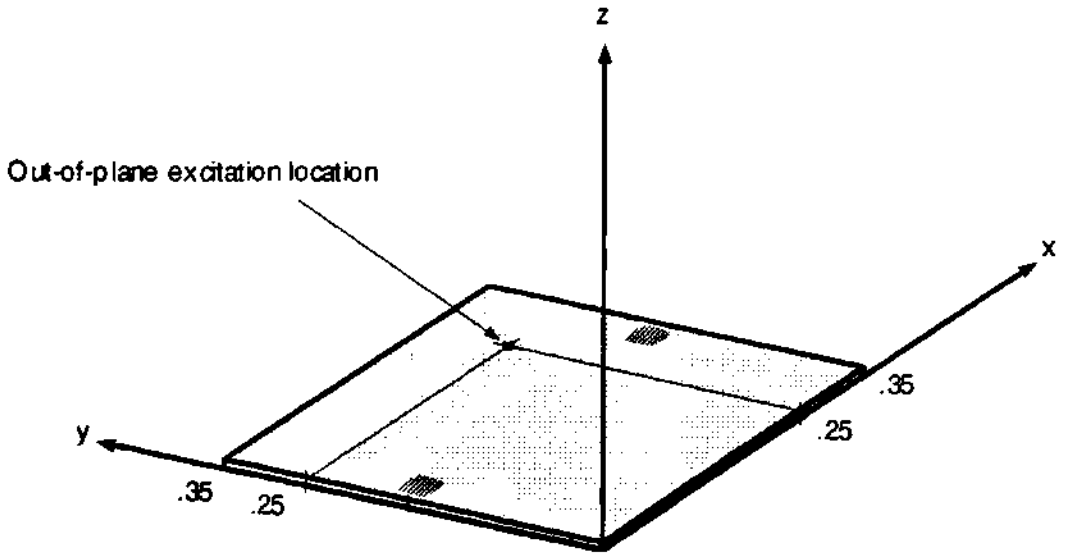

Figure 5.10 Location of out-of-plane excitation

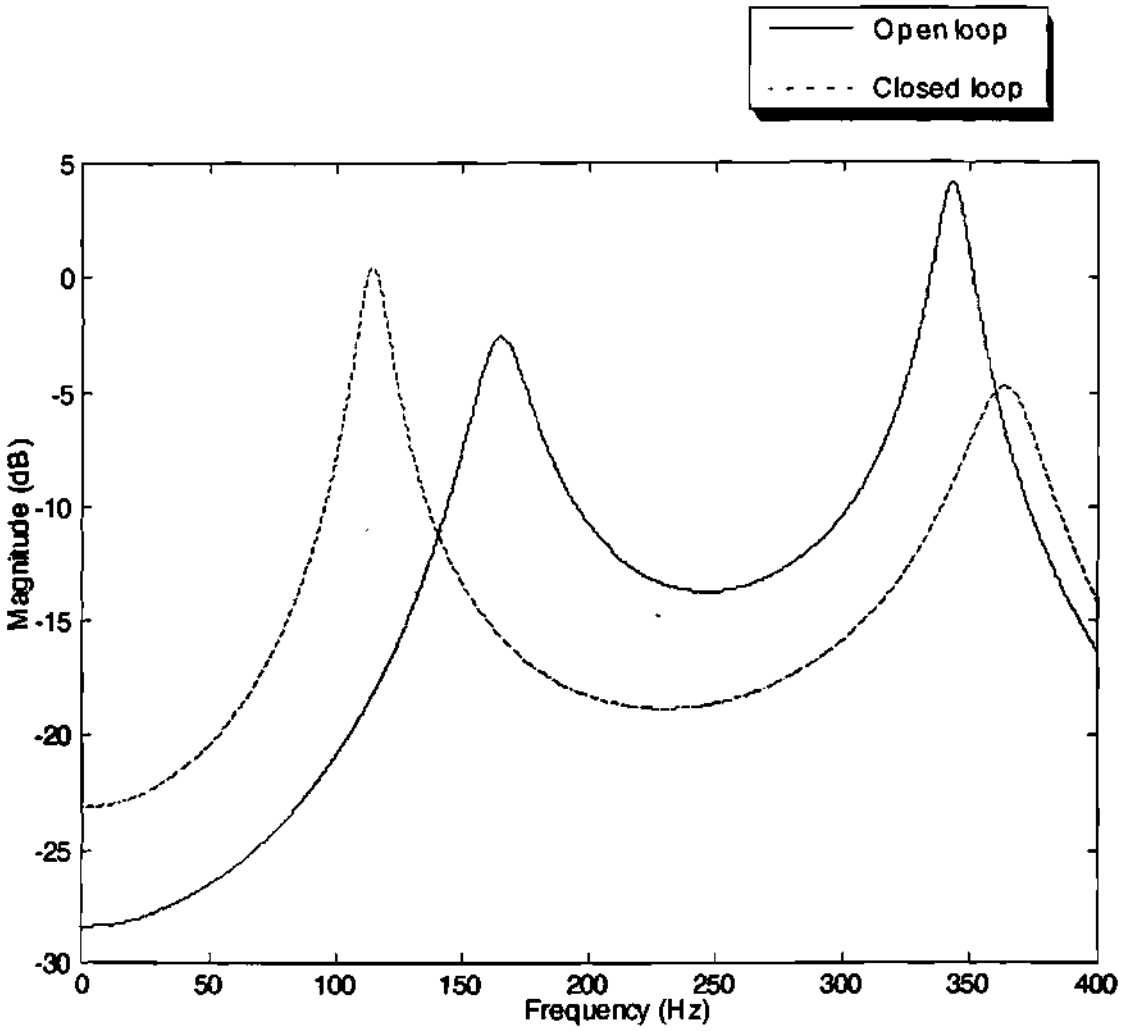

Figure 5.11 - Open and closed loop structural transfer function

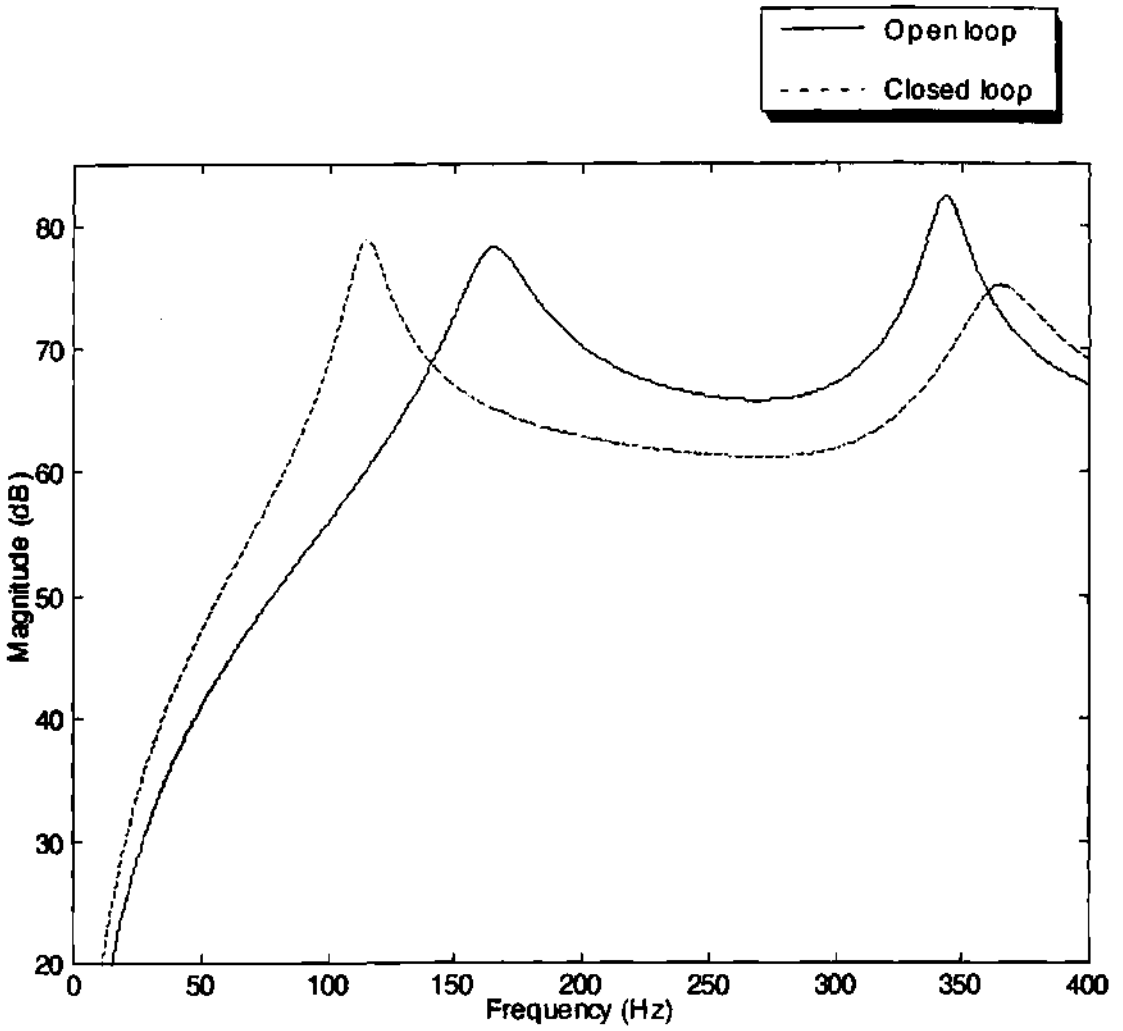

Figure 5.12 - Open and closed loop SPL

CHAPTER VI

CONCLUSIONS AND RECOMMENDATIONS

In this document, the development and solution of three problems of interest in aerospace and other commercial applications are described. In addition, two specific applications are explored, including experiments that confirmed the theoretical development. New research and applications are investigated which had not previously been fully developed. Moreover, this work lays the foundation for future work employing smart structures and structural/acoustic control with the goal of acoustic replication.

6.1 Continuous Model of Cavity-Backed Plate

A spatially continuous structural/acoustic model of a clamped, circular plate backed by a rigid, vented cavity was developed. A Rayleigh integral was used to predict acoustic pressure resulting from both symmetric and antisymmetric plate modes. Pressure resulting from the movement of air in and out of the vent was also included in the model. Inclusion of the effect of antisymmetric plate mode movement was important since this movement has been shown to be an important factor in determining quality in the acoustic guitar application, and past models did not include it. This model could be used, in future studies, to investigate how passive changes in the design of an acoustic guitar affect the sound the instrument makes.

6.2 Discrete Model of Cavity-Backed Plate with Piezoceramics

A spatially discrete structural/acoustic model of a clamped, rectangular plate backed by a rigid, vented cavity was developed. The discrete approach allows solution of complicated problems such as anisotropic plates and plates with varying end conditions using FEM. This approach was also shown to be well suited to the incorporation of piezoceramic sensors and actuators into the model. A discretized form of the Rayleigh integral was used to derive a transfer function between the voltage applied to a piezoceramic actuator mounted on the plate and the resulting acoustic pressure due to movement of the structure and air in the vent. The sensor and actuator modeling approach has the benefit of using FEM to solve the electrically passive, structural part of problem, including piezoceramic and substructure mass and stiffness. This result, along with modal superposition, yielded a state space model of low enough order to be suitable for control design. Future experimental work measuring piezoceramic actuation of plates with relatively low stiffness would be helpful to resolve discrepancies between this work and past models when the plate substructure modulus was relatively low. This is important since plates with relatively low stiffness may be used in acoustic applications.

6.3 Control Approaches for Acoustic Replication

An experimental procedure was introduced for finding good actuator positions for control of structural/acoustic modes. This procedure was based on the reciprocity between measured in-plane motion at a candidate actuator location due to an out-of-plane excitation and measured out-of-plane motion

at the excitation location due to in-plane actuation at the candidate position. Pole placement and a classical frequency response-based method were shown to be effective for control objectives that involved changing damping and frequency of structural/acoustic modes, including intentional enhancement as well as suppression. Regarding acoustic replication, it was necessary to translate desired structural/acoustic properties into specific control objectives. Future approaches would benefit from development of a more autonomous approach, such as the use of a neural network to automatically identify a controller that optimally matches the acoustic radiation of a smart structure to that of a target structure with desired acoustics. However, the control techniques explored in this work are important, even in the context of a more autonomous approach, to define what is a viable target. Finally, future control approaches should also investigate the inclusion of uncertainties in the guitar model in the control approach.

6.4 Acoustic Guitar Application

Structural/acoustic control in a "smart" acoustic guitar was shown to be a means of favorably adjusting factors that ultimately determine quality. This has the potential to make an inexpensive instrument sound like an expensive instrument or to make an instrument with many sounds that correspond to different control laws. Future models could exploit the power of FEM code to obtain a more exact model of the structure, thus increasing the frequency range of modeled behavior to frequencies with more spatially complex mode shapes. An expanded treatment of cavity modes may also be necessary to increase the modeled frequency range. This would also allow extension of

the concept to other acoustic instruments. Future work might also involve psychoacoustic studies comparing various control laws to determine what embodiment a commercial product may take and more experimental work examining the effects of active control on acoustic directivity.

6.5 Aircraft Cockpit Application

The concept of acoustic replication was demonstrated to have potential application in reducing noise transmission into an aircraft cockpit. Acoustic replication may be favorable in noise transmission problems because replication of a target structure might involve less control effort than all-out noise suppression. The potential of acoustic signature modification directed toward a ground-based observer was also demonstrated. Regarding intentional evading of an observer who may be attempting to identify the acoustically radiative structure, future effort may be directed at modifying the acoustic signature of maritime vehicles such as submarines, where acoustic signature is a recognized form of identification. In this case, a new model would have to be developed to account for significant fluid loading. The concept of acoustic signature modification might also have application in modifying the acoustics of windows under laser surveillance, where an observer is attempting to eavesdrop on conversation inside the building.

APPENDIX A

DISCRETE MODEL GLOBAL EQUATIONS

The discrete model for the acoustic cavity is derived by first deriving a finite element to represent each of the piezoelectric, structural, and air spring parts and then assembling a global model which includes the entire acoustic cavity. The generalized form of Hamilton's Principle [91] can be written as

$$\int_{t_1}^{t_2}[\delta(T-U+W_e-W_m)+\delta W]dt=0, \qquad (A.1)$$

where T is kinetic energy U is potential energy, W_e is electrical energy, and W_m is magnetic energy. The kinetic, potential, and electrical energy for a finite element of piezoelectric material from Equations 2.16 are

$$T=\int_{V_p}\tfrac{1}{2}\rho_p\dot{\mathbf{w}}^T\dot{\mathbf{w}}dV_p,\quad U=\int_{V_p}\tfrac{1}{2}\mathbf{S}^T\mathbf{T}dV_p \quad \text{and} \quad W_e=\int_{V_p}\tfrac{1}{2}\mathbf{E}^T\mathbf{D}dV_p. \qquad (A.2)$$

The virtual work density is given by

$$\delta W=\sigma\delta v+\delta\mathbf{w}^T\mathbf{F}, \qquad (A.3)$$

where v is the electric potential, σ is the charge density, and **F** are the applied mechanical point forces.

The piezoelectric constitutive equation can be written as

$$\begin{aligned} \mathbf{T} &= \mathbf{c}^{E}\mathbf{S} - \mathbf{eE}, \\ \mathbf{D} &= \mathbf{eS} + \mathbf{E}^{S}\mathbf{E}, \end{aligned} \tag{A.4}$$

where $\mathbf{c}^E$ is the short circuit elastic stiffness matrix, **E** is the dielectric tensor at constant mechanical strain, and **e** is the piezoelectric tensor [92]. The quantity, **E**, is more conveniently expressed in terms of the d matrix, $\mathbf{E}=\mathbf{dc}^E$, since **d** and $\mathbf{c}^E$ since these are provided by piezoelectric manufacturers.

Taking the variation of each of the quantities in Equations A.2 and substituting in Equations A.3 and A.4, we get

$$\delta T = \int_{V_p} (\rho_p \delta \dot{\mathbf{w}}^T \dot{\mathbf{w}}) dV_p, \tag{A.5}$$

$$\delta U = \int_{V_p} \delta \mathbf{S}^T \mathbf{c}^E \mathbf{S} - \frac{1}{2}(\delta \mathbf{S}^T \mathbf{e}^T \mathbf{E} + \mathbf{S}^T \mathbf{e} \delta \mathbf{E}) dV_p, \tag{A.6}$$

$$\delta W_e = \int_{V_p} \delta \mathbf{E}^T \mathbf{d} \mathbf{c}^E \mathbf{E} + \frac{1}{2}(\delta \mathbf{E}^T \mathbf{e}^T \mathbf{S} + \mathbf{E}^T \mathbf{e} \delta \mathbf{S}). \tag{A.7}$$

Combining equations A.5, A.6, and A.7 into equation A.1 and assuming that the applied charges, body forces, and magnetic energy are zero gives

$$\begin{aligned} &\int_{V_p} -(\rho_p \delta \mathbf{w}^T \ddot{\mathbf{w}}) - \delta \mathbf{S}^T \mathbf{c}^E \mathbf{S} + \frac{1}{2}(\delta \mathbf{S}^T \mathbf{e}^T \mathbf{E} + \mathbf{S}^T \mathbf{e}^T \delta \mathbf{E}) + \\ &\delta \mathbf{E}^T \mathbf{d} \mathbf{c}^E \mathbf{E} + \frac{1}{2}(\delta \mathbf{E}^T \mathbf{e}^T \mathbf{S} + \mathbf{E}^T \mathbf{e} \delta \mathbf{S}) dV_p + \delta \mathbf{w}^T \mathbf{F} = 0. \end{aligned} \tag{A.8}$$

After some algebra, Equation A.8 reduces to

$$\int_{V_p}((\rho_p\delta\mathbf{w}^T\ddot{\mathbf{w}})+\delta\mathbf{S}^T\mathbf{c}^E\mathbf{S}-\delta\mathbf{E}^T\mathbf{e}^T\mathbf{S}-\mathbf{E}^T\mathbf{e}^T\delta\mathbf{S}-\delta\mathbf{E}^T\mathbf{d}\mathbf{c}^E\mathbf{E})dV_p+\delta\mathbf{w}^T\mathbf{F}=\mathbf{0}. \tag{A.9}$$

The strains and the electric field can be expressed in terms of the nodal values of displacement and electric potential as

$$\begin{aligned}\mathbf{S}&=\mathbf{B}_w\mathbf{w}_i,\\ \mathbf{E}&=-\mathbf{B}_v\mathbf{v}_i,\end{aligned} \tag{A.10}$$

where the vector $\mathbf{v}_i$ and $\mathbf{w}_i$ are related to the continuous potential and displacements by

$$\begin{aligned}\mathbf{w}&=\mathbf{f}_u\mathbf{w}_i,\\ \mathbf{v}&=\mathbf{f}_v\mathbf{v}_i.\end{aligned} \tag{A.11}$$

Combining Equations A.10 and A.11 with Equation A.9 and separating each of the coefficients of the varied parameters gives the equilibrium equations for the piezoelectric element in a more compact notation as

$$\begin{aligned}\mathbf{m}_p\ddot{\mathbf{w}}_i+\mathbf{k}_{uu}\mathbf{w}_i+\mathbf{k}_{uv}\mathbf{v}_i&=\mathbf{F}_p,\\ \mathbf{k}_{vu}\mathbf{w}_i+\mathbf{k}_{vv}\mathbf{v}_i&=\mathbf{0},\end{aligned} \tag{A.12}$$

where $\mathbf{m}_p$ is the piezoelectric mass matrix, $\mathbf{k}_{uu}$ is the structural stiffness matrices, $\mathbf{k}_{uv}$ and $\mathbf{k}_{vu}$ are the piezoelectric stiffness matrices, $\mathbf{k}_{vv}$ is the dielectric stiffness matrix, and $\mathbf{F}_p$ are applied point forces. These matrices are

further defined in Table A.1. This result is consistent with the work of Allik and Hughes [42] who also derived a finite element for piezoelectric vibration using a different variational approach. The first of Equations A.12 is analogous to the actuator equation and the second to the sensor equation in reference [91].

Equations A.12 can be further simplified if the piezoceramic actuators will be used with only two opposing surfaces electroded. Further, if it is assumed that only one of the electrode surfaces is active and the other is common with ground, it is possible to define a vector of voltages applied to each actuator, $\mathbf{v}_A$ rather than the voltage applied at each node of actuator piezoceramics, $\mathbf{v}_i$. The relationship between these vectors is $\mathbf{v}_i = \mathbf{n}\mathbf{v}_A$ where $\mathbf{n}$ is a matrix of ones and zeros which maps the voltage applied to each piezoceramic onto the nodes that are common with the active surface. With this modification and the applied point forces set to zero, the first of Equations A.12 becomes

$$\mathbf{m}_p\ddot{\mathbf{w}}_i + \mathbf{k}_{uu}\mathbf{w}_i = -\Theta_A\mathbf{v}_A, \qquad \text{(A.13)}$$

where $\Theta_A = \mathbf{k}_{uv}\mathbf{n}$. Considering that the sensor piezoceramics are electroded in the same fashion, substituting $\mathbf{v}_i = \mathbf{n}\mathbf{v}_S$ into the second of Equations A.12 and multiplying both sides of the equation by $\mathbf{n}^T$ gives

$$\Theta_S^T\mathbf{w}_i = \mathbf{n}^T\int_{V_p}\mathbf{B}_V^T\boldsymbol{\epsilon}\mathbf{B}_V dV_p\mathbf{n}\mathbf{v}_S, \qquad \text{(A.14)}$$

where the definition for $\mathbf{k}_{VV}$, as given in Table A.1, has been included explicitly and $\Theta_S = \mathbf{k}_{vu}^T\mathbf{n}$. Finally, considering the shape function B_v in

Equations A.10 and A.14, if the electroded surfaces of the piezoceramic sensor are applied perpendicular to the z axis and the element considered is an eight-noded solid element, as in Figure A.1, Equation A.10 can be written explicitly as

$$\mathbf{E} = \begin{Bmatrix} E_x \\ E_Y \\ E_Z \end{Bmatrix} = -\frac{1}{4t}\begin{bmatrix} 0 & 0 & 0 & 0 & 0 & 0 & 0 & 0 \\ 0 & 0 & 0 & 0 & 0 & 0 & 0 & 0 \\ 0 & 0 & 0 & 0 & 1 & 1 & 1 & 1 \end{bmatrix} \begin{Bmatrix} 0 \\ 0 \\ 0 \\ 0 \\ v_s \\ v_s \\ v_s \\ v_s \end{Bmatrix} = \mathbf{B}_V \mathbf{v}_i. \quad \text{(A.15)}$$

With this definition for B_V, evaluation of the integral in Equation A.14 and some algebra gives

$$v_s = \frac{\Theta_s^T \mathbf{w}_i}{C_s},$$

where $C_s = \frac{\epsilon_3^s}{t} lw$ is just the blocked sensor capacitance measured across the electroded surfaces.

The base structural material is a specific case of piezoelectric material with $\mathbf{k}_{uv}=\mathbf{k}_{vu}=\mathbf{k}_{vv}=0$. The equilibrium equation is then expressed directly as

$$\mathbf{m}_s \ddot{\mathbf{w}}_i + \mathbf{k}_s \mathbf{w}_i = \mathbf{F}_p, \quad \text{(A.16)}$$

where $\mathbf{m}_s$ and $\mathbf{k}_s$ are the mass and structural stiffness matrix.

As in the continuous model, the acoustic cavity couples the plate motion to that of the entrained air mass in the rose. The air spring and the entrained air mass will be treated as one element in this simplified model of the guitar. The kinetic energy of the air element can be written as

$$T = \frac{1}{2} m_h \dot{z}^2 . \qquad \text{(A.17)}$$

The potential energy can be expressed as

$$V = \frac{1}{2} \beta (\Delta V)^2 , \qquad \text{(A.18)}$$

where $\Delta V = \mathbf{w}_i^T \mathbf{m} + S_h z$ and $\beta = \frac{\gamma P_o}{V}$ Here, as in the continuous model, the change in volume of air in the cavity is dictated by the movement of the plate and the air mass. To represent this in the discrete model, the vector $\mathbf{m}$ is defined such that the product $\mathbf{w}_i^T \mathbf{m}$ represents the volume displaced by the movement of the plate. Again, using Equation A.1, assuming W_e and W_m are zero and that there is no virtual work done in the element gives

$$[m_h \dot{z} \delta z] - m_h \ddot{z} \delta z - \beta (\mathbf{w}_i^T \mathbf{m} + S_h z)(\delta \mathbf{w}_i^T \mathbf{m} + S_h \delta z) = 0. \qquad \text{(A.19)}$$

After some manipulations Equation A.19 gives two equations of motion for the air spring element

$$\begin{aligned} & m_h \ddot{z} + \beta S_h^2 z = -\beta S_h \mathbf{w}_i^T \mathbf{m}, \\ & -\beta \mathbf{m} (\mathbf{m}^T \mathbf{w}_i + S_h z) = 0. \end{aligned} \qquad \text{(A.20)}$$

The first of equations A.20 is the equilibrium equation for the air spring element. The second must be considered along with the other coefficients of the variational parameter $\delta \mathbf{w}_i^T$ in the global equations

$$\begin{aligned} &[\mathbf{m}_p + \mathbf{m}_s]\ddot{\mathbf{w}} + [\mathbf{k}_s + \mathbf{k}_{uu}]\mathbf{w} = -\Theta_A \mathbf{v}_A + \beta \mathbf{m}(\mathbf{m}^T\mathbf{w} + S_h z), \\ &m_h \ddot{z} + \beta S_h^2 z = -\beta S_h \mathbf{w}^T \mathbf{m}, \\ &\mathbf{v}_S = \frac{\Theta_S^T \mathbf{w}}{C_S}, \end{aligned} \tag{A.21}$$

where all matrices have been assembled from the individual matrices of each element. Also, the subscript i has been left off of **w** with the understanding that **w** is the vector of nodal degrees of freedom for the global model. In the first of Equations A.21, $\mathbf{v}_A$ is a column vector of the voltages applied to each actuator. The non zero elements of the column of Θ_A corresponding to a given actuator are assembled from piezoceramic finite elements making up that actuator. Similarly, $\mathbf{v}_S$ is a column vector made up of the voltages generated on each sensor with each row of Θ_S^T corresponding to a sensor. Again, the nonzero elements of the corresponding sensor row are assembled from those piezoceramic elements making up each sensor. All other elements in Θ_A and Θ_S not corresponding to a node that is common with an actuator or sensor are zero. A useful physical interpretation of Θ_A and Θ_S is the applied forces to the corresponding nodal degree of freedom for a unit voltage input into the piezoceramic.

Table A.1 Piezoelectric and structural matrices

$\mathbf{m}_P = \rho_P \int_{V_P} \mathbf{f}_U{}^T \mathbf{f}_U dV_P$	Consistent piezoelectric mass matrix
$\mathbf{m}_S = \rho_S \int_{V_S} \mathbf{f}_U{}^T \mathbf{f}_U dV_S$	Consistent structural mass matrix
$\mathbf{k}_S = \int_{V_S} \mathbf{B}_U{}^T \mathbf{c} \mathbf{B}_U dV_S$	Structural stiffness matrix
$\mathbf{k}_{UU} = \int_{V_P} \mathbf{B}_U{}^T \mathbf{c}^E \mathbf{B}_U dV_P$	Piezoelectric stiffness matrix
$\mathbf{k}_{UV} = \int_{V_P} \mathbf{B}_U{}^T \mathbf{c}^E \mathbf{B}_V dV_P$ $\mathbf{k}_{VU} = \int_{V_P} \mathbf{B}_V{}^T \mathbf{e} \mathbf{B}_U dV_P$	Piezoelectric coupling matrices
$\mathbf{k}_{VV} = -\int_{V_P} \mathbf{B}_V{}^T \boldsymbol{\epsilon} \mathbf{B}_V dV_P$	Dielectric matrix

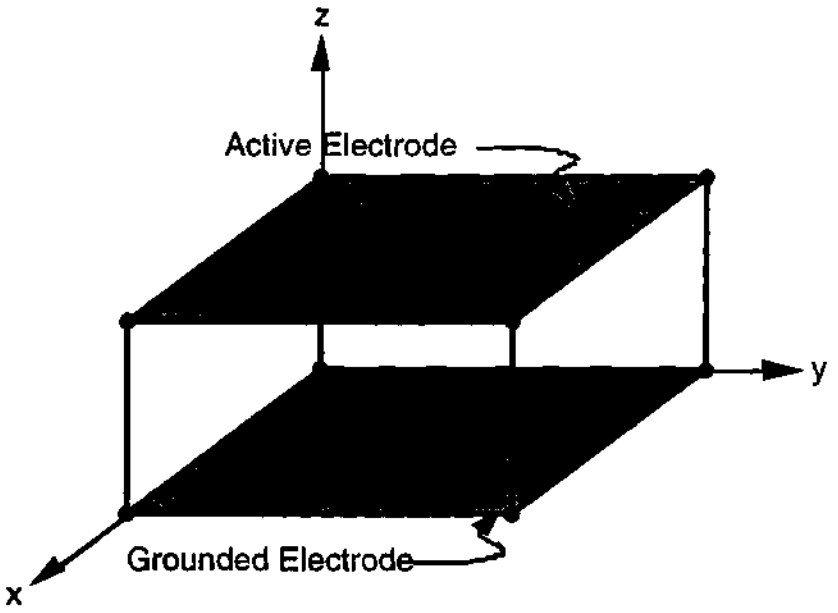

Figure A.1- Piezoceramic element

APPENDIX B

DISCRETE AND ANALYTICAL MODEL COMPARISON

In the approach by Dimitriadis, Fuller, and Rogers [36], an analytical expression is developed for symmetrically located, about the neutral axis, surface mounted piezoceramic actuators. The actuators are connected electrically out of phase so that when one expands, the other shrinks. The net effect is an applied moment to the plate. It is assumed that the actuators are perfectly bonded and that the plate undergoes spherical curvature. It is also assumed that the resulting moment arrived at for an infinite plate and infinite piezoceramics is directly applicable to a segmented actuator. It is recognized that this assumption violates the boundary conditions for the actuator, but this is said to be acceptable as long as the actuators are large in width and length when compared to thickness. It is also assumed the plate is thin, uniform thickness, and isotropic and that the plate ad the actuators are rectangular. The equation that governs the motion of the plate with the bonded piezoceramic actuators is given by

$$D\nabla^4 w + \rho\ddot{w} = \frac{\partial^2 m_x}{\partial x^2} + \frac{\partial^2 m_y}{\partial y^2}. \qquad \text{(B.1)}$$

The terms on the right hand side are due to the piezoceramic and given by

$$\frac{\partial^2 m_X}{\partial x^2} = C_0 \varepsilon_{pe}[\delta'(x-x_1)-\delta'(x-x_2)][h(y-y_1)-h(y-y_2)]$$

and

$$\frac{\partial^2 m_Y}{\partial y^2} = C_0 \varepsilon_{pe}[h(x-x_1)-h(x-x_2)][\delta'(y-y_1)-\delta'(y-y_2)],$$

where $\varepsilon_{pe} = \frac{d_{31} v_A}{t}$, and Co is a coupling term defined by

$$C_0 = -E_P \frac{1+\nu_{pe}}{1-\nu_{pe}} \frac{P}{1+\nu_p-(1-\nu_{pe})P} \frac{2}{3} h^2,$$

where K is a nondimensional geometric parameter defined by

$$K = \frac{3th(2h+t)}{2(h^3+t^3)+3ht^2}.$$

In the approach by Dimitriadis, Fuller, and Rogers, Equation B.1 was applied to a simply supported rectangular plate. In this comparison, the equation will be applied to a rectangular plate that is clamped on all four sides. Unlike the simply supported plate, there is no exact solution to the clamped problem, but there is an approximate solution derived by Young [89] using the Ritz method. The solution is derived based on assumed solution of

$$w(x,y) = \sum_{m=1}^{p} \sum_{n=1}^{q} A_{mn} X_m(x) Y_n(y),$$

where X_m and Y_n are equal to

$$X_r = \cosh\frac{\varepsilon_r x}{l} - \cos\frac{\varepsilon_r x}{l} - \alpha_r(\sinh\frac{\varepsilon_r x}{l} - \sin\frac{\varepsilon_r x}{l})$$

and

$$Y_r = \cosh\frac{\varepsilon_r y}{l} - \cos\frac{\varepsilon_r y}{l} - \alpha_r(\sinh\frac{\varepsilon_r y}{l} - \sin\frac{\varepsilon_r y}{l}).$$

A 36 term series was used to come up with approximations to the first six mode shapes. The modal coefficients A_{mn}, coefficients ε_r and α_r, and frequencies corresponding to each mode are given in tables in reference [89]. The result is a series of approximate mode shapes given by

$$w(x,y,t) = \sum_{m=1}^{6} \eta_m(t)\phi_m(x,y). \qquad \text{(B.2)}$$

Substituting Equation B.2 into Equation B.1, multiplying by ϕ_i and integrating over the plate area gives

$$\int \phi_i^2 dA(\ddot{\eta}_i - \omega_i^2\eta_i) =$$
$$\frac{C_0\varepsilon_{pe}}{\rho}\left[\int_{y_1}^{y_2}(\frac{\partial\phi_i}{\partial x}_{|x=x_1} - \frac{\partial\phi_i}{\partial x}_{|x=x_2})dy + \int_{x_1}^{x_2}(\frac{\partial\phi_i}{\partial y}_{|y=y_1} - \frac{\partial\phi_i}{\partial y}_{|y=y_2})dx\right]. \qquad \text{(B.3)}$$

In order to compare the analytical model with the discrete approach, a a series made up of the first three mode shapes was assumed for the out-of-plane displacement. These are shown graphically in Figure B.1. The actuator position was assumed to be as shown in Figure B.2. Other relevant plate data are given in Table B.1. After substitution of the three term series into Equation B.3 and integration, a transfer function was formulated between

out-of-plane displacement at a given point and voltage into the piezoceramic actuators for plates of two different moduli, 0.69 GPa and 100 GPA. The point chosen to monitor out-of-plane displacement is also shown on Figure B.1. The amplitude and phase of the resulting transfer functions for each plate are shown in Figures B.3 and B.4 where a 3% proportional damping ratio is also assigned to each mode. In both transfer functions, mode 2 was not excited for the given actuator position.

The discrete model was formulated as derived in Chapter 2 without the backing cavity resulting in

$$[\mathbf{m}_p + \mathbf{m}_s]\ddot{\mathbf{w}} + [\mathbf{k}_s + \mathbf{k}_{uu}]\mathbf{w} = -\Theta_A \mathbf{v}_A. \qquad \text{(B.4)}$$

The sensor equation is not necessary since displacement will be compared in the transfer function making the elements of the relevant entries into the C matrix the out-of-plane modal displacements iat the measurement location. The mode shapes, ϕ_i, and frequencies, ω_i, were solved using the FEM code COSMOS/M by Structural Research and Analysis Corporation. Solid 3-dimensional elements were used to accurately reflect the three dimensional characteristics of the piezoceramic elements. Details of the model are the same as that for the lower bout of the guitar described in Appendix C except that the piezoceramics are both actuators and are mounted symmetrically about the neutral axis at the location shown in Figure B.2. The k_{uv} matrix for the piezoceramic elements was computed using the formula in Table A.1. In a process exactly analogous to that described in Chapter 2, Equation B.4 is transformed into a state space model using the first three mode shapes. The the resulting transfer functions between voltage on the actuators and

displacement at the point shown in Figure B.1 are shown in Figures B.5 and B.6 for the low and high modulus plates. Again, a 3% proportional damping ratio is assigned to each mode, and the first antisymmetric mode is not excited at the given actuator postion.

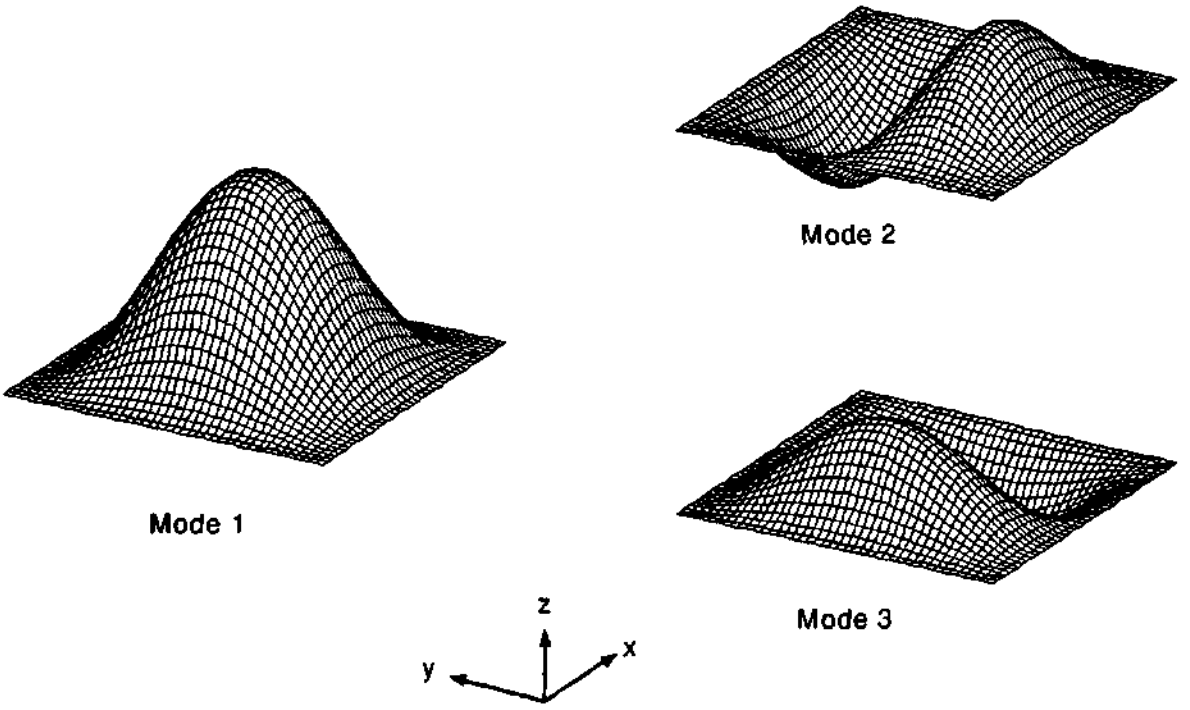

Figure B.1 - Plate mode shapes

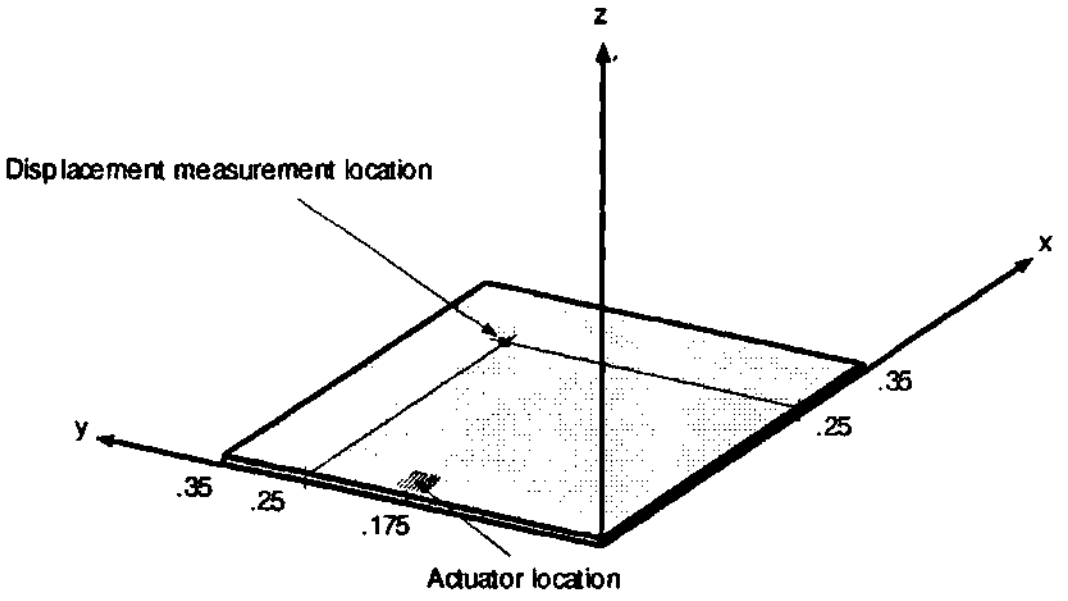

Figure B.2 - Displacement measurement and actuator location

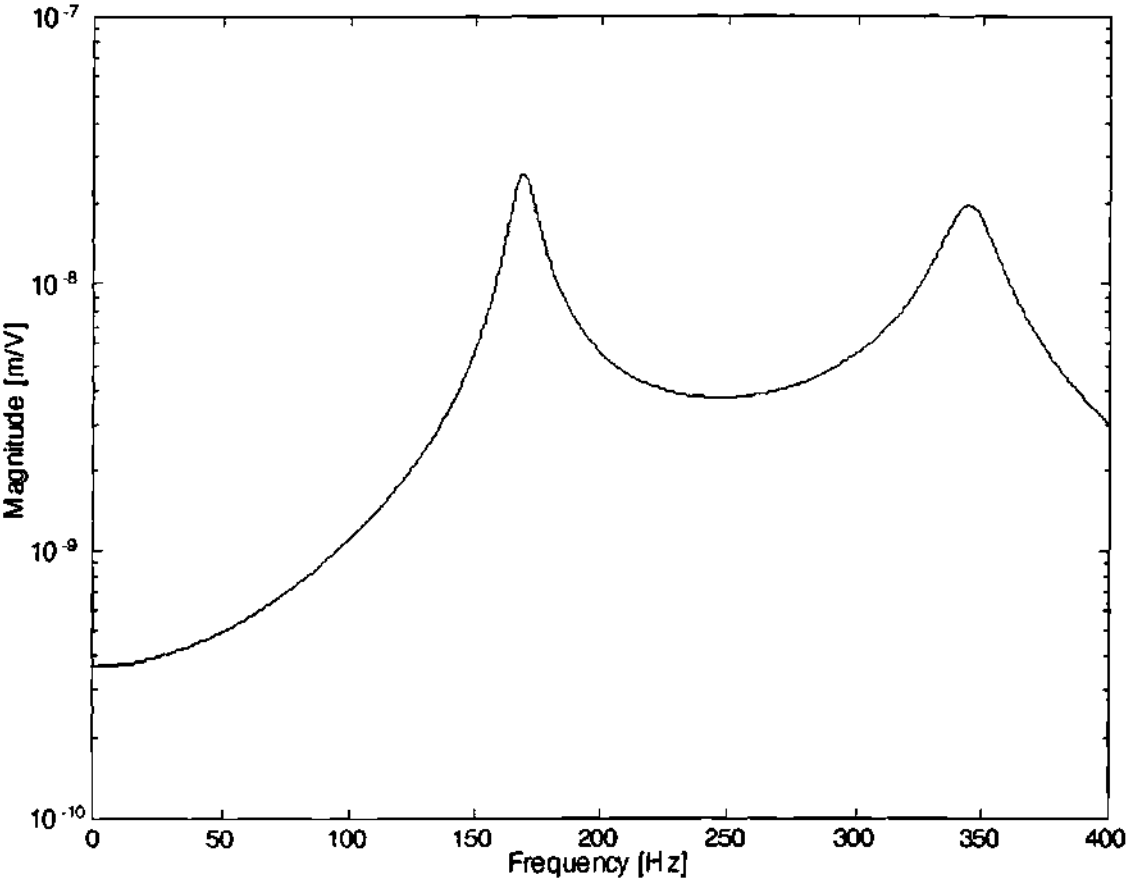

Figure B.3 Dimitriadis model with 3% damping, Ep=.69 GPa

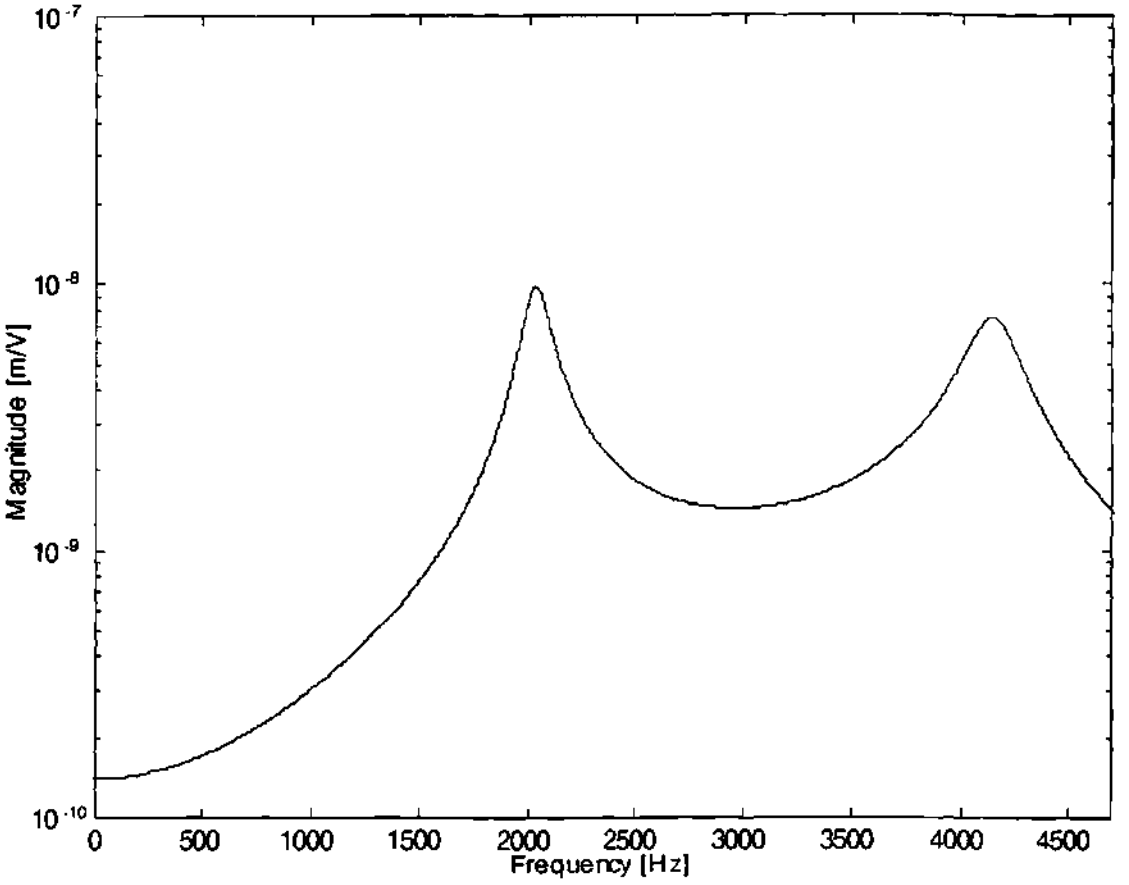

Figure B.4 Dimitriacis model with 3% damping, Ep=100 GPa

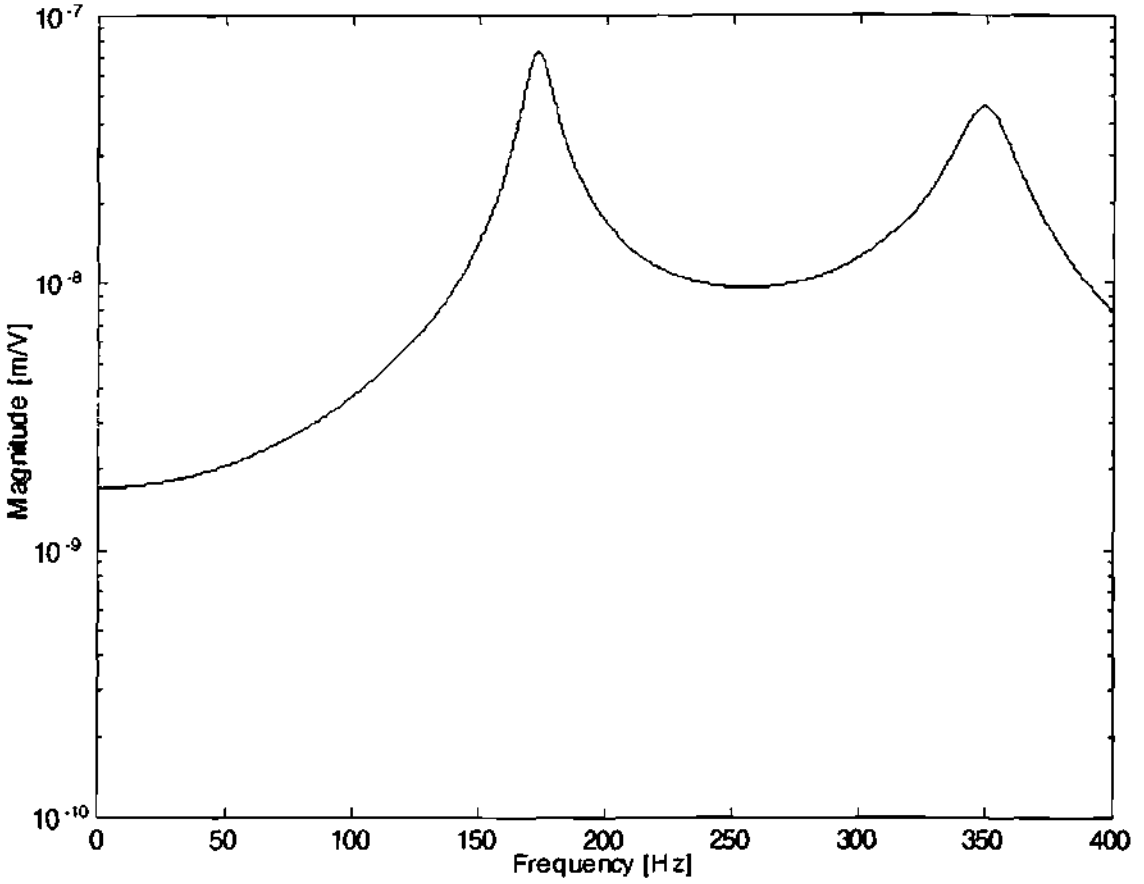

Figure B.5 Discrete model with 3% damping, Ep=.69 GPa

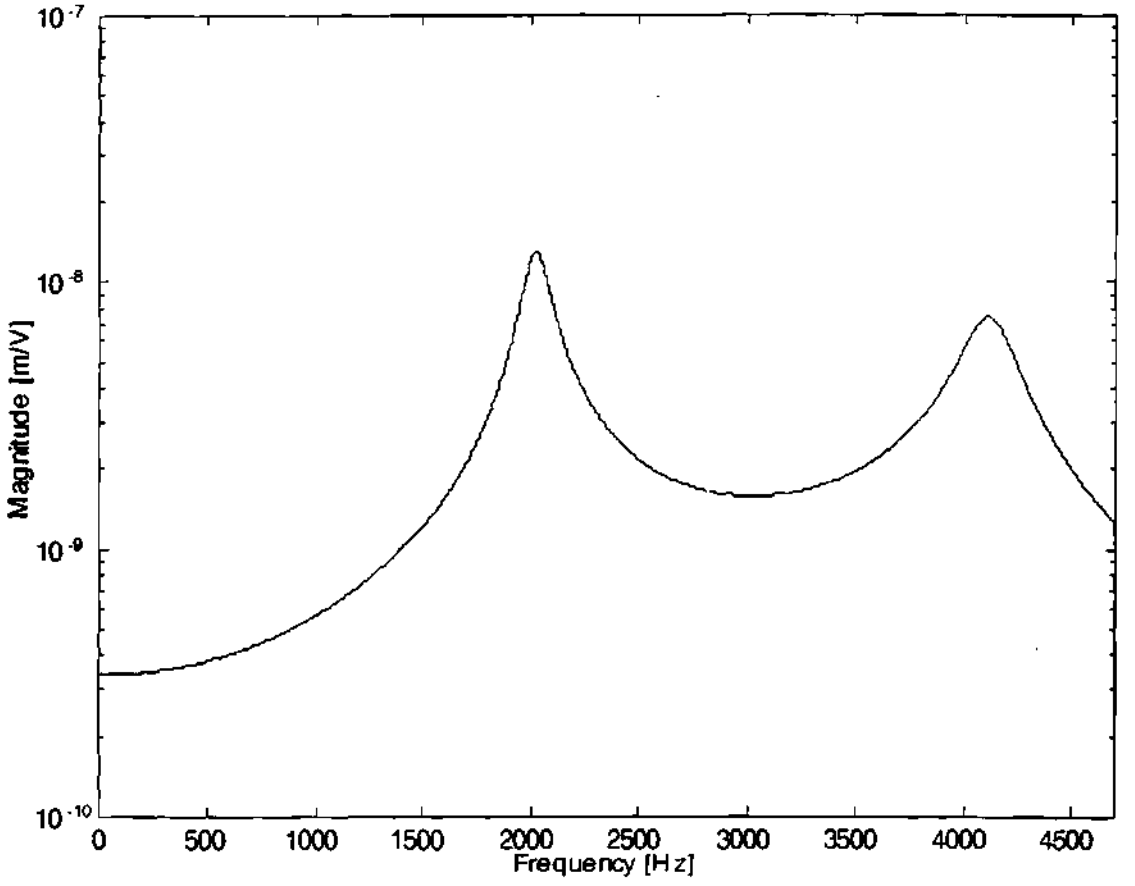

Figure B.6 Discrete model with 3% damping, Ep=100 GPa

APPENDIX C

GUITAR TOP PLATE FINITE ELEMENT MODEL

The finite element model to compute mode shapes and frequencies for the guitar lower bout, with one piezoceramic sensor and one piezoceramic actuator, was constructed using the COSMOS/M finite element software by Structural Research and Analysis Corporation. As in the continuous model, it was assumed that the second plate mode was not well coupled with the air cavity and measurements have confirmed that this mode has relatively low damping making its measured frequency very close to its undamped natural frequency. Also, analogous to the continuous model, two lower plate modes of the clamped, rectangular plate had a reasonably similar shape to the measured mode shapes.

Based on this, the first step was to construct a finite element model of an equivalent rectangular plate that displayed the same second plate mode frequency as was measured in the second modal survey. In this first step, only the plate substructure is considered since the modal survey to get the second plate mode frequency was done before adding piezoceramics. The finite element model was constructed using eight-noded solid elements to allow for the general case of anisotropy. Also, solid elements were chosen because x, y, and z displacement degrees of freedom were desired to be consistent with the rest of the model formulation. A total of 676 elements were

used in a discretization shown in Figure C.1. The pattern of discretization was dictated by the necessity of more elements in potential locations for piezoceramics.

Similar to the continuous model, a smearing of anisotropic properties was done to form an equivalent isotropic plate to model lower frequency function in the guitar. The x and y dimensions of the plate were taken to be equal to the diameter of the plate used in the continuous model. The Young's modulus, Poisson's ratio, and volume density were taken to be $E = 6.9 \times 10^8$ GPa,ν=0.02, and ρ=390 kg/m^3 respectively. These are properties of Sitka Spruce in its low modulus direction [93]. The thickness of the plate was then varied until the second plate mode frequency matched the measured second plate mode frequency in the guitar. The thickness arrived at was t=.00942 m which corresponds to the measured second plate mode frequency of 344 Hz. Reduced order integration in the thickness direction was used to prevent shear locking in the elements. As a double check on the model, the approximate clamped second mode plate frequency by the method in reference [89] gave a second mode frequency that was within 0.4 % of this for the same material properties and geometry. It is noteworthy that 0.00942 m is between the upper plate thickness of 0.003 m and the maximum upper plate plus reinforcing brace thickness of 0.018 m.

Once the thickness of the substructure was set, the second step was to incorporate elements which represented the structural properties of the piezoceramic sensors and actuators. The size of the piezoceramic sensors and actuators were both selected as 0.025 m x 0.025 m in the length and width directions and 0.001 m in the thickness direction. Both the piezoceramic sensor and actuator were made up of 16 elements. Before

assembling the final model, a test case was run using the 16 element assembled plate with clamped edges and isotropic properties to again compare with the approximate solution of reference [89]. The first mode frequencies were within 3% of each other.

The piezoceramic elements were then included in the larger plate model by making common nodes at the intersection of the two materials. The piezoceramics with the plate are shown in Figure C.2. The properties used in the piezoceramics in the assembled model were derived from data given for PZT 5A [94] and are given in Table C.1. The frequencies and mode shapes corresponding to the two modes of the finite element model which closely matched the measured modes were used as inputs in the discrete model formulation for the acoustic guitar. Representations of the mode shapes are shown in Figure C.3 for comparison with the measured mode shapes in Figure 4.3. The numerical values of the calculated first and second plate mode frequencies were 174 Hz and 347 Hz respectively.

Table C.1 Piezoceramic Properties of PZT 5A

E_x	6.09×10^{10} GPa
E_y	6.09×10^{10} GPa
E_z	5.32×10^{10} GPa
ν_{xy}	0.35
ν_{yz}	0.44
ν_{xz}	0.44
G_{xy}	2.26×10^{10} GPa
G_{yz}	2.10×10^{10} GPa
G_{xz}	2.10×10^{10} GPa
ρ (volume density)	7700 kg/m^3

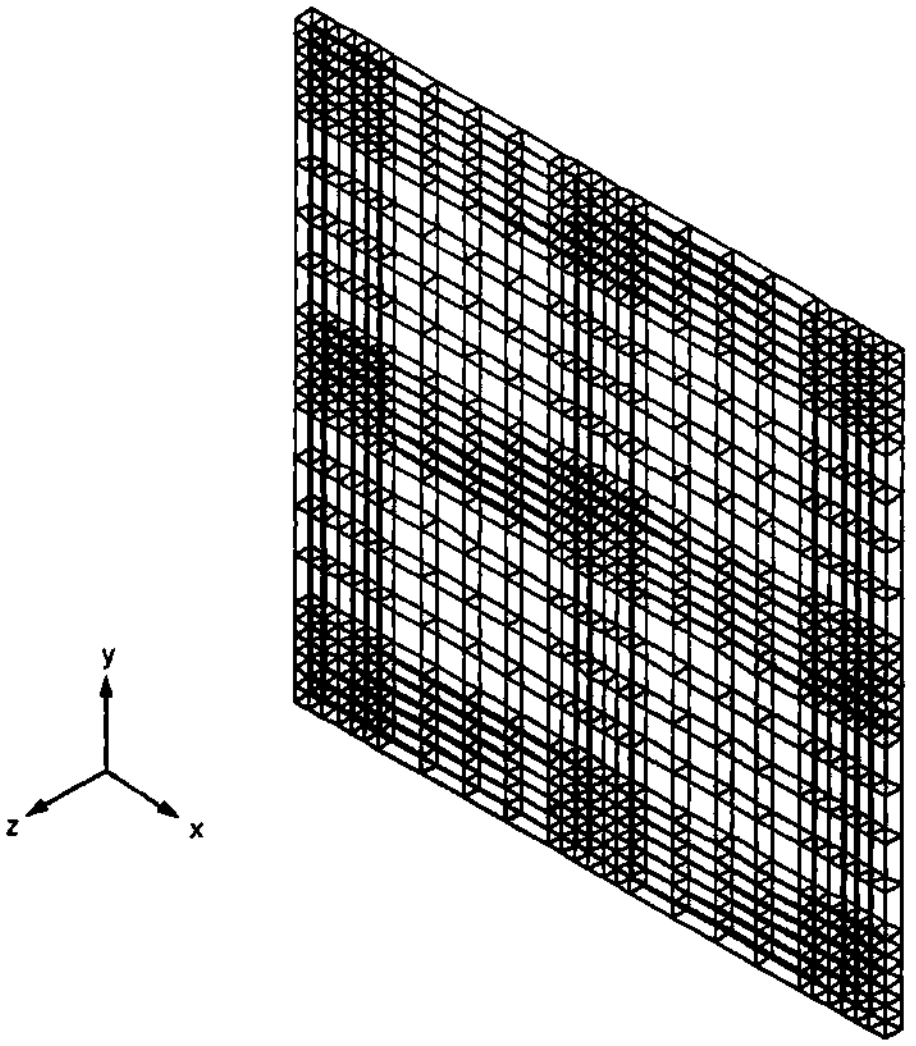

Figure C.1 Finite element model of plate

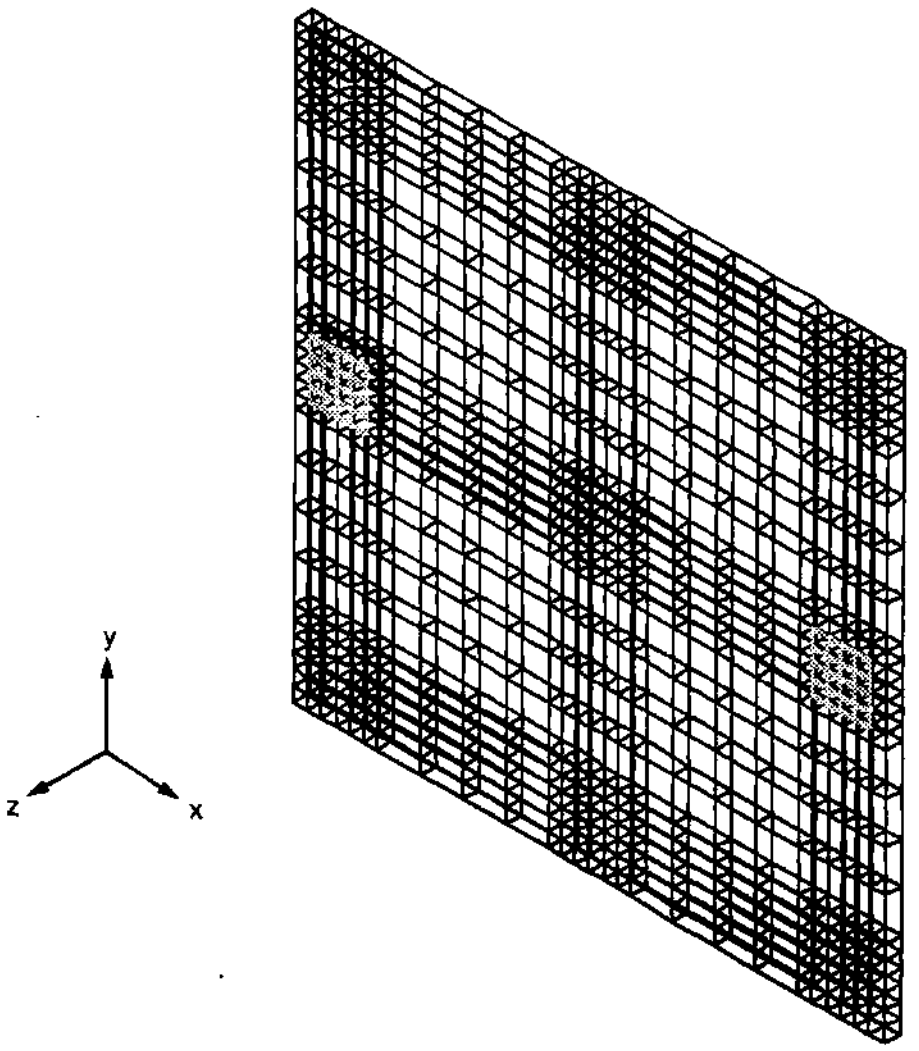

Figure C.2 Finite element model with piezoceramics

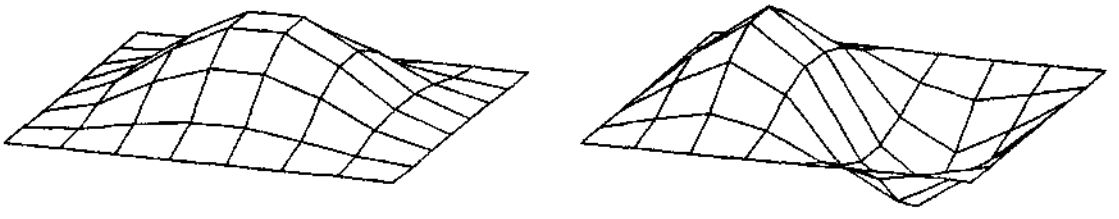

Figure C.3 Finite element model mode shapes

BIBLIOGRAPHY

[1] Pierce, A. D., Acoustics- *An Introduction to Its Physical Principles and Applications*, Acoustical Society of America, Woodbury, New York 1989.

[2] Hunt, F. V., *Origins in Acoustics*, Yale University Press, New Haven 1978.

[3] Stevens, J. C. and Ahuja, K. K., "Recent Advances in Active Noise Control," *AIAA J.*, 1991, 1058-1067

[4] Mangiante, G. A., "Active Sound Absorption," *J. Acoust. Soc. Am.*, **61(6)** 1977, 1516-1523.

[5] Liu, C. Y., and Ma, Y. L., "An Acoustic Field-Fitting Method for Free Field Active Noise Control," *Inter-noise 89*, 1989, 505-508.

[6] Lueg, P., "Process of Silencing Sound Oscillations," U.S. Patent #2,043,416, 1936.

[7] Conover, W., "Fighting Noise with Noise," *Noise Control*, **92(2)** 1956, 78-82.

[8] Berge, T., Petersen, O. Kr. O. and Sorsdal, S., "Active Cancellation of Transformer Noise: Field Measurements," *App. Acoust*, **23(4)** 1988, 309-320.

[9] Warnaka, G. E., "Active Attenuation of Noise- The State of the Art," *Noise Cont. Eng.*, May-June 1982, 100-110.

[10] Olson, H. F., and May, E. G., "Electronic Sound Absorber," *J. Acoust. Soc. Am.*, **25(6)** 1953, 1130-1136.

[11] Beranek, L. L., *Noise and Vibration Control*, INCE Washington 1988.

[12] Wise, S. S., Goodman, S. D. and Dineen, S. H., "Active Control of Low-Frequency HVAC Fan Noise in Building Systems," *ASHRAE trans.*, **99(2)** 1993, 1037-1043.

[13] Kempton, A. J., "The Ambiguity of Acoustic Sources- A Possibility For Active Control," *J. Sound Vib.*, **48(4)** 1976, 475-483.

[14] Lester, H. and Fuller, C. R., "Mechanisms of Active Control for Noise Inside a Vibrating Cylinder," *Noise-Con 87* , 1987, 371-376.

[15] Fuller, C. R. and Jones, J. D., "Experiments on Reduction of Propeller induced Noise by Active Control of Cylinder Vibration," *J. Sound Vib.*, **112(2)** 1987, 389-395.

[16] Jones, J. D. and Fuller, C. R., "Active Control of Sound Fields in Elastic Cylinders by Multicontrol Forces," *AIAA J.*, **27(7)** 1989, 845-852.

[17] Elliott, S. J., Curtis, A. R. D., Bullmore, A. J. and Nelson, P. A., "Active Minimization of Harmonic Enclosed Sound Fields, Part III Experimental Verification," *J. Sound Vib.*, **117(1)** 1987, 35-58.

[18] Angevine, O. L., Gupta, P. K. and Rushden, F. A., "Active Acoustic Absorbers for Low Frequency Hum," *99th Meeting of the Acoustical Society of America*, 1980, Paper LL3.

[19] Fuller, C. R., "Active Control of Sound Transmission/Radiation from Elastic Plates by Vibration Inputs," *J. Sound Vib.*, **136(1)** 1990, 1-15.

[20] Silcox, R. J., Fuller, C. R. and Lester, H. C., "Mechanisms of Active Control in Cylindrical Fuselage Structures," *AIAA J.*, **28(8)** 1990, 1397-1404.

[21] Knyazev, A. S., and Tartakovskii, B. D., "Application of Electromechanical Feedback for the Damping of Plate Vibrations and Radiation," *Sov. Phys.-Acous.*, **12(3)** 1967, 330-331.

[22] Knyazev, A. S., and Tartakovskii, B. D., "Abatement of Radiation from Flexurally Vibrating Plates by Means of Active Local Vibration Dampers," *Sov. Phys.-Acous.*, **13(1)** 1967, 115-117.

[23] Vyalyshev, A. I., Dubinin, B. D. and Tartakovskii, B. D., "Active Acoustic Noise Reduction of a Plate," *Sov. Phys.-Acous.*, **32(2)** 1986, 96-98.

[24] Clark, R. L. and Fuller, C. R. , "Experiments on Active Control of Structurally Radiated Sound using Multiple Piezoceramic Actuators," *J. Acoust. Soc. Am.*, **91(6)** 1992, 3313-3320.

[25] Fuller, C. R., Hansen, C. H. and Snyder, S. D., "Experiments on Active Control of Sound Radiation from a Panel Using a Piezoceramic Actuator," *J. Sound Vib.*, **150(2)** 1991, 179-190.

[26] Forward, R. L., "Electronic Sampling of Vibration in Optical Structures," *Applied Optics*, 1979, 690-697.

[27] Bailey, T. and Hubbard, J. E. Jr., "Distributed Piezoelectric-Polymer Active Vibration Control of a Cantilever Beam," *J. Guid. Control Dyn.*, **8(5)** 1985, 605-611.

[28] Obal, M. W., *Vibration control of Flexible Structures Using Piezoelectric Devices as Sensors and Actuators*, PhD Thesis, Georgia Institute of Technology, Atlanta, GA, 1987.

[29] Hanagud, S., Obal, M. W. and Calise A., "Piezoceramic Devices and PVDF Films as Smart Sensors and Actuators for Intelligent Structures" *Smart Materials, Structures and Mathematical Issues*, C.A. Rogers, ed., Technomic Publishing Co., 1988, 69-80.

[30] Hanagud, S., Obal, M. W. and Calise A., "Control of Sound Transmission into a Closed Cavity Using Smart Structures" *Proc. 28th AIAA SDM Conference* , 1987, 987-997.

[31] Baz, A. and Poh, S., "Performance of an Active Control System with Piezoelectric Actuators," *J. Sound Vib.*, **126(2)** 1988, 327-343.

[32] Crawley, E. F. and Deluis J., "Use of Piezoelectric Actuators as Elements of Intelligent Structures," *AIAA J.*, **25(10)**, 1987, 1373-1385.

[33] Crawley, E. F. and Anderson, E. H., "Detailed Models of Piezoceramic Actuation in Beams," *J. of Intell. Mater. And Struct.*, **1** 1990, 5-25.

[34] Fanson, J. L. and Chen, J. C., "Structural Control by the Use of Piezoelectric Active Members," *Proc. of NASA/DOD Control/Structures Interaction Technology 1986*, 1986, 809-829.

[35] Bronowicki, A. J. and Betros, R. S., *Active Structures Workshop - 1995 Smart Structures and Materials Conference*, SPIE 1995.

[36] Dimitriadis, E. K., Fuller, C. R. and Rogers, C. A., "Piezoelectric Actuators for Distributed Vibration Excitation of Thin Plates," *Journ of Vib and Acoust.*, **113** 1991, 100-107.

[37] Fuller, C. R., Rogers, C. A. and Robertshaw, H. H., "Control of Sound Radiation with Active/Adaptive Structures," *J. Sound Vib.*, **157(1)** 1992, 19-39.

[38] Crawley, E. F. and Lazarus K. B., "Induced Strain Actuation of Isotropic and Anisotropic Plates," *AIAA J.*, **29(6)**, 1991, 944-951.

[39] Kim, S. J. and Jones, J. D., "Optimal Design of Piezoactuators for Active Noise and Vibration Control" *AIAA J.*, **29(12)**, 1991, 2047-2053.

[40] Tzou, H. S. and Fu, H. Q., "A study on Segmentation of Distributed Piezoelectric Sensors and Actuators: Part 1 -Theoretical Analysis," *Proc. of Active Control of Noise and Vibration* ASME 1992, 239-246.

[41] Tzou, H. S. and Fu, H. Q., "A study on Segmentation of Distributed Piezoelectric Sensors and Actuators: Part 2 - Parametric Study and Active Vibration Control," *Proc. of Active Control of Noise and Vibration* ASME 1992, 247-253.

[42] Allik, H. and Hughes, T. Jr., "Finite Element Method for Piezoelectric Vibration," *Int. J. for Num. Meth. in Eng.* **2** 1970, 151-157.

[43] McDearmon, G. F. "The Addition of Piezoelectric Properties to Structural Finite Element Programs by Matrix Manipulations," *J. Acoust. Soc. Am.*, **76(3)** 1984, 666-669.

[44] Ha, S. K., Keilers, C. and Chang, F., "Finite Element Analysis of Composite Structures Containing Distributed Piezoceramic Sensors and Actuators," *AIAA J.*, **30(3)**, 1992, 772-779.

[45] Smith, J. P., Fuller, C. R., and Burdisso, R. A., "Control of Broadband Radiated Sound with Adaptive Structures," *SPIE 1993 Smart Str and Int. Sys.*, **1917**, 1993, 587-597.

[46] Saunders, W. R., Cole, D. G., and Robertshaw, H. H., "Impact of Piezoelectric Sensoriactuators on Active Structural Acoustic Control," *SPIE 1993 Smart Str and Int. Sys.*, **1917**, 1993, 578-586.

[47] Clark, R. L. and Fuller, C. R., "Optimal Placement of Piezoelectric Actuators and Polyvinylidine Fluoride Error Sensors in Active Structural Acoustic Control Approaches," *J. Acoust. Soc. Am.*, **92(3)** 1992, 1521-1533.

[48] Clark, R. L. and Gibbs, G. P., "Feedforward Higher Harmonic Control of Sound Radiation," *SPIE 1993 Smart Str and Int. Sys.*, **1917**, 1993, 598-611.

[49] Clark, R. L. and Fuller, C. R., "Modal Sensing of Efficient Acoustic Radiators with Polyvinylidene Flouride Distributed Sensors in Active Structural Acoustic Control Approaches," *J. Acoust. Soc. Am.*, **91(6)** 1992, 3321-3329.

[50] Clark, R. L. and Fuller, C. R., "A Model Reference Approach for Implementing Active Structural Acoustic Control," *J. Acoust. Soc. Am.*, **92(6)** 1994, 1534-1544

[51] Banks, H. T., Silcox, R. J. and Smith, R. C., "The Modeling and Control of Acoustic/Structure Interaction Problems via Piezoceramic Actuators:2-D Numerical Examples," *Proc. of Active Control of Noise and Vibration* ASME 1992, 83-94.

[52] Guigou, C. and Clark, R. L., "Active Control of Sound Radiation from a Semi-Infinite Elastic Beam with a Clamped Edge," *J. Sound Vib.*, **168(3)** 1993, 507-523.

[53] Van Niekerk, J. L., Tongue, B. H. and Packard, A. K., "Active Control of a Circular Plate to Reduce Transient Noise Transmission," *J. Sound Vib.*, **183(4)** 1995, 643-662.

[54] Banks, H. T. , Fang, W. and Smith, R. C., "Active Noise Control: Piezoceramic Actuators in Fluid/Structure Interaction Models," *Proc. of the 30th Conference on Decision and Control,* 1991, 2328-2333.

[55] Banks, H. T., Fang, W., Silcox, R. J. and Smith, R. C. "Approximation Methods for Control of Structural Acoustics Models with Piezoceramic Actuators," *J. of Intell. Mater. Syst. and Struct.*, 4 1993, 98-116.

[56] Koshigoe, S., Gillis, J. T. and Falangas, E. T. , "A New Approach for Active Control of Sound Transmission Through an Elastic Plate Backed by a Rectangular Cavity," *J. Acoust. Soc. Am.*, **94(2)** 1993, 900-907.

[57] Ellis, G. K. and Koshigoe, S., "An Experiment in Feedforward Control for the Reduction of Sound Transmission Through an Elastic Plate Backed by a Rigid Rectangular Cavity," *Proc. of Smart Structures and Materials 1994* , SPIE 1994, 289-296.

[58] Koshigoe, S. and Ellis, G. K., "A Time Domain Analysis of Active Control of Sound Transmission Through an Elastic Plate Backed by a Rigid Rectangular Cavity," *Proc. of Smart Structures and Materials 1994* , SPIE 1994, 321-329.

[59] Hill, M. L., Chrissos, P., Koval, L. R., Rao, V. S. and Kern, F. J., "Control of Sound Transmission into a Closed Cavity Using Smart Structures" *Proc. of Smart Structures and Materials 1995* , SPIE 1995, 224-235.

[60] Rogers, C. A., Fuller, C. R. and Liang, C., "Active Control of Sound Radiation from Panels Using Embedded Shape Memory Alloy Fibers," *J. Sound Vib.*, **136(1)** 1990, 164-170.

[61] Lyon, R. H., "Noise Reduction of Rectangular Enclosures With One Flexible Wall," *J. Acoust. Soc. Am.*, **35** 1963, 1791-1797.

[62] Meirovitch, L. and Thangjitham, S., "Active Control of Sound Radiation Pressure," *Journ of Vib and Acoust.*, **112** 1990, 237-244.

[63] Fuller, C. R. and Burdisso, R. A., "Wavenumber Domain Approach to the Active Control of Structure-Borne Sound" *J. Sound Vib.* **148(2)** 1991, 355-360.

[64] Clark, R. L. and Fuller C. R., "Active Structural Acoustic Control with Adaptive Structures Including Wavenumber Considerations," *J. of Intell. Mater. Syst. and Struct.*, **3** 1992, 297-315.

[65] Bauman, W. T., Saunders, W. R. and Robertshaw, H. H., "Active Suppression of Acoustic Radiation from Impulsively Excited Structures," *J. Acoust. Soc. Am.*, **90(6)** 1991, 3202-3208.

[66] Bauman, W. T., Ho, F. S. and Robertshaw, H. H., "Active Structural Acoustic Control of Broadband Disturbances," *J. Acoust. Soc. Am.*, **92(4)** 1992, 1998-2005.

[67] Hutchins, C. M. and Fielding, F. L., "Acoustical Measurement of Violins," *Physics Today* **35** 1968, 35-40.

[68] Caldersmith, G., "Guitar as a Reflex Enclosure," *J. Acoust. Soc. Am.*, **63(5)** 1978, 1566-1575.

[69] Hutchins, C. M., "A History of Violin Research," *J. Acoust. Soc. Am.*, **73(5)** 1983, 1421-1440.

[70] Firth, I. M., "Physics of the Guitar at the Helmholtz and First Top-Plate Resonances," *J. Acoust. Soc. Am.*, **61(2)** 1977, 588-593.

[71] Christensen, O. and Vistisen, B. B., "Simple Model for Low-Frequency Guitar Function," *J. Acoust. Soc. Am.*, **68(3)** 1980, 758-766.

[72] Rossing, T. D., Popp, J. and Polstein, D., "Acoustical Response of Guitars," *Proc. SMAC 83* Royal Swedish Academy of Music, 1983 311-332.

[73] Christensen, O., "Quantitative Models for Low-Frequency Guitar Function," *J. Guitar Acoustics* **6** 1982, 1-15.

[74] Christensen, O., "An Oscillator Model for Analysis of Guitar Sound Pressure Response," *Acustica* **54** 1984, 289-295.

[75] Fletcher, N. H. and Rossing, T. D., *The Physics of Musical Instruments,* Springer-Verlag, New York 1991.

[76] Gridnev, M. V. and Porvenkov, V. G., "Appraisal of the Quality of Violins and Guitars," *Sov. Phys. Acoust.,* **22(5)** 1976, 385-389.

[77] Meyer, J., "Quality Aspects of the Guitar Tone," *Function, Construction, and Quality of the Guitar* E. V. Jansson, ed., Royal Swedish Academy of Music, Stockholm 1983, 51-75.

[78] Christensen, O., "The Response of Played Guitars at Middle Frequencies," *Acustica* **53** 1983, 45-48.

[79] Bathe, K., *Finite Element Procedures in Engineering Analysis,* Prentice-Hall Inc., New Jersey 1982.

[80] Borwick, J., *Loudspeaker and Headphone Handbook*, Butterworths, London, 1988.

[81] Meirovitch L., *Analytical Methods in Vibrations*, Macmillan, New York 1967.

[82] Cremer, L. and Heckl, M., *Structure-Borne Sound*, Springer-Verlag, New York 1973.

[83] Lamancusa, J. S., "Numerical Optimization Techniques for Structural-Acoustic Design of Rectangular Panels," *Computers & Structures* **48(4)** 1993, 661-675.

[84] Ogata K., *Modern Control Engineering*, Prentice-Hall, New Jersey 1990.

[85] Brogan, W. L., *Modern Control Theory,* Prentice-Hall, New Jersey 1991.

[86] Griffin, S. F., Bronowicki A. J. and Betros, R. S., "Piezoceramic Sensors and Actuators for Smart Composite Structures, "*proc. of 30th IEEE Conference on Decision and Control,* IEEE 1991 2543-2545.

[87] Bronowicki A. J., Innis, J. W., Betros, R. S., Kuritz, S. P. and Griffin, S. F., "ACESA Active Member Damping Performance," *proc. of Smart Structures and Materials 1993: Smart Structures and Integrated Systems,* SPIE 1993 836-847.

[88] Kwak, M. K., Denoyer, K. K. and Sciulli, D., "Dynamics and Control of Slewing Active Beam," *J. Guid. and Cont.* **18(1)** 1995, 185-187.

[89] Young, D., "Vibration of Rectangular Plates by the Ritz Method," *J. of Appl. Mech.* **17**, 1950 448-453.

[90] Dress, W. B. and Kercel, S. W., "Wavelet-Based Acoustic Recognition of Aircraft," *proc. of Wavelet Applications*, SPIE 1994 778-791.

[91] Anderson, E. H. and Hagood, N. W., "Simultaneous Piezoelectric Sensing/Actuation: Analysis and Application to Controlled Structures," *J. of Sound Vib.*, **174(5)**, 1994 617-639.

[92] Institute of Electrical and Electronics Engineers *1987 IEEE Standard on Piezoelectricity, ANSI/IEE Std.* 1987.

[93] *CRC Handbook of Materials Science*, C. T. Lynch ed., CRC Press, Cleveland, Ohio 1974.

[94] *Piezoelectric Technology Data for Designers*, Morgan Matroc Inc., Vernitron Division, Bedford, Ohio.

[95] Hsu, J. and Ahuja, K., "Smart Window Project", unpublished Internal Research and Development work for Georgia Tech. Research Institute, 1995.

VITA

Steven Fulton Griffin was born on August 27, 1965 in Fargo, North Dakota. He grew up in central Florida, where he and his family moved in 1969. He enrolled at the University of Florida in 1983, received a Bachelor of Science in Aerospace Engineering in 1988, and was also commissioned as an Air Force Officer. He served for four years at Edwards Air Force Base in California, also completing his Master of Engineering in Engineering Mechanics from University of Florida in 1990. After military service, he was accepted into the Air Force Palace Knight Program and enrolled in the Ph. D. program at the Georgia Institute of Technology in 1992.